2011

WETTING TRANSITIONS AT NANOSTRUCTURED SURFACES

Yazdi Jamileh Seyed
Virginia Commonwealth University

WETTING TRANSITIONS AT NANOSTRUCTURED SURFACES

A thesis submitted in partial fulfillment of the requirements for the degree of Master of Science in Chemistry at Virginia Commonwealth University

by

Jamileh Seyed Yazdi

Master of Science in Chemistry

Virginia Commonwealth University
College of Humanities and Sciences
Department of Chemistry
Richmond, Virginia

2011

Director: Dr. Alenka Luzar, Professor of Chemistry

Department of Chemistry

Acknowledgment

I would like to dedicate this work to my advisor, Professor Alenka Luzar, for all her support and mentorship. Also I would like to give my special thanks to Professor Dusan Bratko, for his help and support during my study at VCU. I would like to thank Dr. Chris Daub for his help and Dr. Davide Vanzo and Mr. John Ritchie for their contributions. In addition, I appreciate financial support from Chemistry Department at Virginia Commonwealth University (Lidia M. Vallarino Scholarship) and National Science Foundation and Altria Group and Office of Global Education. I would like to thank my committee members for their help and their support. I would also like to thank Professor Jose Teixeira from LLB Saclay, France, for his valuable discussion. All supports from my family and my friends is highly appreciate.

To

my husband Mohammad Reza

and

my son Daniel

Table of Contents

List of Figures

List of Tables

Abstract

WETTING TRANSITIONS AT NANOSTRUCTURED SURFACES

By Jamileh Seyed Yazdi

A thesis submitted in partial fulfillment of the requirements for the degree of
Master of Science at Virginia Commonwealth University.
Virginia Commonwealth University, 2011
Major Director: Alenka Luzar
Ph.D, Professor, Department of Chemistry

Shape of a droplet atop a surface heterogeneity at a nanoscale. *Small aqueous droplets on homogeneous surfaces, surrounded by a reservoir of vapor are inherently unstable. In contact with supersaturated vapor, the drops will keep growing until they coalesce and form a contiguous aqueous phase. Alternatively, if vapor pressure is below that of the droplets, the droplets gradually evaporate. Departing from this common picture, when nanoscale droplets sit above hydrophilic patches on a heterogeneous surface, at certain conditions they can maintain a stable volume, determined by the pertinent contact angle and the size of the patches. Only the region under the droplet perimeter controls the contact angle, which in turn determines the drops curvature for given volume and the vapor pressure of the liquid in the drop. The drop size may therefore stop changing when its base just covers the hydrophilic patch. The finite range of water-substrate interactions, however, blurs the patch boundaries hence the nanodrop geometry varies with the patch size in a gradual manner. We use molecular simulations to examine this dependence on graphene-like surfaces with topological heterogeneity as complementing studies of chemical heterogeneity (John Ritchie, Master Thesis, VCU, 2010). We measure the microscopic analogue of the contact angle of aqueous nanodrops above circular hydrophilic or hydrophobic patches of varied size. For both the chemically and topographically heterogeneous surfaces, the results confirm the contact angle of a nanodroplet can be predicted by the local Cassie-Baxter mixing relation applied to the area within the interaction range from the drop's*

perimeter, which, in turn, enables predictions of condensation and saturated vapor pressure above nanopatterned hydrophilic/hydrophobic surfaces.

Switchable nanowetting dynamics. *Understanding the dynamic response of contact angle on switchable hydrophobic-hydrophilic surfaces is key to the design of nanofluidic and optical devices. We use molecular dynamics simulation for water droplets with different number of molecules on a molecularly smooth and corrugated substrate. We monitored the relaxation of the droplet geometry in response to a change in surface hydrophobicity. From the time correlation function for the height of the drop's center of mass we estimate the rates of relaxation for wetting/dewetting processes following the change between hydrophobic and hydrophilic character of the surface. On molecularly smooth surfaces, we find similar forward/backward rates revealing insignificant hysteresis. Calculations on corrugated surfaces, however, reveal quite different relaxation times for forward (Cassie state to Wenzel state) and reverse processes. The observed hysteresis is associated with different friction forces between the droplet and the surface during advancing and receding processes. We calculate the friction coefficient of the corrugated surface for the forward process following the increase in surface hydrophilicity. We compare continuum hydrodynamic (HD) and molecular kinetic theories (MKT) for calculation of the friction coefficient. Although the small size of our system suggests the use of molecular description of the surface, incorporated in MKT, we obtain essentially equal friction coefficients from both theories. This information indicates an overlap between continuum hydrodynamics and molecular dynamics regimes, with both the HD and MKT theories being applicable at the nanoscopic lengthscales we consider.*

Water dynamics inside nanospheres. *Chemical nature of a spherical confinement has significant effect on dynamics of water molecules outside the cage. In a separate study we examined the effect of chemical nature of the cage on the dynamics of water molecules inside the cage. Calculations have been made for variety of time correlation functions of water in four different sizes of spherical hydrophobic/hydrophilic confinements,* C_x *x=320, 500, 720, 1500 based "hollow buckyballs", with different spherical pore diameters. Calculated water hydrogen bond lifetimes, diffusion coefficients and rotational relaxation times in these systems reveal a distinctly different water dynamics compared to interfacial water dynamics outside the cage:*

interestingly we find insignificant changes in time scales for water dynamics in hydrophilic and hydrophobic carbon cages. Even adding partial charges to hydrophilic confinement did not make a big effect on results compared to hydrophobic case. These findings are suggesting that in highly symmetric confinement water molecules do not care about the type of interaction with the wall because of cancellation of forces in different directions.

Chapter 1. Introduction

For a macroscopic drop, Young's equation relates the contact angle θ to the three interfacial free energies[1]

$$\cos\theta = \frac{\gamma_{SV} - \gamma_{SL}}{\gamma_{LV}} \qquad (1\text{-}1)$$

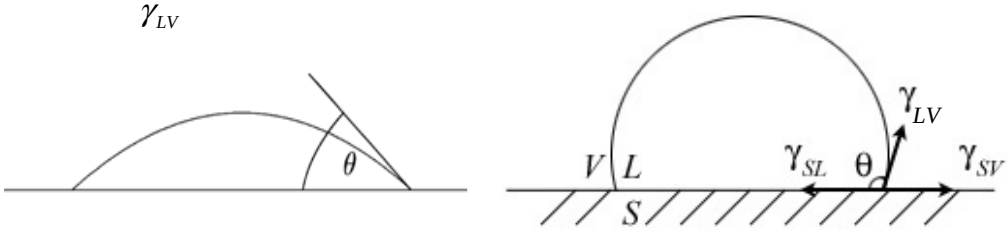

Figure 1.1. Young's contact angle.

where γ_{SL}, γ_{LV}, and γ_{SV} are the surface free energies of the solid-liquid, the liquid-vapor and the solid-vapor interfaces. Cassie and Baxter generalized Young's equation to composite surfaces whose cosine of contact angle is presumed to represent the area average of $\cos\theta_i$ of individual components covering fractional areas f_i [2]

$$\cos\theta_C = f_1\cos\theta_1 + f_2\cos\theta_2 \qquad (1\text{-}2)$$

The Cassie-Baxter equation (1-2) implicitly presumes any heterogeneities to occur on length scales that are small compared to the size of the drop (macroscopic drops), thus there is no dependence on the drop location[3,4]. Recently McHale proposed using the local form of the Cassie-Baxter equation where only the region covered by the three phase contact line is used in determining f_1 and f_2 in equation (2)[5]. However, no equation of the proposed local form was presented.

When a drop is touching a surface to wet it, at very early stage contact angle has its highest value. As time passes the drop shape undergoes evolution by reducing the contact angle. Finally the drop will reach to equilibrium state and contact angle will have its minimum value. This equilibrium contact angle is called static contact angle while the non-equilibrium, time dependent contact angle is called dynamic contact angle. In wetting events that contact angle is growing, it named as advancing contact angle, however, in dewetting processes that contact angle is reducing, it known as receding contact angle. Depending on the surface, advancing contact angle is always smaller or

equal to the receding contact angle. The difference between advancing and receding contact angle is called contact angle hysteresis.

To develop new technologies like nanofluidic devices, medical and basic sciences, understanding the properties and behavior of water at the nanoscale is extremely important. In this regards the importance of surface modification for specific chemical and physical properties is absolutely crucial[6]. Construction and design of new materials having surface heterogeneities can be used to change/predict wetting properties based on the knowledge about detailed pattern of the surface[4].

Since most of the works have been done in macroscopic scale, a question that can be asked is "what happens at a nanoscale?" Cassie-Baxter equation is not supposed to be always valid for relatively small (microscopic) drops[7]. For nanoscale drop on a nanoscale roughness only local Cassie-Baxter equation may work[8]. Kwon and coworkers[9] pointed out that in the case of roughness pinning/depinning processes are a major cause of hysteresis and any deviations from the Cassie-Baxter prediction. Thus if a surface is devoid of pinning (ideal smooth surface) it will show no hysteresis and will follow Cassie-Baxter formula[9,10].

Conventional Cassie-Baxter predictions for wetting of heterogeneous surfaces relate the contact angle to the average properties of the substrate under the drop. When surface heterogeneities occur on the lengthscale close to the size of the drops McCarthy and coworkers[11] pointed out that the nature of the substrate at the droplet perimeter controls the contact angle. This distinction is relevant when the properties of this region deviate from the average under the drop. In the case of nanodrops the situation is further complicated, because the finite range of water-substrate interactions makes the definition of the perimeter region somewhat arbitrary[12]. Using molecular simulations we try to understand which parameters are involved to determine the shape of a sessile nanodrop in contact with a heterogeneous surface. In the case of macroscopic drops it is well known that the characteristic of the perimeter of the drop is determining the contact angle. Recent chemical heterogeneity[58] studies, has proved that in the case of a nanodrop this fact is also valid and now we are going to validate this fact for topological heterogeneity. Therefore in a complementary study we generated a set of corrugated graphite-like model surfaces with different patterns for topological heterogeneity and we measured the

microscopic analogue of the contact angle of nanodrops containing 2000 water molecules above a surface patch. Our results confirm it is exclusively the border characteristics of the base that determine the contact angle of a nanodrop on these topologically heterogeneous surfaces. We showed the observed contact angle dependence on the size of the patch can be predicted by the local Cassie-Baxter mixing relation applied to the area within the interaction range from the drop's perimeter. The important effects of surface heterogeneities on saturated vapor pressure of water above the droplet have been discussed.

Diverse modification procedures have been used to permanently alter wettability. Control of wettability has been demonstrated by elegant methods including light-induced and electrochemical surface modifications[15]. These systems require chemical reactions in order to control wettability.

Surface properties and functionality can change by applying external stimuli and therefore produce changes in the molecular structure and nanoscale features of the surface[13]. Interfacial properties, such as wetting behavior, are defined by the molecular-level structure of the surface. It is very useful to have a surface whose properties are actively under control. These surfaces are named smart surfaces/devices in surface engineering. Electrical switching, electrochemical switching, photo-switching, thermal switching, mechanical switching, environmental switching and so on are all different methods to switch the surface interaction to change hydrophilicity/hydrophobicity[13]. Electrowetting for example has been proposed as a novel principle for a reflective display[14]. In systems where the ratio of surface area to volume is large, the surface forces dominate. Therefore, switchable surfaces are ideal for nano/micro scale systems[13].

Understanding and knowing the dynamic properties and response of the hydrophobic/hydrophilic switchable devices will definitely help finding new applications for these devices in new technologies[15]. It is known that two physically different wetting states exist on structured surfaces. A droplet may fully wet the structured surface, i.e. completely fill the crevices of the surface, or, alternatively, rest on top of the structure with air trapped below the droplet. The former case is referred to as the Wenzel state, as the droplet senses a rough but homogeneous surface (the Wenzel regime with wet grooves between the posts), while the latter case is referred to as the Cassie state, as the

droplet senses a flat but heterogeneous surface (the Cassie regime with empty grooves between the posts under the drop). These two wetting states and related intermediate states (partial penetration of the liquid into the surface structure) have been studied extensively because of very different wetting behaviors observed. Transitions between Cassie and Wenzel states may be triggered by switching surface wettability[16]. Ralston and co-workers[17,18,72] performed extensive experimental studies on droplets in Cassie and Wenzel states on smooth and structured surfaces and they were able to measure the friction coefficient of the surface. They used molecular kinetic theory (MKT)[71] and hydrodynamics model[73,74 ,19] to do so and all of their studies are for macroscopic drops.

We followed their method to find friction coefficient for nanodrop on a nanorough surface to validate if the theory that they are using can be applied for nanoscale systems. After finding the timescale of the droplet's relaxation on the smooth surface and scaling with the system size, we created a structured surface that is able to show both Cassie and Wenzel states upon switching the hydrophilicity/hydrophobicity of the surface. In our studies switching is induced by changing the water-surface attraction[50]. After finding the relaxation time of the water drop for this surface and scaling with the system size we used molecular kinetic theory and hydrodynamics model to estimate friction coefficient of the surface.

Encapsulation of molecules at the nano-scale provides the possibility of exploring the behaviour of solutions and liquids under conditions that are completely different from the bulk systems. Confined water has been studied in different structures like graphite channels[20], carbon nanotubes[21,22,23], silica pores[24,25], and mica surfaces[26], and other systems. Water confined in reverse micelles, RMs[27,28,29], has attracted many investigations theoretically[30,31,32,33] and experimentally[34,35,36,37]. As an example metal oxide based nanocapsules have been shown[38] to provide a suitable system to study the behaviour of confined liquids, especially water and aqueous solutions. These studies all reveal general trends of confined water that differ from bulk phase. Recent computational study[39] of water inside nanopores in general shows that water molecules organize in layers depending on the size and geometry of the confinement. For example, the most

important factors affecting the structure and dynamics of water in the confinement are water interactions with the confining surface and the geometry of the container.

A perfect spherical confinement is molybdenum based nanocapsule. These materials are Mo_{132}-ACET or Mo_{132}-PHOS balls in which acetate and phosphate groups will result in different interaction energy between wall and water molecules. These materials are synthesized during last decade and there is an ongoing neutron spin echo experiment on this particular system that is taking place by Jose Teixeira, Marc Henry and Stephane Longeville in LLB, CEA Saclay, France. But there is only one recent computational study so far on this system by a group of scientists in Spain[39]. These giant spherical confinements with large internal cavities are capable of encapsulating guest molecules. By tuning the overall charge and geometry of the internal surface with addition of specific ligands, the structure of the encapsulated molecules can vary. X-ray experiments show that water can form two well defined concentric layers with dodecahedral symmetry and buckyball-like structure followed by a coordination layer. This simulation study[39] mainly used $MO_{132}(SO_4)$ which is behaving as a hydrophilic sample and has a similar space for water molecules as (AOT RMs) reverse micelles with ratio between the total water to the total surfactant concentrations, w_0, is equal to 4. They studied the structure of water and they found four peaks for oxygen-oxygen pair correlation function, g(r). They divide the cavity into 10 concentric shells. They calculate average number of hydrogen bonds per water molecules and they found the characteristic three-dimensional hydrogen bond network present in the bulk water is distorted inside the cavity where water organizes instead in concentric layered structures similar to those belonging to the buckyball family. They calculate hydrogen bond correlation function and they found its decay to be much slower for external layers compared to internal layers. Also they found hydrogen bond bridges between layers are less correlated in time than intralayer hydrogen bonds. They claim that their results show switches of water molecules between layers are rare events and involve the simultaneous switch of two water molecules. Another finding of their study is at long times: the system show power law decay in properties like the fluctuations in the number of molecules in the structures. We are going to validate if a simple spherical geometry without all detailed of the structure can lead us to the results that they found. We would like to consider the simplest

approximation that can still capture essential physical properties, therefore we performed our computer simulations in spherical geometry of “hollow buckyballs”. Our aim was to study the dynamics of water in these ordered confined spaces. In this recent simulation study only one size of the confinement with hydrophilic interaction was reported. We, on the other hand, studied confinements with different sizes and with different degrees of hydrophobicity/hydrophilicity. We studied the difference in dynamics of water in these confinements by calculating diffusion coefficients and rotational relaxation time and hydrogen bonds time correlation functions.

Chapter 2. Methods and models

Water Model. We studied structure and dynamics of water droplets at a nanoscale on smooth and structured surfaces as well as dynamics of water in the confinements. For all these studies we apply the extended simple point charge (SPC/E) model[40] for water. Despite its limitations associated with the lack of molecular flexibility and polarizability, SPC/E captures qualitatively and often quantitatively a large number of properties of water[41,42]. Since in our studies water properties like surface tension and diffusion coefficient are important and SPC/E reproduces well these two quantities, we used this model for water. The sketch of SPC/E water model is shown in Figure 2.1, in addition to the partial charges on all of the three sites. Oxygen site has Lennard-Jones parameters $\varepsilon = 0.6502$ kJ/mol , and $\sigma = 3.166$ Å.

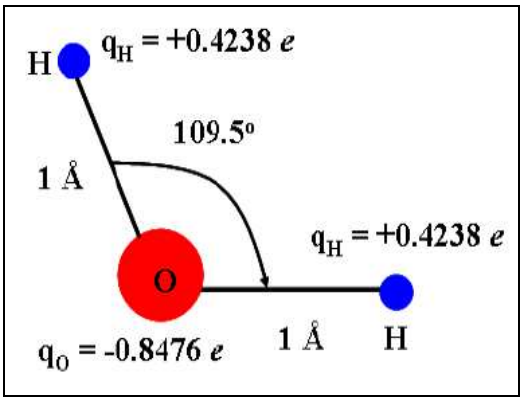

Figure 2.1. SPC/E water model.

Surface Models. For smooth surfaces we took a graphene sheet consisting of carbon-like atoms on a hexagonal lattice. The bigger the drop that we are going to put on the surface, the bigger the graphene sheet required. For corrugated surface we used three-layers of graphite. Many atoms from second and third layers will be removed and only atoms in desired locations will stay to build pillars. The details of atom positions of 2nd and 3rd layers are based on particular problem that we need to solve. Therefore we can create pillars with different thickness, pillars with different empty space between them (different number of pillars per unit area) and different pillar's height by starting with more

graphene sheets. After preparation of the surface we put a water droplet on the surface. To start the simulation we need to specify type of water-carbon interactions.

Water surface interaction (mixing rules). The essential features of intermolecular interaction can approximate well by Lennard-Jones potential, which can be written as

$$U_{LJ} = 4\varepsilon\left[(\sigma / r)^{12} - (\sigma / r)^{6}\right] \qquad (2\text{-}1)$$

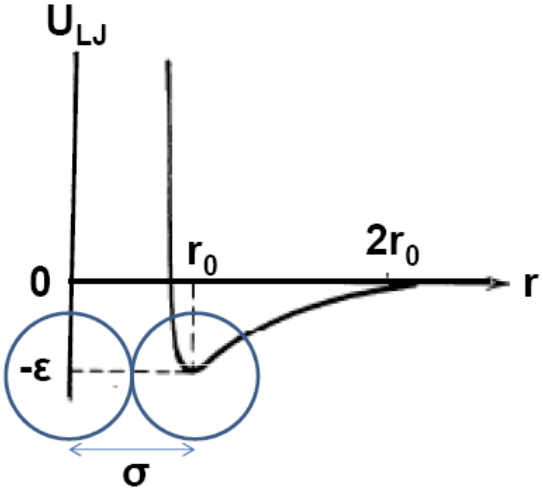

Figure 2.2. Lennard-Jones potential.

For applying water-surface interaction we have to use mixing rule based on parameter values for carbon, oxygen and hydrogen.

Geometric mixing rules is using geometric mean for sigma and epsilon as below

$$\varepsilon_{CI} = (\varepsilon_{CC}\,\varepsilon_{II})^{1/2} \qquad \sigma_{CI} = (\sigma_{CC}\,\sigma_{II})^{1/2} \qquad I = O, H \qquad (2\text{-}2)$$

Lorentz-Berthelot mixing rules is using arithmetic mean for sigma values and geometric mean for epsilon as follow

$$\varepsilon_{CI} = (\varepsilon_{CC}\,\varepsilon_{II})^{1/2} \qquad \sigma_{CI} = \frac{1}{2}(\sigma_{CC} + \sigma_{II}) \qquad I = O, H \qquad (2\text{-}3)$$

Simulation Method. ***Molecular Dynamics (MD)***[43,44]**.** MD is one of widely used methods for simulating many-body systems in which their particles are obeying Newtonian

mechanics. This method is a very powerful technique with excellent approximations for our studies. The only restriction of using MD is for very light particles such that we cannot ignore quantum effects. In this method we accommodate particles in simulation box and then based on the temperature that we want, we apply initial random velocity to all particles (for example using Gaussian distribution). Then we compute forces on all particles based on the potential that we define (for example Lennard-Jones potential). Then by having the force we can integrate the Newton's equations of motion to get new velocity and new position of particles. These steps will repeat until the system reaches equilibrium and then we can sample the parameters that we are interested in. To integrate Newton's equations of motion, there are numerous methods. The most common one is Verlet algorithm. As other versions of Verlet algorithms we can name velocity Verlet and Leap Frog. Another main algorithm is predictor-corrector that is also commonly used. There are few softwares available for MD calculations that are open source. For two projects, chapters 3 and 4 we used LAMMPS ("Large Scale Atomic/Molecular Massively Parallel Simulator") molecular simulation package, 2010 and 2011 versions. LAMMPS is distributed by Sandia National Laboratories, a US Department of Energy laboratory[45]. For project in chapter 5 we used DLPOLY v2.15 code[46], developed at Daresbury Laboratory, UK, by adding additional subroutines adopted from Christopher Daub and modified by Jamileh Seyed-Yazdi.

Verlet algorithm. To find new velocity and position with this algorithm we can start with Taylor expansion of the position of a particle, around time t,

$$r(t+\Delta t) = r(t) + v(t)\,\Delta t + \frac{F(t)}{2m}\Delta t^2 + \frac{\Delta t^3}{3!}\dddot{r} + O(\Delta t^4)$$

$$r(t-\Delta t) = r(t) - v(t)\,\Delta t + \frac{F(t)}{2m}\Delta t^2 - \frac{\Delta t^3}{3!}\dddot{r} + O(\Delta t^4)$$

By summing these two, we get

$$r(t+\Delta t) + r(t-\Delta t) = 2r(t) + \frac{F(t)}{m}\Delta t^2 + O(\Delta t^4)$$

This can be rewrite

$$r(t+\Delta t) \approx 2r(t) - r(t-\Delta t) + \frac{F(t)}{m}\Delta t^2 \qquad (2\text{-}4)$$

In this algorithm to find new position there is no need for using velocity. Calculation of new velocity however, can be done as follows

$$r(t+\Delta t)-r(t-\Delta t)=2\,v(t)\,\Delta t+O(\Delta t^3)$$

Therefore

$$v(t)=\frac{r(t+\Delta t)-r(t-\Delta t)}{2\Delta t}+O(\Delta t^2) \qquad (2\text{-}5)$$

Long range electrostatic interactions. Electrostatic interaction, (Coulomb interaction), which falls off at the rate of r^{-1} (equation 2-6), is a long-ranged interaction. Long-ranged interactions in molecular simulation are usually difficult to calculate.

$$E_{Coulomb}=\sum_{i\neq j}\frac{q_i\,q_j}{4\pi\varepsilon\,r_{ij}} \qquad (2\text{-}6)$$

where q_i and q_j are the partial charges on atoms *i* and *j* respectively, and ε is dielectric constant. Ewald summation method[47], and its other extensions like SPME[48] (Smooth Particle Mesh Ewald) and PPPM[49] (Particle-Particle-Particle Mesh). In this method electrostatic interaction can be split to two parts using an error function and a complementary error function.

$$erf\,(x)=\frac{2}{\sqrt{\pi}}\int_0^x e^{-t^2}dt \qquad (2\text{-}7)$$

$$erfc(x)=1-erf\,(x) \qquad (2\text{-}8)$$

$erfc(x)$ quickly vanishes to zero as x increases so this part is a short-ranged interaction that can be summed in real space. $erf\,(x)$ is Fourier transformed into a reciprocal space that also called k space, since its sum converges quickly in k space. Equation (2-9) has electrostatic interaction after Ewald sum treatment.

$$\begin{aligned}U_{electrostatic}=&\frac{1}{V}\sum_{k\neq 0}\frac{4\pi}{k^2}\left|\sum_{i=1}^{N}q_i\exp\left(i\vec{k}.\vec{r}_i\right)\right|^2\exp\left(-k^2/4\alpha\right)\\&-\left(\alpha/\pi\right)^{1/2}\sum_{i=1}^{N}q_i^2+\frac{1}{2}\sum_{i\neq j}^{N}\frac{q_i\,q_j\,erfc\left(\sqrt{\alpha}\,r_{ij}\right)}{r_{ij}}\end{aligned} \qquad (2\text{-}9)$$

Structural and Thermodynamics properties

a) Contact Angle Calculations. Contact angle of water droplet has been calculated using standard procedures. We adapted the technique developed by Werder et al.[50] to determine the microscopic analogue of the contact angle, which basically entails fitting the cross-section of the droplet to a truncated circle. We obtained water isochore profiles from simulation trajectories by introducing cylindrical bins using a reference level and the surface normal through the center of mass of the droplet as reference axis. The bins have a height of 0.5 Å in the z-direction and are of equal volume. The radial bin boundaries are located at $r_i = \sqrt{i\,\delta A/\pi}$ for i=1,…,N_{bin} with a base area per bin of δA=50Å^2. To find the water contact angle, we used a two-step procedure as described by de Ruijter et al.[51]. First, the location of the equimolar dividing surface is determined within every single horizontal layer of the binned drop. The equimolar dividing surface is defined as the surface where the average density of the water drop decreases by 50 percent from the density of liquid water. This dividing surface is found by sectioning the water drop into horizontal layers. Each layer is divided into radial bins where the density profile is measured. From this profile the equimolar dividing line is calculated. Second, a circular best fit through these points is extrapolated to the graphite surface where the contact angle, θ, is measured.

b) Hydrogen bonds. There are two most common definitions of hydrogen bonds, geometric[52,53] and energetic[54,55]. In geometric definition two water molecules are considered to share a hydrogen bond when oxygen-oxygen distance $r_{OO} < 3.5$ Å, the oxygen-hydrogen distance $r_{OH} < 2.45$ Å and the angle between r_{OO} and r_{OH} vectors is less than 30°. In our analysis, interfacial hydrogen bonds involve at least one molecule within σ_{CO} (3.19 Å) of one of the substrate atoms. Energetic definition considers two water molecules to be hydrogen bonded if their oxygen-oxygen distance $r_{OO} < 3.5$ Å and

their interaction energy is less than the threshold energy E_{HB} over a duration exceeding a minimum threshold time.

Dynamic properties

a) Time Correlation Functions. Using definitions from statistical mechanics[56] we can define and calculate time correlation functions. If $\delta A(t)$ show instantaneous deviation or fluctuation in A(t) from its time independent equilibrium average $\langle A \rangle$

$$\delta A(t) = A(t) - \langle A \rangle \tag{2-10}$$

The correlation between $\delta A(t)$ and an instantaneous or spontaneous fluctuation at time zero is

$$C(t) = \langle \delta A(0)\, \delta A(t) \rangle = \langle A(0)\, A(t) \rangle - \langle A \rangle^2 \tag{2-11}$$

In equilibration, the correlation between dynamical variables at different times should depend on the separation between theses times only, and not the absolute value of time. Thus

$$C(t) = \langle \delta A(t')\, \delta A(t'') \rangle, \qquad for \;\; t = t'' - t' \tag{2-12}$$

As a special case,

$$\begin{aligned} C(t) &= \langle \delta A(0)\, \delta A(t) \rangle \\ &= \langle \delta A(-t)\, \delta A(0) \rangle \end{aligned} \tag{2-13}$$

Switching the order of these two averaged quantities, gives

$$\begin{aligned} C(t) &= \langle \delta A(0)\, \delta A(-t) \rangle \\ &= C(-t) \end{aligned} \tag{2-14}$$

At small times,

$$C(0) = \langle \delta A(0)\, \delta A(0) \rangle = \langle (\delta A)^2 \rangle \tag{2-15}$$

At large times, $\delta A(t)$ will become uncorrelated to $\delta A(0)$. Thus

$$C(t) \to \langle \delta A(0)\, \delta A(t) \rangle, \quad as \;\; t \to \infty \tag{2-16}$$

And since $\langle \delta A \rangle = 0$

$$C(t) \to 0 \qquad as\ t \to \infty \tag{2-17}$$

Values close to one show a high degree of correlation and values close to 0 are indicating no correlations. We can calculate correlation time by doing time integral of correlation function from 0 to ∞. There is a high interest toward correlation functions in computer simulation:

a) in studying of fluid these functions give a clear picture of the dynamics,

b) we can often relate the time integral of these functions directly to macroscopic transport coefficients,

c) Fourier transform of these functions often can be related to experimental spectra.

b) Diffusion Coefficient. Diffusion coefficient, *D*, in three dimensions is given by integration of the velocity autocorrelation function

$$D = \frac{1}{3}\int_0^\infty dt\ \langle \vec{v}_i(t).\vec{v}_i(0)\rangle \tag{2-18}$$

$\vec{v}_i$ is the velocity of center of mass of a single molecule. The corresponding Einstein relation that is valid at long time is based on mean square displacement

$$2t\,D = \frac{1}{3}\left\langle \left|\vec{r}_i(t).\vec{r}_i(0)\right|^2 \right\rangle \tag{2-19}$$

$\vec{r}_i$ is the molecule position. In using Einstein relation we should not switch from one periodic image to another.

c) Rotational Dynamics. A useful quantity to measure is the time required for water molecules to reorient themselves. It can be measured by computing the time autocorrelation functions of n'th Legendre polynomial of the cosine of the angle spanned by the axes of each water molecule between time 0 and time t,

$$C_{n,\alpha} = \left\langle P_l\left(\vec{u}_\alpha(t).\vec{u}_\alpha(0)\right)\right\rangle \tag{2-20}$$

$\vec{u}_\alpha(t)$ is a unit vector along the molecular axis of interest measured at *t*. The reorientational times will be obtained by integrating the orientational correlation function of 2nd Legendre polynomial, $P_2(t)$, which is

$$P_2(\cos\theta) = \frac{1}{2}\left(3\cos\theta^2 - 1\right) \quad (2\text{-}21)$$

The rate of decay, τ_2, is determines the nuclear magnetic resonance, NMR, relaxation time which is associated with intramolecular dipole-dipole coupling.

Chapter 3. Shape of a droplet atop a surface heterogeneity at the nanoscale

Our present study reaffirms the importance of surface properties in the region adjacent to the three phase contact line of a nanoscale droplet. This approach tests generalizations of conventional surface thermodynamics to small length scale system relevant to nanofluidics and design of surface-patterned nanomaterials. We examine the differences that inevitably separate macroscopic and nanoscale systems, as a continuum picture holds only approximately at the nano and molecular levels. Our computer experiments test how water-substrate interaction beneath the drop's core or at its perimeter determines the contact angle. Secondly, we examine changes in contact angle as a hydrophilic surface beneath the drop's core approaches and eventually extends beyond the three phase contact line. We specifically consider surface heterogeneities whose sizes are comparable to the size of the droplets. Experimentally, this situation has been tested on surfaces with macroscopic drops and surface patches[57]. We used molecular simulations to probe the role of tiny heterogeneities comparable to the size of the nanodroplets on the surface. Molecular simulations provide an ideal framework for studies of nanoscale systems which are not accessible to laboratory measurements. We consider model graphene-like surfaces with hydrophobic and hydrophilic domains. In the model, the hydrophilicity is controlled by degree of surface roughness. We performed calculations for a sequence of systems to study topological heterogeneity by increasing the radius of a circular hydrophilic patch and measuring the contact angle by starting from a pure corrugated surface in which a water droplet can only be in Cassie state. In analogy with studies of chemical heterogeneity[58], we confirmed that the surface properties at the drop's perimeter determined the contact angle on surfaces with topological heterogeneity. We further investigated the influence of the range of water/surface interaction as the patch contour approaches the drop's three phase contact line. To this end we examined the contact angle as a function of the radius of an expanding circular patch beneath the drop. Plotting the contact angle as a function of patch radius we identify a threshold patch size corresponding to a considerable decrease in contact angle. In our molecular simulations we incrementally increased the radius of

the circular hydrophilic patch beneath the drop until the contact angle converged to the value of our pure hydrophilic surface (that means a surface with fully occupied 2nd and 3rd graphite layers and hence no corrugation). We found essentially identical behavior for our topological heterogeneities with what has been found for chemical heterogeneity (the work has been done by John Ritchie[58]).

Simulation Methodology. In the case of water droplets on chemical and topological heterogeneous surfaces, the computer simulations are carried out by the LAMMPS molecular simulation package 2010 and 2011 versions[45] in NVT ensemble with temperature 300K maintained by Nose-Hoover thermostat[59] with 100fs time constant. Because of vapor/liquid coexistence, the average pressure in the system corresponded to the saturated vapor pressure above the drop at given T. Verlet integrator was used with simulation time step 1 fs. Lennard-Jones interactions are truncated at 14.0 Å. Long-range electrostatic interactions are treated by particle-particle-particle mesh solver (pppm) with a real space cutoff of 14.0 Å, and precision tolerance of 10^{-5}. Simulation box is a rectangular prism, with box edges L_x = 117.9 Å, L_y = 119.1 Å, and L_z = 300 Å and periodic boundary conditions are imposed throughout. In order to speed up the calculations, the surfaces are frozen in place during the simulation and the SHAKE algorithm[60] is used to maintain the internal geometry of the water molecules.

Water droplets containing 2000 molecules are simulated interacting with a corrugated surface for topological heterogeneity, with expanding a patch in the middle of these surfaces. The water-graphene interaction parameters (Table 3.1) were calculated using the geometric averages shown in the equations below.

$$\varepsilon_{CO} = (\varepsilon_{CC}\,\varepsilon_{OO})^{1/2}$$
$$\sigma_{CO} = (\sigma_{CC}\,\sigma_{OO})^{1/2} \qquad (3\text{-}1)$$

where σ_{co}, σ_{cc}, and σ_{oo} are the carbon-oxygen, carbon-carbon, and oxygen-oxygen separation distance at minimum potential, and ε_{co}, ε_{cc}, and ε_{oo} are the Lennard-Jones minimum potential energies[50]. These choices have been made for consistence with

completed studies on chemically heterogeneous surfaces with which we compare our new results.

Water-Carbon Interaction. We used Lennard-Jones surface interactions corresponding to a hydrophilic surface with a carbon-oxygen interaction energy ε_{CO} of 0.120 kcal/mol for entire surface and all our simulations following Werder and coworkers[50].

Table 3.1. Lennard-Jones parameters used in the simulations.

	ε_{CO} (kcal/mol)	σ_{CO}(Å)	ε_{CC} (kcal/mol)	σ_{CC}(Å)	ε_{OO} (kcal/mol)	σ_{OO}(Å)
Topological Heterogeneity	**0.120**	**3.190**	**0.092**	**3.214**	**0.155**	**3.165**

Topological heterogeneity. We created a corrugated surface with pillars made from two layers of atoms grown on the graphene surface consisting of 5376 carbon-like atoms. The positions of pillar atoms in the 2nd and 3rd layers were the same as positions of carbon atoms of graphite in the first layer with lateral coordinates of the pillars, while we leave all other atom positions in these two layers unoccupied (empty spaces between pillars). The distances between pillars in x and y directions are Δx=4.912 Å and Δy=4.254 Å (Figure 3.1). These distances are sufficiently small to prevent any penetration of water into the grooves. This corrugated surface was made from 8064 carbon-like atoms. We start to grow a circular patch in the middle of this corrugated surface by replacing the pillars and intervening space by fully occupied graphite in 2nd and 3rd layers (with the patch radius starting from 10 Å and increased to 55 Å in 5 Å intervals). Subnanoscale corrugations render the surface more hydrophobic, a behavior deviating from predictions of Wenzel equation[61], as demonstrated in previous work done in Dr. Luzar's group[62], and by Mittal and Hummer[63]. When the patch radius is zero this particular surface is uniformly hydrophobic. The hydrophilic extreme is the case with infinite radius of the patch, meaning that the 'patch' is extended over the entire surface with 16128 carbon-like atoms.

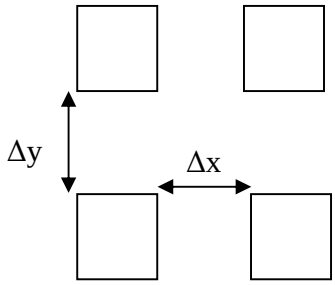

Figure 3.1. Schematic description of the surface covered with pillars for the case of topological heterogeneity.

After preparing topological heterogeneity as explained in chapter 2, our simulations were initiated by putting a water droplet with 2000 molecules on these surfaces at the center of the patch. We equilibrated the system and then used configurations from 1 to 3ns trajectories to measure the contact angle (Figure 3.3). Figure 3.2 shows snapshots of three surfaces with different patch radius (top row) as well as water droplet on these surfaces (bottom row). The whole set of surfaces and snapshots of equilibrated drops are shown in Appendix I.

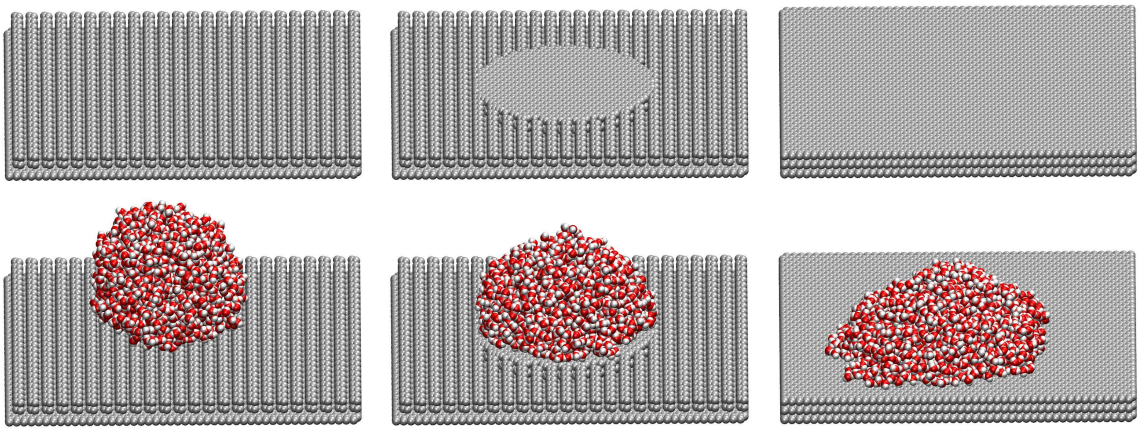

Figure 3.2. Three surfaces with r_p (patch radius) r_p=0 Å, r_p=30Å and r_p=∞ from left to right (top row). Snapshots of 2000 molecule water droplet on corresponding surfaces (bottom row).

Contact angles have been measured using the method explained in chapter 2. Figure 3.2 shows typical drop profiles for three different surfaces.

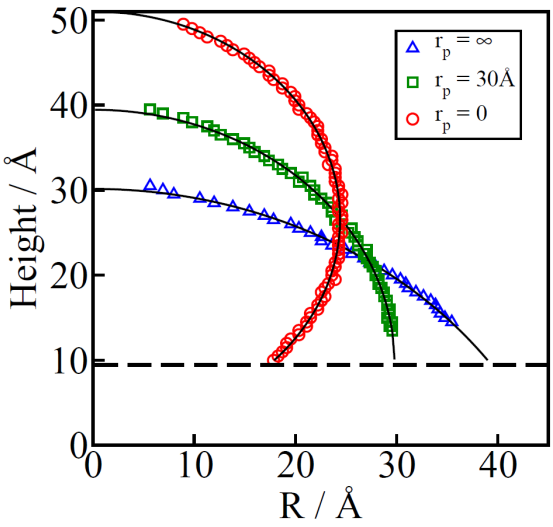

Figure 3.3. Drop profiles for three different surfaces, the most hydrophilic (homogeneous surface, $r_p \rightarrow \infty$ Å), the most hydrophobic (r_p=0 Å) and an intermediate patch size r_p=30 Å. Black solid lines are fitted to the simulated data. Dashed line represents the surface, where the contact angles were measured. R is the distance from the main axis of the drop and height is the height of the drop measured from the top layer, 9.89 Å.

In Figure 3.4 we show contact angles for all different patch radii for topological heterogeneity (blue points). We compare our results with those obtained on surfaces with chemical heterogeneity[58].

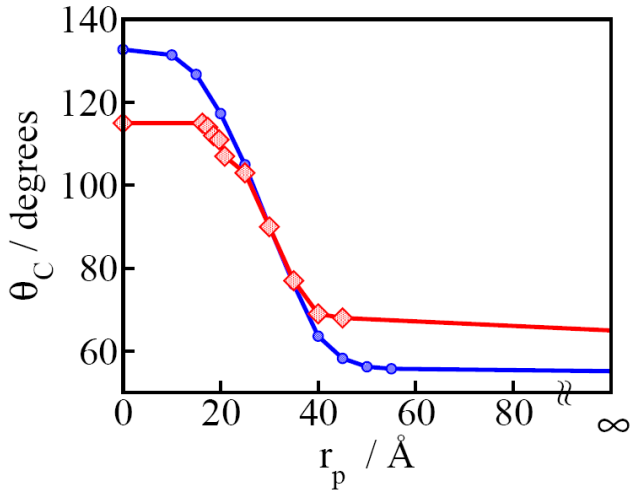

Figure 3.4. Simulated contact angle for topological (blue circles) and chemical (red diamonds) heterogeneity vs. the radius of the patch. Error bars are within the symbol sizes. Data points for chemical heterogeneity (red diamonds) are taken from ref. 58 for comparison to our simulation results (blue circles). Lines are guides to the eye.

Analysis. Because of perpetual droplet shape fluctuations and finite range of water/substrate interactions, the apparent surface properties affecting the droplet near the patch perimeter change in a gradual rather than abrupt fashion. This gradual change is incorporated in the local form of Cassie-Baxter equation[5] where we used fractions f_1 and f_2 calculated within the range of interaction from the drop's perimeter. To enable a consistent comparison of our results for topological heterogeneity with the results of the work done by John Ritchie for chemical heterogeneity[58] we used identical form of local Cassie-Baxter relation for our simulation. The area of the hydrophilic patch, (A_{pi}), and the net area of the range of interaction, (A_{ri}), were calculated to estimate the apparent fractional areas f_1 and f_2 in the proximity of the perimeter as follows:

$$A_{ri} = \pi(r_d + r_i)^2 - \pi(r_d - r_i)^2 \tag{3-2}$$

$$A_{pi} = \pi r_p^2 - \pi(r_d - r_i)^2 \tag{3-3}$$

Above, r_d is the radius of the drop's base obtained from the simulation (i.e. $r_{perimeter}$), r_p the radius of the patch, and f_1 is the fractional area of hydrophilic patch overlapping the area of the range of interaction (all introduced parameters are shown in Figure 3.5)

$$\begin{aligned} f_1 &= 1 \qquad if\ r_p > r_d + r_i \\ f_1 &= \frac{A_{pi}}{A_{ri}} \quad if\ r_d - r_i < r_p < r_d + r_i \\ f_1 &= 0 \qquad if\ r_p < r_d - r_i \end{aligned} \tag{3-4}$$

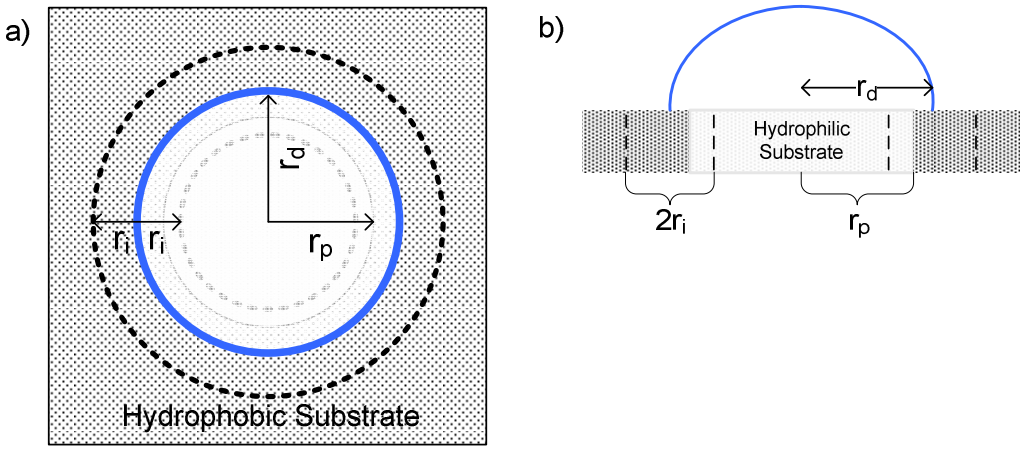

Figure 3.5. Parameters used to calculate local form of the Cassie-Baxter equation. Figures are taken from John Ritchie's Master Thesis[58].

f_2 is the area fraction of the hydrophobic patch overlapping the area of range of interaction $f_2 = 1 - f_1$. Local values of f_1 and f_2 are substituted into equation (1-2) to calculate Cassie-Baxter contact angles for comparison with our simulation results (topological heterogeneity) knowing θ_1=55.2° and θ_2=132.7°. Related results for chemical heterogeneity from the work done by John Ritchie[58] are shown as well (Figure 3.7).

Because of their nanoscale dimensions, the geometry of small droplets we consider may deviate from the ideal shape of a truncated sphere and may only approximately follow the Young equation (equation 1-1). A recent systematic analysis[64], and previous works[50,62] show Young equation is obeyed surprisingly well for O(10^3) molecule drops, with small deviation observed primarily on very hydrophilic surfaces. In this work, we examined the sphericity of nanodrops on varied surfaces. As we observe significant temporal shape fluctuations, we concentrated on long-time averages. Specifically, in Figures 3.6a and 3.6b we compare the average perimeter radii from simulations with the values corresponding to the shape of the ideal truncated sphere described[5] by the equations of

$$R_{spherical\,drop} = \left(\frac{3V}{\pi\beta}\right)^{1/3} \quad , \quad r_d = R_{spherical\,drop}\sin\theta \tag{3-5}$$

Here $R_{spherical\ drop}$ is the radius of curvature of the spherical drop, r_d is $r_{perimeter}$, V is the volume of the drop (with good approximation we multiply the number of water molecules by 30 Å^3 which is the volume of one water molecule) and $\beta(\theta)$ is a function of contact angle defined as

$$\beta(\theta) = 2 - 3\cos\theta + \cos^3\theta = (1-\cos\theta)^2(2+\cos\theta) \qquad (3\text{-}6)$$

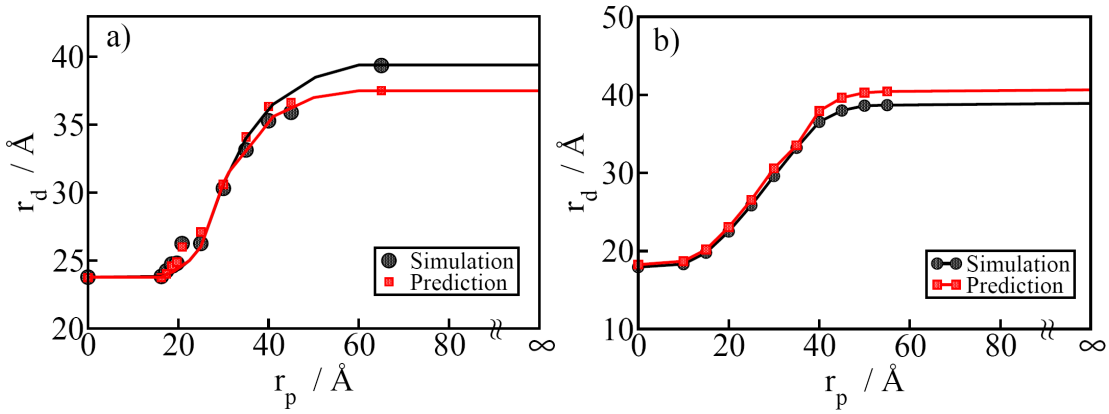

Figure 3.6. Comparison of radius of the perimeter, r_d, obtained from molecular simulation (solid circles) and predicted values (solid squares) from equations (3-5) and (3-6) as a function of patch radius for (a) chemical and (b) topological heterogeneity. Lines are guides to the eye. Error bars are within the symbol sizes. (a) is based on the results of John Ritchie[58] for chemical heterogeneity for comparison.

The good agreement between simulated radii and spherical-drop predictions indicate negligible droplet distortion when surfaces are predominantly hydrophobic. Increasing the size of chemical or topological heterogeneity with hydrophilic characteristics results in small deviations between the two sets of data, consistent with comparisons between geometric and thermodynamic contact angles of nanodroplets in the literature[64]. We also note the increased uncertainty in simulated contact angle determination on hydrophilic surfaces.

Interfacial Hydrogen Bonds. We used geometric definition in calculation of hydrogen bonds[52,53]. In our analysis, interfacial hydrogen bonds involve at least one molecule within σ_{CO} (3.19 Å) from one of the substrate atoms. In the case of topological heterogeneity we used snapshots from 1 to 3ns simulation to calculate the number of

interfacial hydrogen bonds in solid-liquid interface for two extreme cases (pure hydrophilic, 100% coverage and pure hydrophobic, 25% coverage). We defined coverage as the number of atoms in the top layer divided by number of atoms in the bottom layer. We found the number of interfacial hydrogen bonds per molecule for 100% coverage 3.1 ± 0.1 and for 25% coverage 2.6 ± 0.6 in good agreement with previous results[62]. The changes we observe can be attributed to density depletion of water molecules in the interfacial layer when the drop on the corrugated surface assumes a Cassie-like state as opposed to the higher density in aqueous surface layer on the more hydrophilic high-coverage surfaces.

Results and Discussion. Comparing the relation between contact angle and the patch radius shows the same trend for chemical and topological heterogeneity (Figure 3.7) but for smaller patch radius the topological heterogeneity shows higher values of contact angle compared with chemical heterogeneity. The reason is that in the topologically heterogeneous systems we have three layers of atoms with separation of graphite sheets (3.4 Å), compared with chemically heterogeneous systems that have only one layer of atoms. The extra atoms in topological heterogeneous systems cause the difference in contact angles for lower and higher patch radii. Based on the results from Figure 3.4 we can conclude that with interaction range $r_i \sim 5$ Å for both cases we find the transition distance at about twice the interaction range added to the difference of the perimeter radius of the drop at the lowest and the highest patch radius, $2r_i + \Delta r_d$. This model works for both systems, with chemical and topological heterogeneity[65]. Figure 3.7 shows that for these two systems local Cassie-Baxter equation gives a good agreement with simulation results for entire data sets. That is consistent with findings of others[8,10]. Figures 3.6a and 3.6b show that predicted values for the radius of the perimeter of the drop are in close agreement with simulation results.

The average number of interfacial hydrogen bonds calculated for a pure hydrophilic surface (extended patch, 100% coverage) that has a direct impact on the interfacial free energy of the water-surface interface, which affects the contact angles, shows that the droplet is in tighter contact with the surface (lower θ_C) compared with the case of hydrophobic surface (pure corrugated surface, zero patch radius, 25% coverage)

that shows the droplet is in the Cassie state (higher θ_C). Because of its thermal motion, the droplet is moving and bouncing on hydrophobic surface. The instability of the droplet position in contact with the surface explains large error bars of the reported data.

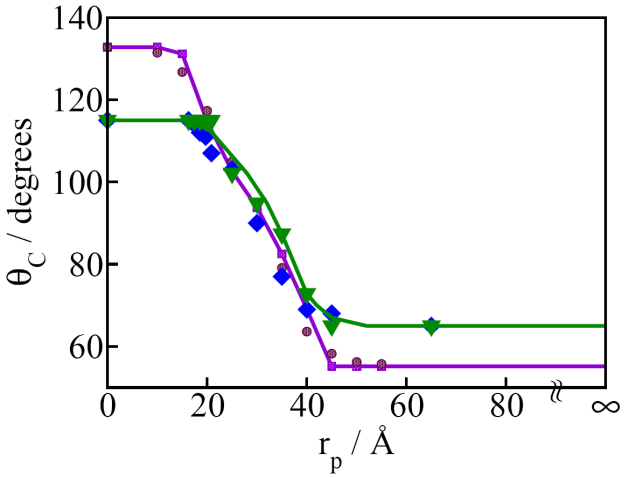

Figure 3.7. Comparison of contact angles based on simulation and local Cassie-Baxter predictions for topological (maroon circles: simulation results, purple squares: predicted Cassie-Baxter values) and chemical heterogeneity (blue diamonds: simulation results, green downward triangles: predicted Cassie-Baxter values). Error bars are within the symbol sizes. Solid lines are guide to the eye. Data points for chemical heterogeneity are taken from John Ritchie's results[58] for comparison.

Conclusion. We examined the relation between the contact angle of an aqueous nanodrop and surface-water interaction energy at the perimeter and beneath the drop. We simulate nanodroplets on graphene-like surfaces having hydrophobic and hydrophilic interaction energy at the perimeter and beneath the drop. The microscopic analogue of the contact angle was extracted from simulation trajectory data. We confirm the contact angle is exclusively related to the surface interaction energy in the region adjacent to the drop's perimeter. We test the role of finite range of substrate-water interaction when the area of a circular hydrophilic patch beneath the drop's core is incrementally expanded until the contact angle is equivalent to that on the pure hydrophilic surface. We identify a range of interaction corresponding to a considerable drop in contact angle when plotting contact angle as a function of patch size. We show the observed contact angle dependence on the size of the patch can be predicted by the Cassie-Baxter mixing relation

when limited to the area within the interaction range from the drop's perimeter which is about 5 Å for both topological and chemical heterogeneities.

Finally we discuss implications of surface heterogeneities on saturated vapor pressure of water above the droplet. In equilibrium, the droplet curvature alone defines the chemical potential inside a drop and hence the saturated vapor pressure in the system, independently of the nature of the substrate. The vapor pressure above the drop is bigger than the corresponding value above the bulk liquid. Considering Kelvin equation we have three situations. First, if μ (chemical potential) inside the drop exceeds μ outside the drop, evaporation exceeds condensation (the drop will gradually decrease in size) but the thermodynamic contact angle and curvature will stay the same (metastability due to perimeter pinning can cause deviations from Young's contact angle) unless the droplet perimeter crosses the patch border. Second, if μ inside the drop is equal to μ outside the drop, the drop size will stay the same. Last, when μ inside the drop is below μ outside (supersaturation), condensation and droplet growth will take place.

When, due to the droplet growth, or shrinking, the droplet perimeter crosses the border of the underlying hydrophilic patch, the drop's contact angle, curvature, and water chemical potential will be affected. If, due to condensation, the droplet base outgrows the size of the hydrophilic patch, the curvature and chemical potential will increase, thus slowing and eventually preventing further droplet growth. In the opposite scenario, the perimeter of a shrinking droplet can move over from a hydrophilic region to the area covered by the hydrophilic patch. In response, the curvature will be reduced, and the chemical potential decrease. Again, the droplet shape can reach an apparent equilibrium as chemical potentials in the drop and vapor converge. Static situations we discuss above are metastable with respect to the bulk liquid and require vapor supersaturation.

Chapter 4. Switchable Nano-Wetting Dynamics

Surface properties can change by external stimuli and therefore produce changes in the molecular structure and nanoscale features of the surface. Interfacial properties, such as wetting behavior, are determined by the composition and molecular-level structure of the surface. It is very useful to have surface properties where are actively under control. These surfaces are named smart surfaces/devices in surface engineering. One of the ways in which surfaces can be controlled is by switching its properties.

The wetting and dewetting of solid surfaces occur in nature and are also central to a number of biological processes and industrial applications. Systematic studies of wetting processes have predominantly involved equilibrium, or static, measurements. However, in most cases it is the dynamic wetting and dewetting behavior that is of practical relevance. The wetting behavior is generally characterized by the contact angle. In the dynamic systems the contact angle varies with the speed and direction of movement of the contact line. Investigators have developed models that relate the perimeter velocity and hence the rate of contact angle change to readily measured properties such as liquid viscosity, surface or interfacial tension, and the static contact angle and friction coefficient. Most of the models may be broadly classified as emphasizing hydrodynamic or molecular kinetic aspects or combinations of the two, with a recent more general theory proposed[66]. In the hydrodynamic approach the role of the solid surface is discounted, whereas in the molecular kinetic approach the microscopic properties of the solid surface are explicitly taken into account[66]. The velocity of wetting depends on the intrinsic wettability of the solid surface in such a way that there exists an optimum contact angle at which the velocity of wetting has the highest value[67].

Simulation Methodology. Computer simulations are carried out by the LAMMPS package in NVT ensemble with temperature 300K maintained by Nose-Hoover thermostat with 100fs time constant. Because of vapor/liquid coexistence, the average pressure in the system corresponds to the saturated vapor pressure above the drop at given T. Verlet integrator is used with simulation time step 1 fs. Lennard-Jones and Coulomb nonbonded pair-wise interactions are truncated at 11.0 Å for smooth surface

and 20.0 Å for corrugated surfaces. Long-range electrostatic interactions are treated by particle-particle-particle mesh solver (pppm) with a real space cutoff of 11.0 Å and 20.0 Å respectively, and precision tolerance of 10^{-5}. Simulation box is a rectangular prism, with box edges L_x = 117.9 Å, L_y = 119.1 Å, and L_z = 300 Å and periodic boundary conditions are imposed throughout. In order to speed up the calculations, the surfaces are frozen in place during the simulation and the SHAKE algorithm[60] is used to maintain the internal geometry of the water molecules.

We simulated water drops containing 500, 1000, 2000, 4000 and 8000 molecules on a smooth surface and water droplets with 1000, 2000 and 4000 water molecules on corrugated surface. We change hydrophilicity and hydrophobicity of the surface by changing Lennard-Jones energy parameters according to Werder et. al[50]. The water-graphene interaction parameters were calculated using the Lorentz-Berthelot mixing rules shown in the equations below for consistency with Werder et al. and others.

$$\varepsilon_{CO} = (\varepsilon_{CC}\,\varepsilon_{OO})^{1/2}$$
$$\sigma_{CO} = \frac{1}{2}(\sigma_{CC} + \sigma_{OO}) \qquad (4\text{-}1)$$

where σ_{co}, σ_{cc}, and σ_{oo} are the carbon-oxygen, carbon-carbon, and oxygen-oxygen separation distance at minimum potential, and ε_{co}, ε_{cc}, and ε_{oo} are the Lennard-Jones minimum potential energies. Table 4-1 contains all Lennard-Jones parameters that have been used in these simulations. In smooth and corrugated surfaces we start the simulation by putting a droplet on a hydrophobic surface and then we switch the surface to hydrophilic by changing the interaction between water and the surface (see details below).

Table 4-1. Lennard-Jones parameters used in these simulations.

	ε_{CO} (kcal/mol)	σ_{CO}(Å)	ε_{CC} (kcal/mol)	σ_{CC}(Å)	ε_{OO} (kcal/mol)	σ_{OO}(Å)
Hydrophobic Smooth	0.060	3.190	0.023	3.214	0.155	3.165
Hydrophilic Smooth/structured	0.150	3.190	0.144	3.214	0.155	3.165
Hydrophobic Structured	0.075	3.190	0.036	3.214	0.155	3.165

Smooth surfaces. *Smooth Surfaces.* For smooth surfaces we took a graphene sheet consisting of 5376 carbon-like atoms for smaller droplets with 500, 1000 and 2000 water molecules and a surface of a graphene sheet consisting of 21504 carbon-like atoms for bigger droplets containing 4000 and 8000 water molecules. In each case we started with a water droplet pre-equilibrated on a hydrophobic surface of a graphene sheet. Using the Lennard-Jones parameters mentioned above, see Appendix II (case 21 from Werder et. al.[50] for hydrophilic surface, corresponding to contact angle ~29° and case 17 for hydrophobic surface, corresponding to contact angle ~128°), pure hydrophobic and hydrophilic surfaces were created. Following an equilibration time (~300 ps) of a water droplet on hydrophobic surface, by changing Lennard-Jones parameters we switch the surface into hydrophilic and measure the relaxation time of the water droplet (we call this a forward process). Relaxation times depend on the size of the droplet (see Table 4.2). After the new equilibration time, by changing the Lennard-Jones parameters, we switch the surface back to hydrophobic and measure the relaxation time of the water droplet (we call this as backward/reverse process). Figure 4.1 shows a relaxation process of a water droplet with 2000 molecules on a smooth surface.

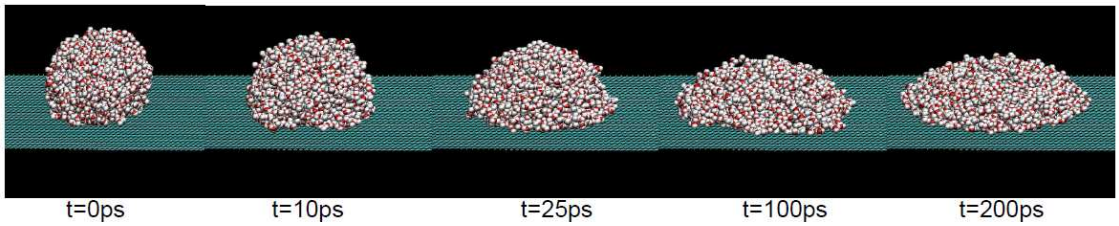

Figure 4.1. From left to right starting from hydrophobic surface, snapshots of 2000 molecule droplet's relaxation on a smooth surface.

Corrugated surfaces. *Corrugated surface with Cassie and Wenzel features.* We created a corrugated surface with pillars made from two layers of atoms grown on the graphene surface consisting of 5376 carbon-like atoms as bottom layer to create a structured surface with 6048 atoms. If we define the coverage for structured (corrugated) surfaces as the number of atoms on the top layer divided by number of atoms on the bottom layer, our constructed surface has the coverage of 1/16.

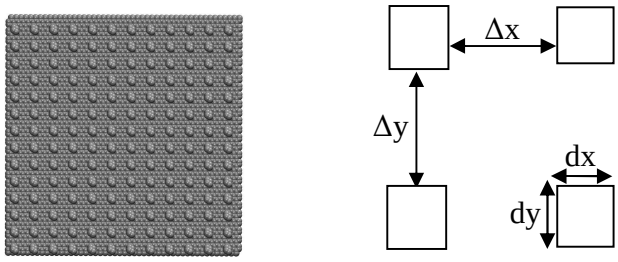

Figure 4.2. Left: snapshot of corrugated surface (top view). Right: schematic description of the surface covered with pillars for the case of corrugated surface with Cassie and Wenzel features.

We created a corrugated surface with pillars made from two layers of atoms grown on the graphene surface consisting of 5376 carbon-like atoms as bottom layer to create a structured surface with 6048 atoms (Figure 4.2). The distance between pillars in x and y directions are Δx=8.6 Å and Δy=7.8 Å and pillars have a thickness of dx=1.22 Å and dy=0.7Å (Figure 4.2). Lennard-Jones parameters used for this case are fixed as shown in Table 4.1 (case 21 from Werder et. al.[50] for hydrophilic surface, that corresponds to contact angle ~29°, and case 2 from Werder et. al. for hydrophobic surface, that corresponds to contact angle ~110°). See Appendix II.

This particular structured surface has been selected out of many trial surfaces with different coverages because of its ability to undergo a transition between Cassie-Baxter and Wenzel states upon switching the surface from hydrophilic to hydrophobic and vice versa. Snapshots of the water droplet for the case of 2000 water molecules are presented in Figure 4.3 for structured (corrugated) surfaces.

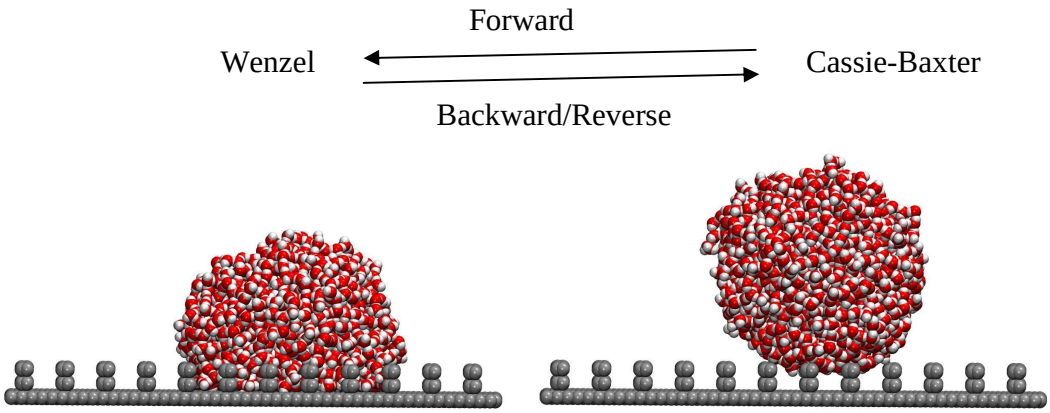

Figure 4.3. Snapshots of water droplet on corrugated surfaces from molecular dynamics trajectory. Left: droplet in Wenzel state; Right: droplet in Cassie state.

After equilibration of the droplet on hydrophobic surface in Cassie state, we change Lennard-Jones parameters to apply a hydrophilic interaction which means we switch the surface from hydrophobic to hydrophilic. After ~300 ps equilibration time, the droplet reaches the Wenzel state. Interestingly, if we switch the surface back to hydrophobic again, by changing Lennard-Jones parameters to their original values, the droplet will return to the Cassie state. We name these two processes forward and backward/reverse. In general there is a free energy barrier between these two states on every surface. For our corrugated surface going from Cassie to Wenzel state and vice versa is relatively fast (~45 and ~38 ps respectively) which means the free energy barrier between these two states (Cassie/Baxter and Wenzel) is rather small. When the drop reaches the Cassie state, because of its thermal motion, it moves around, wetting- and dewetting the surface over time occasionally it bounces away from the surface. This can happen if the water-surface interaction is very weak and the drop is elevated above the height that is out of the interaction range with the surface. In these cases the droplet tends to assume a nearly spherical shape. If the starting configuration corresponds to say a 120° contact angle, as the droplet approaches a more spherical shape, there will be a net force pushing the drop away from the surface, and it can suffice to push the drop out of contact in the absence of gravity (we should notice that roughness of hydrophobic surfaces enhances their hydrophobicity[62]). Of course all of these depend on the initial velocity distribution of the water molecules in the drop at the switching time. The detachment happened in about ten percent for a droplet with 2000 water molecules and more than seventy percent of the cases for droplets with 1000 water molecules and about five percent of the cases for the drop with 4000 water molecules. The likelihood of detachment hence rapidly decreased with the mass of the droplet and its size. To study the rate of the droplet response characterized in terms of droplet relaxation times in reverse (hydrophilic to hydrophobic) process we analyzed the runs during which the drop stayed close to the surface over ~5 ns simulation time and discarded those at which the drop flew away from the surface.

Analysis and Results. *Time Correlation Functions.* For water droplet on smooth and corrugated surfaces, calculation of the time correlation functions for the height of the

center of mass, h(t), of the nanodrop enabled us to estimate the rates of the microscopic analogue of the contact angle relaxation for wetting/dewetting processes (Figure 4.4). We used two characteristic time correlation functions, C(t) and R(t) to characterize the dynamics:

C(t) describes dynamics of fluctuations around equilibrium (using many time origins)

$$C(t) = \frac{\langle \delta h(t)\ \delta h(0) \rangle}{\langle \delta h(0)^2 \rangle} \tag{4-1}$$

R(t) is defines by the same equation as C(t), but the time origin is fixed at surface switching time (Figure 4.5)

$$R(t) = \frac{\langle h(t) - h(\infty) \rangle}{\langle h(0) - h(\infty) \rangle} \tag{4-2}$$

In these equations h(t) is the height of the center of mass of the droplet as a function of time (Figure 4.4), h(0) is the initial value of the height of the center of mass and h(∞) is equilibrated value for the height of the center of mass.

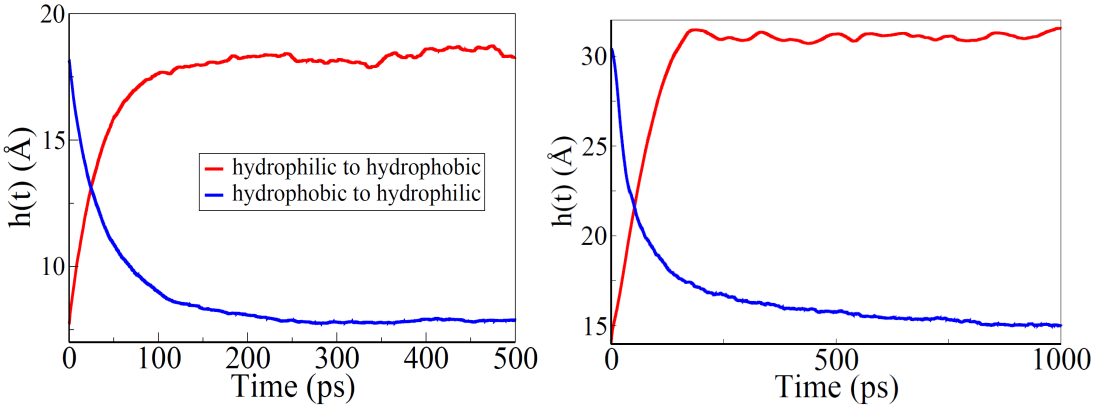

Figure 4.4. Variation of the height of the center of mass for smooth (left) and corrugated surface (right).

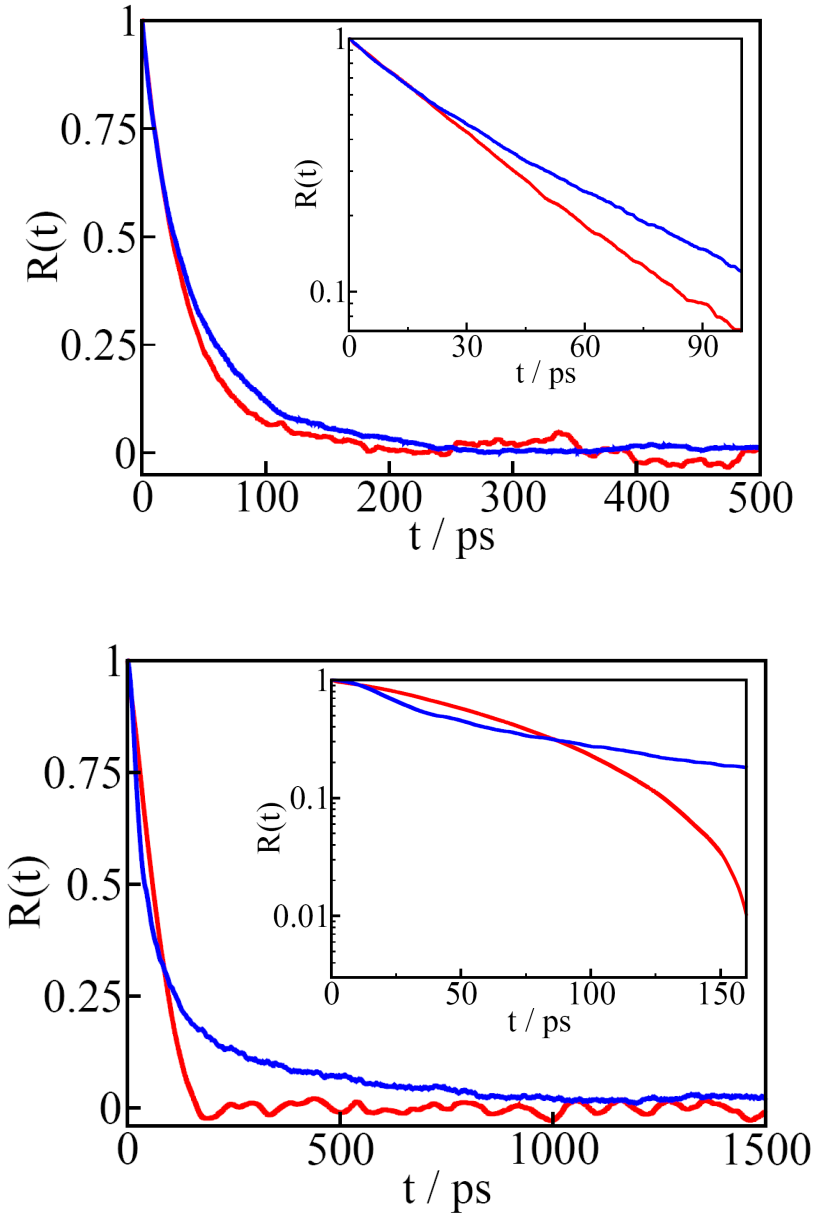

Figure 4.5. Time correlation functions, R(t), of the height of the center of mass for smooth (top) and corrugated surfaces (bottom). Insets are time correlation functions in logarithmic scale.

Scaling with the system size. In order to study scaling of relaxation time with the system size first we modelled droplets containing 500, 1000, 2000, 4000 and 8000 molecules of SPC/E water on a molecularly smooth substrate and 1000, 2000 and 4000 molecules on corrugated surface. We completed time correlation functions calculations for these different system sizes of the droplet to see how the relaxation times scale with system

size. Table 4.2 shows the results for characteristic time scaling of C(t) and R(t) on smooth surfaces. Results show that reverse process (switching from hydrophilic to hydrophobic) is always faster than forward process (switching from hydrophobic to hydrophilic) for both smooth and corrugated surfaces. The difference can be rationalized by stronger perimeter pinning on surfaces with comparatively stronger substrate/water attraction. A similar difference has been observed when comparing experimental spreading and retraction times of microscopic ionic-liquid droplets on switchable surfaces, controlled by the application of electric field[68].

Table 4.2. Size dependence of droplet dynamics on smooth surfaces. N is the number of water molecules in the droplet. All numbers with standard deviation are relaxation times in ps that are calculated using R(t).

N (smooth)	Forward $\tau_{C(t)}$ /ps	Reverse $\tau_{C(t)}$ /ps	Forward $\tau_{R(t)}$ /ps	Reverse $\tau_{R(t)}$ /ps
500	31.4± 2.0	25.3±2.5	25.9±1.1	25.6±1.6
1000	39.0±1.5	30.1±1.5	31.7±0.7	27.5±1.1
2000	52.5±0.5	36.7±1.1	45.2±0.9	38.0±1.8
4000	64.8±1.0	43.4±1.3	55.3±1.0	43.4±1.5
8000	87.6±1.1	58.0±1.4	73.8±1.2	59.2±1.6

The slopes on the log-log plots of characteristic time versus droplet size on smooth surfaces (Figure 4.6) give scaling exponents of 0.38 for forward process (triangles, switching from hydrophobic to hydrophilic) and 0.3 for backward process (circles, switching from hydrophilic to hydrophobic), or ~ 0.34 on average. It means that for smooth surfaces time scale is proportional to $N^{0.34}$. This value is consistent with a simple analytic estimate obtained as follows.

The driving force for spreading the droplet is related to the surface tensions of the liquid times the circumference of the droplet (l) which is a circle with radius R_c as follows

$$F_{df} \sim \sum_i \gamma_i \frac{\partial A_i}{\partial r} l \propto 2\pi R_c \qquad (4\text{-}3)$$

The sum comprises solid/liquid, solid/vapour and liquid/vapour terms. For any specified contact angle, the volume of the drop, is proportional to $R_c^{\,3}$. Therefore $R_c \propto N^{1/3}$.

From dynamics we know that the distance traveled by a particle in one direction is proportional to the acceleration and time squared. So in the case of water droplet, from Newton second law we can replace the driving force with $F \propto R_c \propto N^{1/3}$ and also mass, $m \propto N$, then acceleration is proportional to $N^{-2/3}$. $a = F/m = N^{1/3}/N \rightarrow a = N^{-2/3}$. As a result from Newton second law, time will be proportional to $N^{1/3}$ that is $s \approx a t^2/2 \rightarrow t \propto 1/\sqrt{a}$ therefore $t \propto 1/\sqrt{N^{-2/3}} \Rightarrow t \propto N^{1/3}$ which agrees with our results for the scaling of relaxation time with droplet size on smooth surfaces, considering computational error.

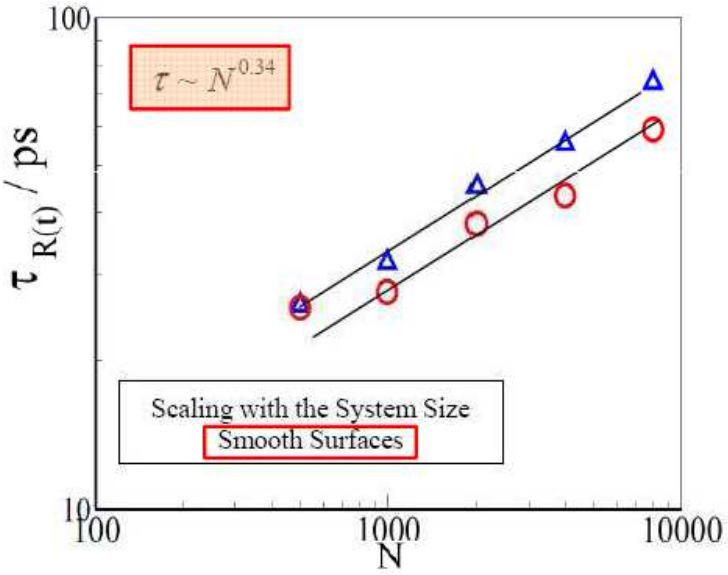

Figure 4.6. Scaling with the system size for smooth surfaces. Y-axis is relaxation time from R(t) and x-axis is number of water molecules in the droplet both in logarithmic scale. Error bars are within the symbol sizes.

For molecularly smooth surfaces, the initial relaxation rates reveal insignificant contact angle hysteresis. This means that response rates upon imposition and cessation of hydrophilicity are very similar. The scaling results suggest linear behaviour on log-log plot (Figure 4.6).

For corrugated surface however, this is not the case. During drop relaxation following the transition from hydrophobic to hydrophilic (forward process) the drop has to overcome high friction because of strong pinning on the posts. The posts and surface

are both hydrophilic and because of the presence of the posts and droplet's pinning to them there is a higher barrier to pass; therefore it will take longer for the droplet to relax to a new equilibrium state. However, for relaxation following the transition from hydrophilic to hydrophobic (reverse process) the situation is quite different. Here, the surface and posts are hydrophobic helping water to recede from the wells between the corrugations, as it approaches the new equilibrium state. In fact the posts do not pin the drop significantly in this case. The friction is therefore much weaker and it takes less time for the droplet to relax. Table 4.3 shows the results of time scales on corrugated surface. In the case of corrugated surfaces, when switching from hydrophilic to hydrophobic state, the transition is more or less exponential, however, when switching from hydrophobic to hydrophilic state, the relaxation is non exponential because of pinning as explained above. Therefore, advancing and receding processes have different frictions: the high friction regime corresponds to forward process (switching from hydrophobic to hydrophilic), because the relaxation process takes place on the surface which is already hydrophilic, with strong pinning to the posts, and low friction regime corresponds to the reverse process (switching from hydrophilic to hydrophobic), i. e. posts do not pin or pin less. We can relate the friction to the combined effect of all barriers that the droplet should pass to reach the new equilibrium state.

Table 4.3. Size dependence of relaxation times for corrugated surfaces. N is the number of water molecules in the droplet. All numbers with standard deviation are relaxation times in ps.

N/corrugated	Forward $\tau_{R(t)}$ / ps	Reverse $\tau_{R(t)}$ / ps
1000	111 ± 13	60 ± 5
2000	150 ± 14	64 ± 3
4000	165 ± 5	68 ± 4

The slope of scaling results for corrugated surface (Figure 4.7) is 0.58 ± 0.1 for forward process (switching from hydrophobic to hydrophilic) and 0.28 ± 0.05 for reverse process (switching from hydrophilic to hydrophobic). These results suggest that for corrugated surfaces time scales are different for the two different processes, with scaling exponent in the range 1/2 – 2/3 for advancing, and 1/4 – 1/3 for retraction. The underlying physical relations behind these exponent values remain to be explained.

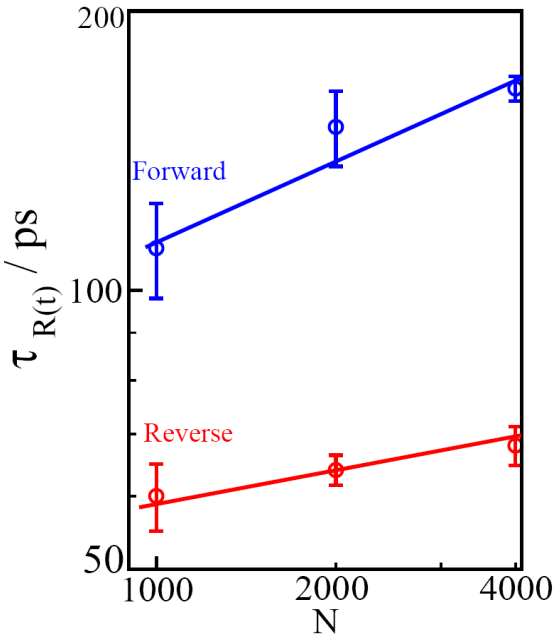

Figure 4.7. Scaling with the system size for corrugated surfaces. Y-axis is relaxation time calculated using R(t) and X-axis is number of water molecules in the droplet both in logarithmic scale.

Interfacial hydrogen bonds. Geometric definition has been used to calculate hydrogen bonds. One of the waters participating in the bond must be within σ_{CO} (3.19 Å) of one of the surface (carbon-like) atoms for calculation of interfacial bonds. We used equilibrated systems considering snapshots from 1 to 5ns trajectories obtained by simulation to calculate the number of interfacial hydrogen bonds in solid-liquid interface for smooth and corrugated surfaces. Table 4.4 contains the results of hydrogen bonds calculation of bulk and solid-liquid interface for smooth and corrugated surfaces.

Table 4.4. Number of hydrogen bonds calculated for smooth and corrugated surfaces for bulk and liquid-solid (l-s) interfaces.

N = 2000 H_2O	Smooth surface	Corrugated surface
Hydrophilic	2.49 l-s (5 Å)	3.03 l-s (15 Å)
	3.35 bulk	3.31 bulk
hydrophobic	2.15 l-s	1.88 l-s
	3.49 bulk	3.37 bulk

***Contact angle calculation*.** Contact angle of water droplet with 2000 water molecules on hydrophilic corrugated surfaces has been calculated using the method described in chapter 2. We measured contact angles for three different reference levels (which are the bottom layer, 3.19 Å, middle layer, 6.54 Å, and top layer of structured surfaces, 9.89 Å). We calculate contact angles on these hydrophilic corrugated surfaces and we found that the angle changed from ~29° on smooth surface to ~79° on our corrugated surfaces. That means corrugation will increase the contact angle and the change depends on the height and density of the posts on the surface. Our results show that for this special structured (corrugated) surface with coverage 1/16, contact angle has been increased by ~50 degrees. Table 4.5 contains the results from contact angle measurements and Figure 4.8 shows a typical drop profile and spherical fitting to that for contact angle measurement.

Table 4.5. Contact angle calculated for droplet on a corrugated surface with three reference levels (bottom layer, middle layer, and top layer of structured surfaces).

Reference level	0+3.19 = 3.19 Å	3.348+3.19 = 6.538 Å	6.696+3.19 = 9.886 Å
$\overline{\theta}_C^{\circ}$	92 ± 3	85 ± 3	79 ± 3

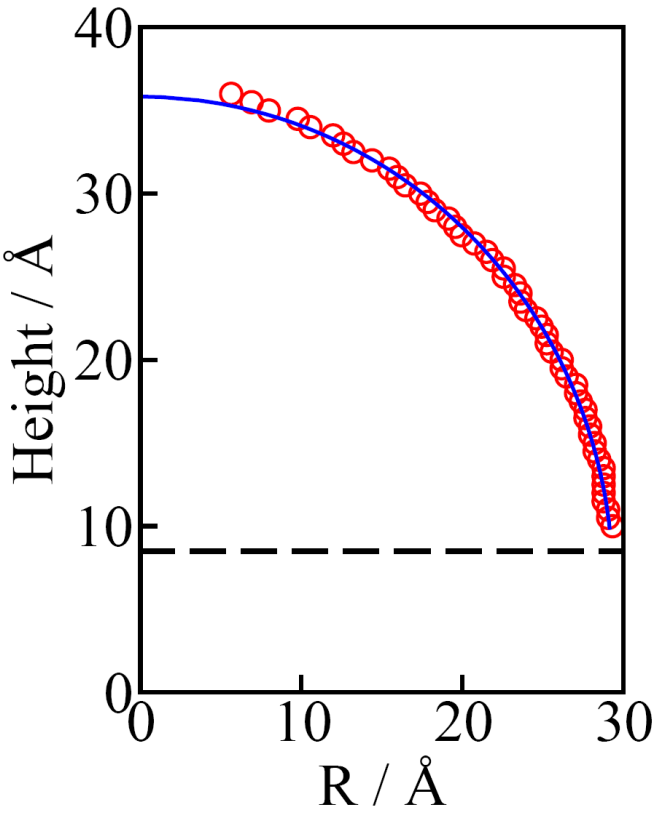

Figure 4.8. Typical drop profiles for 2000 water molecule on a corrugated surface, for the hydrophilic case. Blue solid line is fitted to the simulated data. Dashed line represents the surface, where the contact angles were measured. R (x-axis) is the distance from the main axis of the drop and height (y-axis) is the height of the droplet.

We did not take into account the points of the equimolar surface below the height of 10 Å (the height of the upper layer of atoms in structured surfaces) to avoid the influence from density fluctuations at the liquid-solid interface. Contact angle is the angle between the substrate surface and the circular best fit of the drop's profile along the equimolar dividing surface, measured at the carbon-oxygen equilibrium distance of 3.19 Å for droplets on smooth surfaces (the same convention was used in studies of chemical heterogeneity: Master thesis by John Ritchie VCU 2010[58]). In the case of structured surfaces (also topological heterogeneity, chapter 3), however, the contact angle was measured at the height of 9.89 Å corresponding to the height of the pillars.

Influence of Nanoroughness on the Contact line motion. Roughness influences the wetting properties of solid surfaces. The dependence of wetting behavior on roughness is of great relevance in many practical applications. Topological features, both on the nanometer and micrometer scales affect the equilibrium wettability of a substrate, as well as the static contact angle hysteresis and pinning forces acting on the three phase contact line. For both smooth and nanorough surfaces, contact line motion is governed by two distinct regimes: one based on hydrodynamic dissipation which dominates at small water contact angles, and the other can be described well by the molecular kinetic theory and describes contact line motion at large contact angles[69].

Background. ***Macroscopic Predictions***. When a liquid droplet touches a solid surface it will spread spontaneously to achieve the equilibrium contact angle, i.e. the state of minimum free energy. The surface tension force[70], $\gamma_{SV} - \gamma_{SL} - \gamma_{LV} \cos\theta$ (θ is the dynamic contact angle that was introduced in chapter 1), and which drives the contact line while friction resists the spreading of the liquid, Figure 4.9. Resistance can be due to viscous friction in the bulk liquid and/or molecular friction at the contact line. Previous works[73,74,71] identified two different dissipation regimes on a macroscopic scale: viscous dissipation within the bulk liquid (hydrodynamic models) and molecular dissipation near the three-phase contact line (molecular-kinetic theory, MKT). Hydrodynamic dissipation dominates for small water contact angles, while the molecular kinetic theory describes the contact line motion at large contact angles. The hydrodynamic description assumes viscous shear within the liquid wedge to be the predominant dissipation mechanism during the contact line motion. On the other hand, nonhydrodynamic friction at the contact line is considered in the molecular kinetic theory. Based on Eyring's activation rate theory, local displacements occur at the contact line due to the thermal energy $k_B T$, where k_B is the Boltzmann constant, and T is the absolute temperature. Both kinds of dissipation can exist simultaneously or one can dominate[72].

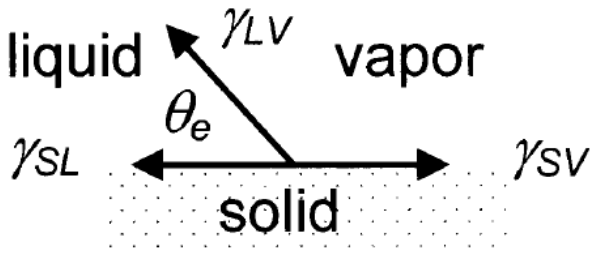

Figure 4.9. Schematic of force balance for equilibrium contact angle on smooth, chemically homogeneous surface.

A relationship between the contact line velocity (V) and dynamic contact angle (instantaneous), θ, is given by Cox[73]

$$g(\theta) = g(\theta_0) \pm \frac{\eta V}{\gamma_{LV}} \ln\left(\frac{L}{L_s}\right) \tag{4-4}$$

where the plus sign holds for advancing liquid fronts and the minus sign for receding ones. θ_0 is the static (equilibrium) contact angle, γ_{LV} denotes the liquid–vapor surface tension, L characterizes a typical macroscopic length scale (e.g., the droplet size), and L_S denotes a microscopic slip length, which is expected to be of the order of the molecular size. In this model, viscous friction dominates and the viscous force F_V is given by

$$F_V = \mu V = \frac{3\eta}{\theta} \ln\left(\frac{L}{L_s}\right) V \tag{4-5}$$

where $\mu = 3\eta \ ln(L/L_S)/\theta$ is the friction coefficient in the bulk. For a liquid–vapor system, if $\theta < 150^\circ$, then $g(\theta) \approx \theta^3/9$ (with a 1% accuracy) and the Voinov equation is obtained[74]

$$\theta^3 = \theta_0^{\,3} \pm \frac{9\eta V}{\gamma_{LV}} \ln\left(\frac{L}{L_s}\right) \tag{4-6}$$

The free parameters in equation (4-6) are the static contact angle, θ_0, and the logarithmic ratio of the two relevant length scales, $ln(L/L_S)$.

In the molecular-kinetic theory, MKT, thermally activated liquid displacements control the contact line motion and the energy dissipation is dominated by non-hydrodynamic effects. According to this model, the contact line moves through

individual molecular jumps, with an equilibrium frequency k_0 and a displacement distance λ. The relation between dynamic contact angle and velocity is given by

$$V = 2k_0\lambda \sinh\left[\frac{\gamma_{LV}\lambda^2}{2k_BT}(\cos\theta_0 - \cos\theta)\right] \tag{4-7}$$

If the argument of sinh is small, equation (4-7) reduces to

$$V = \frac{k_0\lambda^3}{k_BT}\gamma_{LV}(\cos\theta_0 - \cos\theta) \tag{4-8}$$

Equation (4-8) can be rewritten as $F_W = \zeta V$, where F_W is the driving force and $\zeta = k_BT/k_0\lambda^3$ is the friction coefficient at the contact line. It has the physical dimension of a shear viscosity, determines the dissipation rate within the three phase contact line and can be compared with the bulk viscosity of the liquid.

For contact angles approaching 180° the argument of sinh will typically be greater than one, so equation (4-7) will reduce to a single exponential form. The maximum wetting speed will be[75]

$$V_{180} = k_0\lambda \exp\left[\frac{\gamma_{LV}\lambda^2(\cos\theta_0 + 1)}{2k_BT}\right] \tag{4-9}$$

k_0 can be related to the bulk liquid viscosity η and the activation free energy of wetting per molecule arising from solid–liquid interactions, ΔG_S^*, as

$$k_0 = \frac{h}{\eta v_L}k_S = \frac{k_BT}{\eta v_L}\exp\left(-\frac{\Delta G_S^*}{k_BT}\right) \tag{4-10}$$

where v_L is the unit volume and h is Planck's constant. The frequency k_0 is influenced by both the interactions at the surface and the viscous interactions with neighboring molecules, whereas k_S is considered to be affected only by surface forces. v_L is anticipated to correspond to the molecular volume for simple liquids. If the specific activation free energy of wetting per unit area $\Delta g_S^* = \Delta G_S^*/\lambda^2$ is taken to be equal to the work of adhesion (W_a) between the liquid and the solid,

$$\frac{\varsigma}{\eta} = \frac{v_L}{\lambda^3}\exp\left(\frac{\lambda^2\gamma_{LV}(1+\cos\theta_0)}{k_BT}\right) \tag{4-11}$$

The last equation predicts that contact-line friction increases linearly with liquid viscosity but exponentially with work of adhesion. Experimental study of dynamic wetting on surfaces of widely varying wettability with a single liquid provides strong evidence in support of this equation[17].

Energy dissipation can of course occur both in the bulk and near the moving three-phase contact line. Petrov and Petrov[76] proposed a combined molecular-hydrodynamic approach, assuming that both the viscous friction in the intermediate region of the meniscus and the nonhydrodynamic friction in the vicinity of the three-phase contact line play a role in determining the dynamic contact angle. In order to accommodate both kinds of dissipation, Brochard-Wyart and de Gennes divided the total energy dissipation (P) into a hydrodynamic term (P_{HD}) and a molecular-kinetic term (P_{MK}):

$$P = P_{HD} + P_{MK} = (F_V + F_W)V = (\mu + \varsigma)V^2 \qquad (4\text{-}12)$$

The friction coefficients for the hydrodynamic (μ) and molecular (ζ) terms can be obtained from the experimental data of dynamics contact angle as a function of perimeter velocity[72].

Nanoscale Dynamics. Using our simulation results of 2000 water molecule drop we calculate dynamic contact angle and velocity of drop perimeter's radius and we obtain dynamics contact angle (θ) versus velocity of drop perimeter (Figure 4.10), $cos(\theta)$ versus velocity of drop perimeter (Figure 4.11), and θ^3 versus velocity of drop perimeter (Figure 4.12). To get these values first we need to calculate velocity of the drop perimeter, dr_d/dt, that can be calculated in two steps with partial derivatives

$$\frac{dr_d}{dt} = \frac{dr_d}{dh_{com}} \cdot \frac{dh_{com}}{dt} \qquad (4\text{-}13)$$

To get $\frac{dr_d}{dh_{com}}$ and dynamic contact angle, θ, we wrote a program (Appendix III) using equations (3-5) and (3-6), which considers a hemi-spherical drop. $\frac{dh_{com}}{dt}$ can be obtained directly from simulation results. By multiplying these two values at similar h_{com} (height of the center of mass), we can estimate the velocity of the drop perimeter. Based on

comparisons in Figure 3.6, the accuracy of the droplet contact angle and perimeter radius, calculated from the height of the center of mass will be better at higher contact angles.

We calculate the static contact angle of the drop on hydrophilic surface in Wenzel state (Table 4.5), as explained in chapter 2. However, the static contact angle of the drop on a hydrophobic surface and intermediate states in Cassie state could not be determined accurately because of droplet bouncing on the surface due to its thermal motion. Instead, dynamic contact angles were estimated from the height of the drop's center of mass (Appendix III). The procedure also requires precise knowledge of the height of the droplet bottom plane. This plane is easily determined for the Cassie state where it coincides with the pillar height, but cannot be defined precisely for the Wenzel state and intermediate Cassie-to-Wenzel states, when water droplet is entering between the pillars. The final contact angle estimated from the center of mass (Figure 4.10) is about 40°, well below the equilibrium value of 79° (Table 4.5). Given the drop geometry is known accurately only at high contact angles, we use only the initial portion of our data (Figures 4.10-4.12), corresponding to high contact angle, for our calculations.

We considered simulation results of 2000 water droplet on a corrugated surface initially equilibrated in the Cassie, as it relaxes to the Wenzel state. Using our data along with hydrodynamics theory (equation 4-6) and MKT (equation 4-7) we obtain fitting parameters $Ln(L/L_s)$, k_0 and λ and corresponding friction coefficients: ζ, the friction coefficient at the contact line, and μ, the friction coefficient in the bulk, following the methods presented by Ralston[72]. To do so we need surface tension and viscosity for SPC/E water at 300K. These values have been calculated[77,78] at 63.6 ± 1.5 mJ/m^2 and 0.82 ± 0.09 mPa s. Experimental values are respectively 71.6 mJ/m^2 and 0.85 mPa s.

We use the equilibrium value of 79°, however, at high initial dynamic contact angles, the difference θ^3-θ_0^3 is not very sensitive to θ_0 and even the use of the approximate final contact angle, θ_0, from the center-of-mass calculation gives very similar results.

Using equation (4-6), hydrodynamic theory, with drop geometry data calculated from the initial time evolution of the position of center of mass, and SPC/E values for surface tension and viscosity we estimate the "bulk" friction coefficient, $\mu \sim 0.002$ (1 ± 25%) kg/sm. We obtain very similar value (0.0025 kg/sm) using

equation 4-7, MKT theory, for "contact line" friction coefficient, ζ. This seems to be understandable in the case of nanoscale drop where it is difficult to define a clear boundary between hydrodynamics and MKT, and there is likely an overlap between the two regimes.

Based on our results slip length L_s varies around 1/6 drop size L in the more reliable large contact angle part of the plots (Figure 4.13) and k_0 and λ are 0.94×10^{10} /s, and 5.6 Å.

Our results for a nanosized water drop (Figures 4.9 - 4.11) agree qualitatively with results of J. Ralston[72] for a macroscopic ionic drop (See Appendix IV). However, the microscopic drop has much higher velocity of perimeter's radius, about two orders of magnitude difference, due to weaker friction. This indicates that our microscopic roughnesses are much smaller than the roughness on a macroscopically smooth surface used in their experiment.

The product of k_0 and λ^2 gives an estimate of the diffusion coefficient, using fitting parameters above it gives 2.95×10^{-9} m^2/s.

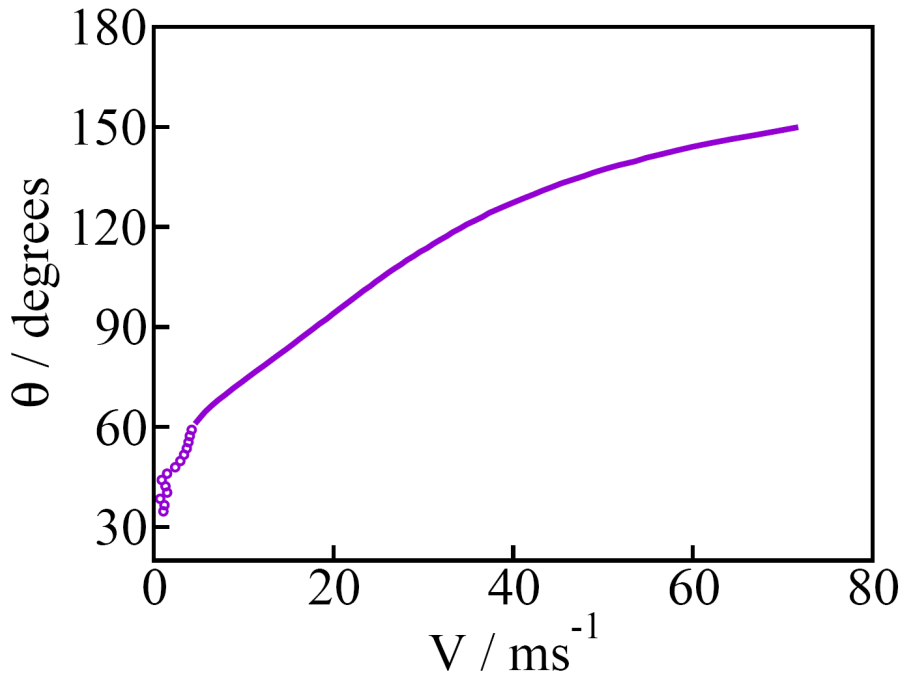

Figure 4.10. Dynamic contact angle (θ) versus velocity of the drop perimeter that has been calculated from the height of the center of mass (Appendix III).

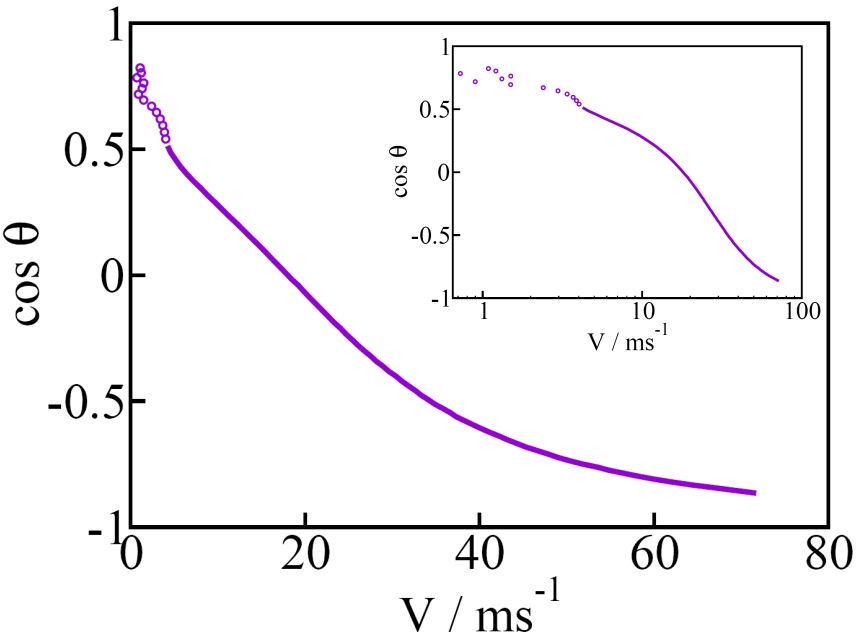

Figure 4.11. Cosine of dynamic contact angle, cos(θ), versus velocity of the drop perimeter. Inset is cos(θ), versus velocity of the drop perimeter in logarithmic scale.

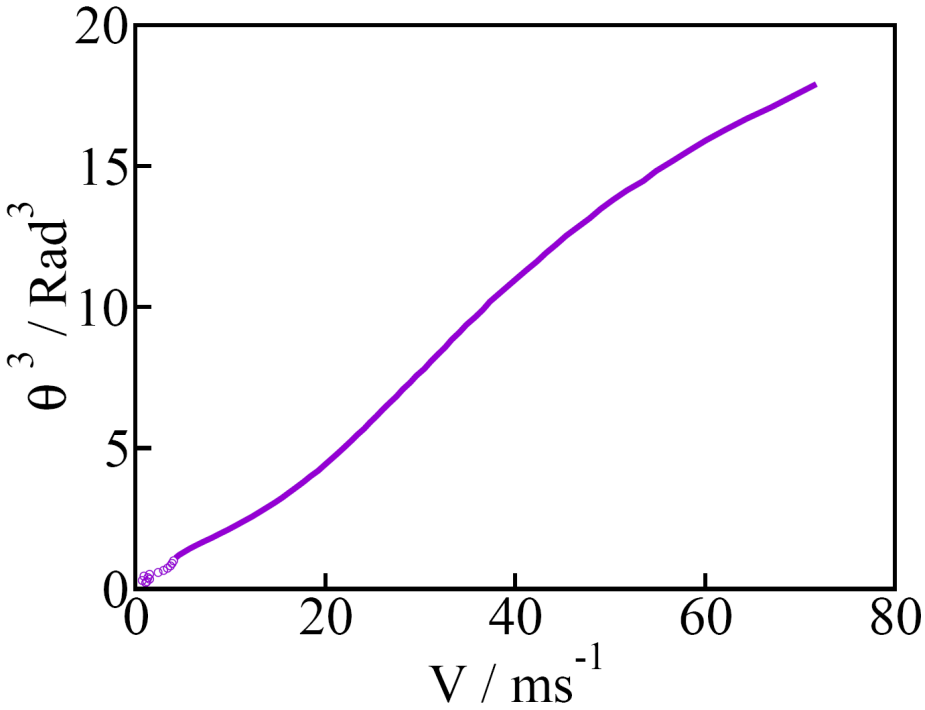

Figure 4.12. Dynamic contact angle cubed, θ^3, versus velocity of the drop perimeter.

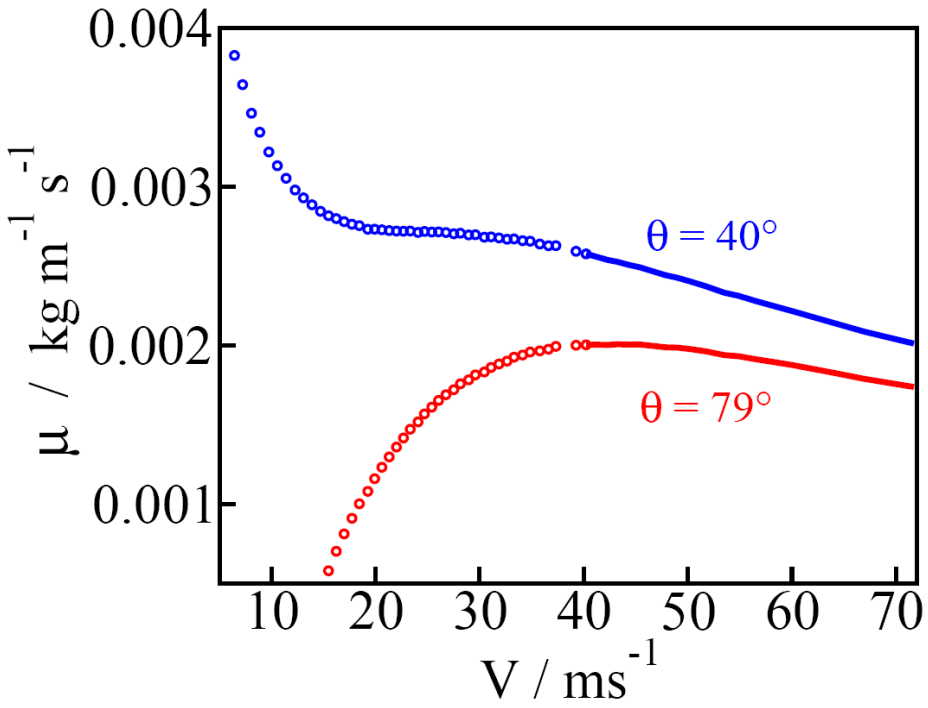

Figure 4.13. Nanodroplet friction coefficient μ (Eq. 4.6) on corrugated substrate, shown as a function of perimeter velocity V at early stages of droplet relaxation following a change from hydrophobic to hydrophilic character of the surface. The red line relies on the direct measurement of the equilibrium contact angle (79°). The blue line utilizes the estimate from the drop's equilibrium position of the center of mass. Note the center of mass data, including the final value, become increasingly inaccurate as the drop enters the Wenzel regime (left portion of the graph).

Discussion. Monitoring the height of the center of mass of the droplet gives a good representation of the relaxation process. Figures. 4.4a-4.4b show changing of the height of the center of mass versus time during the equilibration process for smooth and structured (corrugated) surface for the case of 2000 water droplet. Results for smooth surface show symmetry for evolution of height of the center of mass between hydrophilic and hydrophobic systems, however, results for structured (corrugated) surface show asymmetry. Based on the evolution of the height of the center of mass we calculate time correlation functions C(t) and R(t) from equations (4-1) and (4-2). Figures 4.5a-4.5b shows R(t) for smooth and structured (corrugated) surface, all for the case of 2000 water droplet. Following the symmetry of evolution of the height of the center of mass for water droplet on smooth surface, we see similar relaxation in both, R(t) and C(t). These graphs on a semi-logarithmic scale are almost linear indicating an exponential decay. At the very beginning of the process, at least up to 20 ps, there is complete overlap between

time correlation functions of forward and backward processes. That means that in the case of smooth surfaces studied here, contact angle hysteresis is negligible. In the case of corrugated surfaces, the asymmetry of evolution of the height of the center of mass for two systems is manifested by different behaviors of time correlation functions. This dis-similarity is more obvious in semi-logarithmic scale. It shows that the backward process (going from hydrophilic to hydrophobic) is faster and is completed much sooner than the forward process. These observations can be explained by pinning/depinning mechanisms. When the droplet is equilibrated on a hydrophobic surface and suddenly feels hydrophilic interaction (by switching the surface) it will undergo spreading that involves many pinning/depinning events between individual water molecules and posts until it reaches the equilibrium shape. However in the case of reverse process, when the droplet is equilibrated on a hydrophilic surface, suddenly reversed to hydrophobic interaction (by another switching), contraction involves only depinning between water molecules and posts and therefore proceeds much faster.

Figure (4.14) indicates the occurrence of pinning (i.e. forming a water/substrate bond in the wells) as follows: the drop is confined between pillars and acquires a squarer shape due to pinning to the edge pillars. It seems that the ratio of number of times that pinning is taking place to the number of times that depinning is taking place can be an indication of how far or close the droplet is to the equilibration. That means before equilibration the number of times that pinning and deppining are taking place are almost the same but when the drop reach to the equilibrium state and perimeter velocity is going toward zero, the number of pinning events is much higher than the number of depinning events.

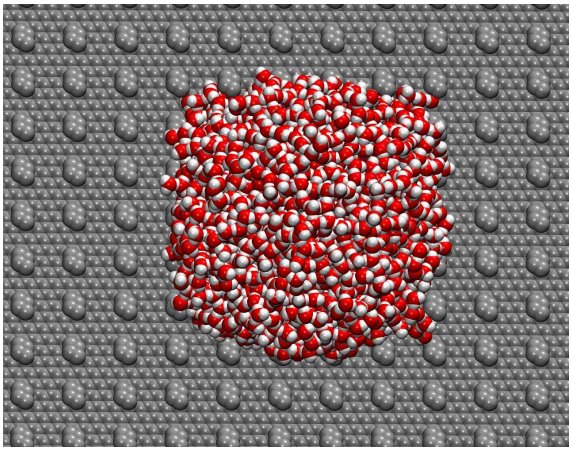

Figure 4.14. Top view of water droplet after 500 ps equilibration time on a corrugated surface. Because of pinning, the drop perimeter looks more like a square than a circle.

Conclusion. There are several conclusions we can get from these observations[79]. First the results clearly show contact angle hysteresis for corrugated surface on a nanoscale between forward and backward processes, which was known only for macroscopic systems before. Second, our studies show the result for scaling of the relaxation time with the system size. For a smooth surface, we found that the relaxation time versus number of molecules, in a logarithmic scale, gives a linear plot for forward and reverse processes with similar slopes. However for corrugated surface we obtained linear fitting for relaxation time versus number of molecules, in a logarithmic scale too, but with different slopes for forward and reverse processes. This difference is an indication of negligible hysteresis and friction for smooth surface, but considerable hysteresis and therefore friction for the case of corrugated surface.

Third, our study is showing there is a friction force in the case of structured surfaces studied here that is applying in different ways in the case of forward and backward processes due to the energy dissipation processes. We calculate the friction coefficient of the 2000 water droplet on a corrugated surface for the case of hydrophilic interaction, droplet going from Cassie to Wenzel state, using hydrodynamic and molecular kinetic theory. Another interesting finding of our calculations for friction coefficient shows that hydrodynamic and molecular kinetic theory can describe our data for this relaxation process very well giving very similar values for friction coefficients at nanoscale. Therefore we conclude that because of nanoscopic scale the boundary between

hydrodynamic and molecular kinetic regimes is not as well defined as it is in the macroscopic world.

Our results also show that although the perimeter of water droplet is a circle in the case of smooth surface, it depends on the pattern of the structured surface it can be far from a circle because of pinning effects for hydrophilic interactions.

Future task that need to be completed:

Use molecular dynamics simulation to compute molecular diffusion within posts and compare its value to diffusion in the nanodrop. While inspecting the trajectories via VMD (Visual Molecular Dynamics, molecular graphics software) we can visually inspect that they differ.

Chapter 5. Water Dynamics inside Nanospheres

It is well realised that water in the confined geometry exhibits modified behaviour in both structural and dynamic properties. Nano-spheres are very well defined confined structures that are ideal for studying the properties of confined liquids as opposed to other disordered porous material that are also used by experimentalists[80,81].

Simulation Systems. In silico samples. Experimental and simulation works[82,38] show that physical properties of water in spherical nano-confinements can be described using buckyball cage geometry (except for the layer directly in contact with the wall). Therefore as a first approximation for nano-sphere confinements, we have used spherical cages of "hollow buckyballs" of four different sizes (sphere radius: 8.37 Å, 10.45 Å, 12.52 Å and 17.52 Å that correspond to C320, C500, C720 and C1500 buckyballs).

Confined Water. To access the correct number of water molecules inside C_x, hollow buckyballs, GCMC (Grand Canonical Monte Carlo) method needs to be performed. Instead we adjusted the number of water molecules inside a buckyball based on available free volume and using 30 $Å^3$ an approximate volume of one water molecule. For the volume of a hollow buckyball we considered the effective volume by subtracting the sigma value (Lennard-Jones distance parameter, σ=3.19 Å) of “carbon” atoms because water molecules cannot get closer to the wall than $\sigma/2$ value and we approximate all these cages as a sphere. Using these assumptions we calculate number of water molecules in each of these samples (i.e. 20 water molecules in C320, 57 water molecules in C500, 100 water molecules in C720 and 500 water molecules in C1500).

We examined effects of different interactions between water and interior wall resembling hydrophilic/hydrophobic scenarios. The strength of water-wall interaction resembles that of hydrocarbon (hydrophobic), or that of glass (hydrophilic). Lennard-Jones parameters for wall-oxygen, to make these different interactions, are presented in (Table 5.1):

Table 5.1. Lennard-Jones parameters used in the simulations.

	$\sigma_{(W\text{-}O)}$ [kJ/mol]	$\varepsilon_{(W\text{-}O)}$ [kJ/mol]
Hydrophobic	3.19 Å	0.18810
Hydrophilic	3.19 Å	0.62700

this σ value of carbons means for example for a cage with 8.37 Å radius only ~5.2 Å is available to water molecules, for a cage with 10.45 Å radius only ~7.3 Å is available and for a cage with 12.52 Å radius only ~9.3 Å is available for water molecules and so on. Figures (5.1a-5.1b, 5.2a-5.2b, 5.3a-5.3b and 5.4a-5.4b) show snapshots for these two different (hydrophilic/hydrophobic) systems for each system size.

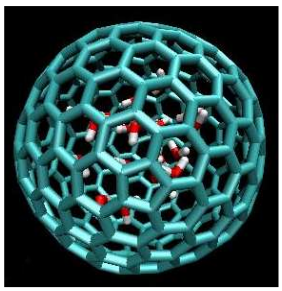

Figure 5.1a. Snapshot for hydrophilic C320 sample.

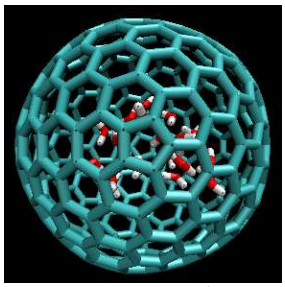

Figure 5.1b. Snapshot for hydrophobic C320 sample.

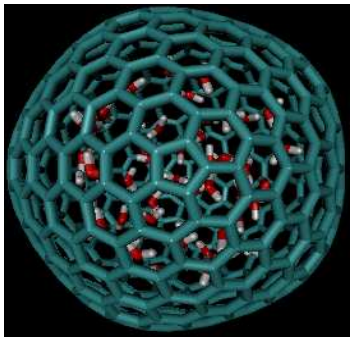

Figure 5.2a. Snapshot of hydrophilic, C500, sample.

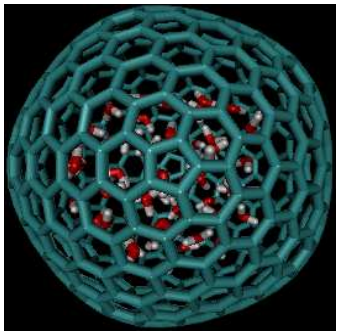

Figure 5.2b. Snapshot of hydrophobic, C500, sample.

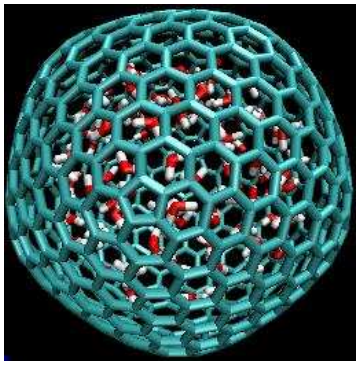

Figure 5.3a. Snapshot of hydrophilic, C720, sample.

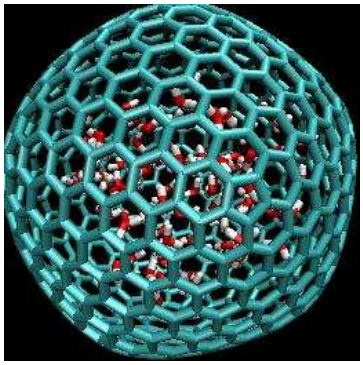

Figure 5.3b. Snapshot of hydrophobic, C720, sample.

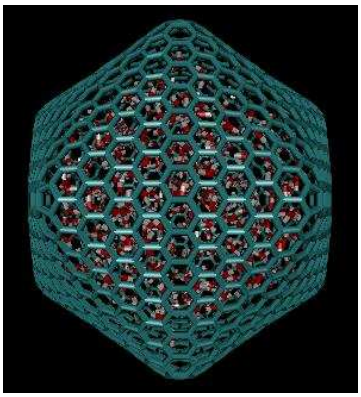

Figure 5.4a. Snapshot of hydrophilic, C1500, sample.

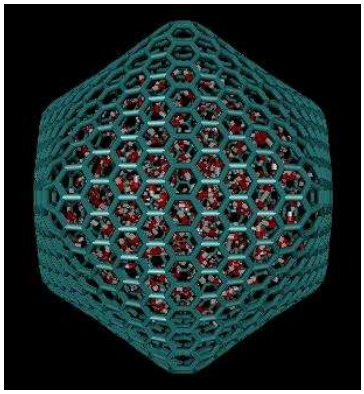

Figure 5.4b. Snapshot of hydrophobic, C1500, sample.

Simulation Details. We used DLPOLY[46] code (version 2.15) to do classical molecular dynamic simulations in the NVT ensemble, using a Nose-Hoover thermostat[83] to maintain a temperature of 300 K. Verlet integrator was used with time step 0.5 fs for all simulations. We have made 10 different systems for each case and total simulation time in most of them (except C1500) is about 65 ns. The Lennard-Jones cut-off values has been chosen to be 19, 25, 28 and 36 Å for C320, C500, C720 and C1500 respectively which are a little bigger than the hollow buckyball's size. The hydrogen bond calculation is based on geometry criteria that is mentioned in chapter 2. Correlation functions have been calculated for up to 1.2 ns to get sufficient statistics. In these systems there is not need to apply periodic boundary conditions. Therefore the system contains only one simulation box that is occupied by an almost spherical confinement with confined water molecules inside and vacuum outside. The volume of the simulation box is equal to

69×69×69 $Å^3$. The technique we used for dealing with long ranged electrostatic potentials is direct Coulomb sum for accurate simulation of isolated (nonperiodic) systems. Both water and confinement have been modelled as rigid molecules. We also performed simulation in NVE ensembles to get the correct dynamics starting from equilibrated configuration. Extra subroutines were added to carry out hydrogen bond dynamics calculations (Appendix V: some subroutines that are adopted from Christopher Daub and modified by us to be applicable for our confined systems).

Correlation Functions. Hydrogen bond correlation function c(t), have been calculated using[84,85]

$$c(t) = \frac{\langle h(0)\, h(t) \rangle}{\langle h \rangle} \tag{5-1}$$

where dynamical variable h(t) equals unity, if the particular tagged pair of molecules is hydrogen bonded, and is zero otherwise. Figures 5.5a, 5.6a, 5.7a and 5.8a, shows c(t) for both hydrophobic/hydrophilic systems with different sizes. The rate of relaxation to equilibrium is characterized by the reactive flux hydrogen bond correlation function[84,85] k(t), (Figures 5.5b , 5.5c , 5.5d ; 5.6b , 5.6c , 5.6d ; 5.7b , 5.7c , 5.7d; 5.8b , 5.8c , 5.8d).

$$k(t) \equiv \frac{-\, d\, c(t)}{dt} = \frac{\langle \dot{h}(0)\, h(t) \rangle}{\langle h \rangle} = -\frac{\langle \dot{h}(0) [1 - h(t)] \rangle}{\langle h \rangle} \tag{5-2}$$

Overdots denote the time derivatives.

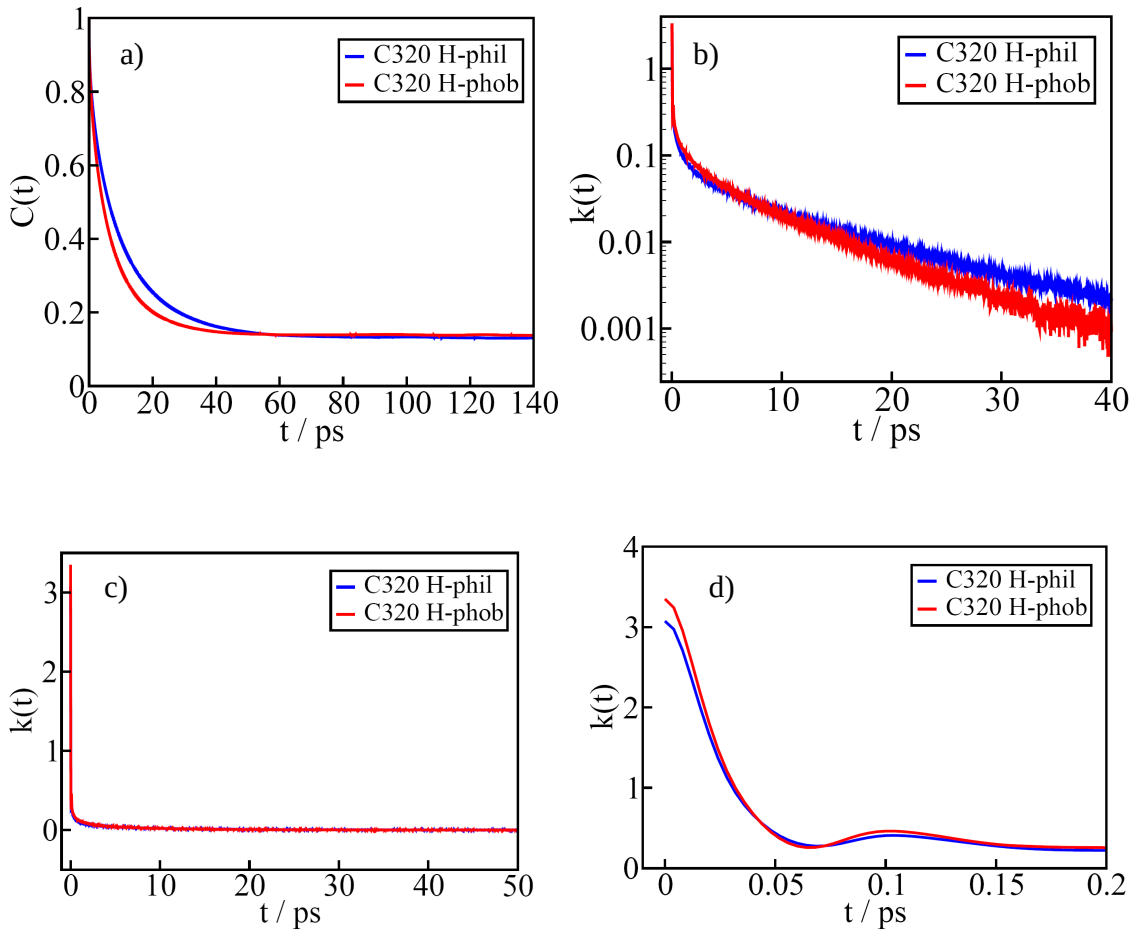

Figure 5.5. C320 samples, hydrophilic (blue) and hydrophobic (red), with 20 water molecules inside. a) Hydrogen bond correlation function, C(t). b) reactive flux hydrogen bond correlation function, k(t) in logarithmic scale. c) k(t) up to 50 ps. d) k(t) up to 0.2 ps, transient time is ~ 0.2 ps.

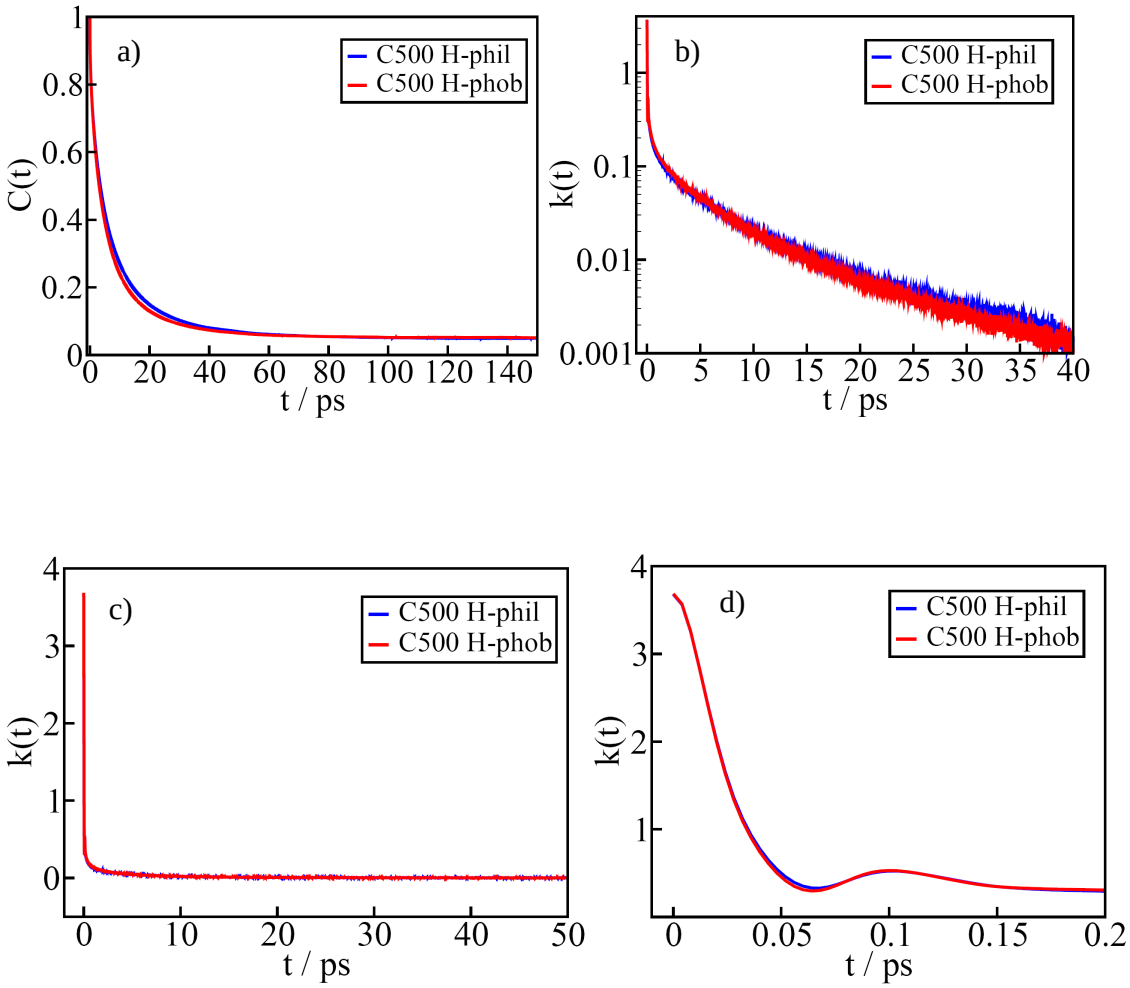

Figure 5.6. C500 samples, hydrophilic (blue) and hydrophobic (red), with 57 water molecules inside. a) Hydrogen bond correlation function, C(t). b) reactive flux hydrogen bond correlation function, k(t) in logarithmic scale. c) k(t) up to 50 ps. d) k(t) up to 0.2 ps, transient time is ~ 0.2 ps.

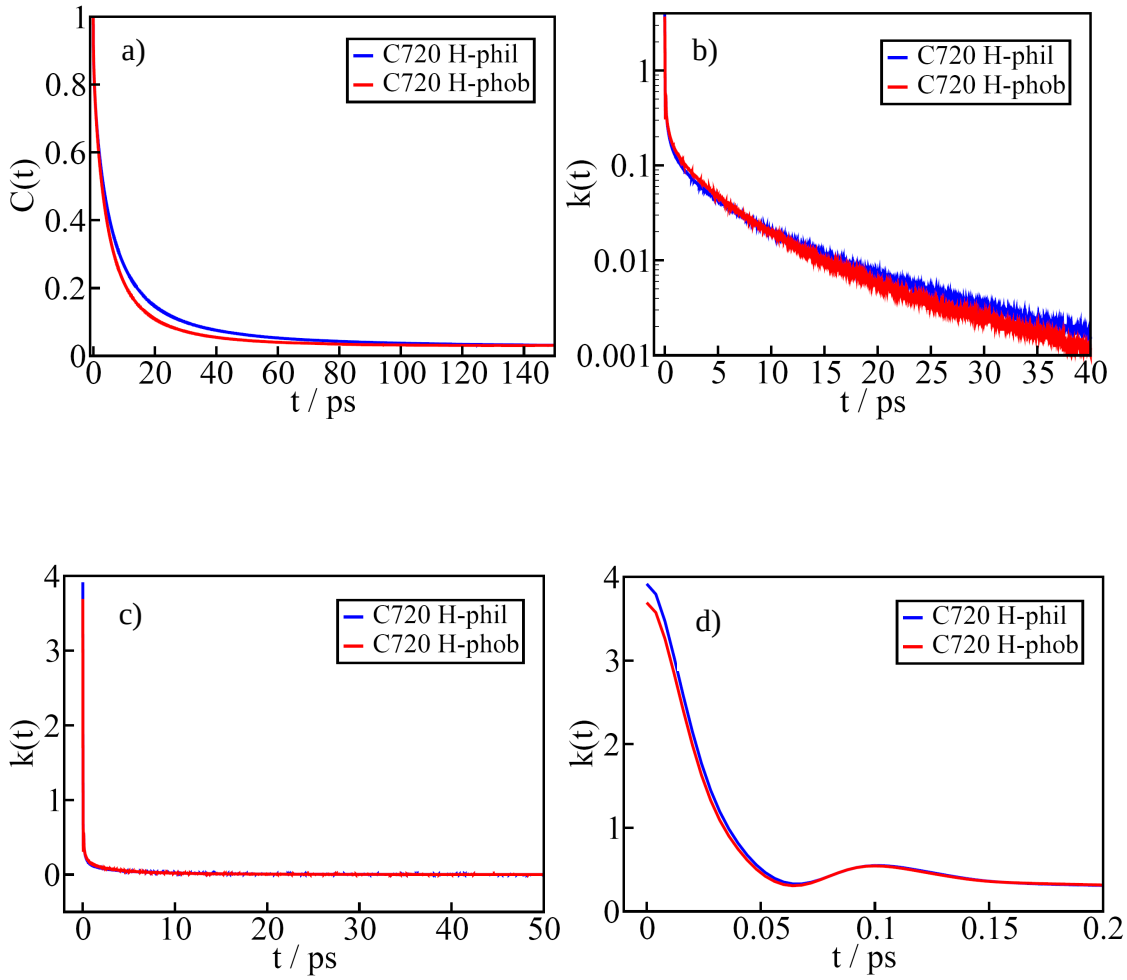

Figure 5.7. C720 samples, hydrophilic (blue) and hydrophobic (red), with 100 water molecules inside. a) Hydrogen bond correlation function, C(t). b) reactive flux hydrogen bond correlation function, k(t) in logarithmic scale. c) k(t) up to 50 ps. d) k(t) up to 0.2 ps, transient time is ~ 0.2 ps.

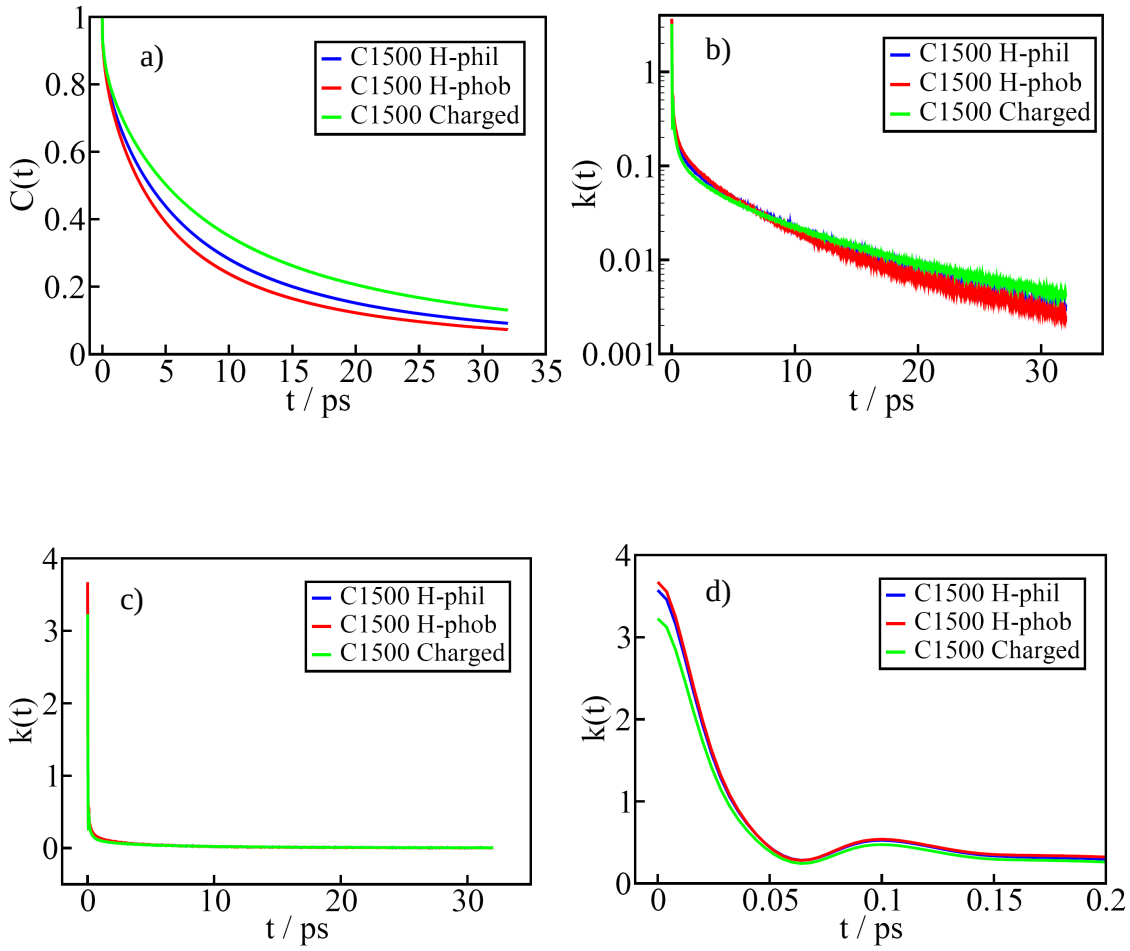

Figure 5.8. C1500 samples, hydrophilic (blue) and hydrophobic (red), and charged sample (green), with 500 water molecules inside. a) hydrogen bond correlation function, C(t). b) reactive flux hydrogen bond correlation function, k(t) in logarithmic scale. c) k(t) up to 50 ps. d) k(t) up to 0.2 ps, transient time is ~ 0.2 ps.

In Table 5.2 we have reported k(t) at starting time which is k_{TST}, transition state theory rate constant. This value depends on hydrogen bond definition[85]. Another value that has been reported in Table 5.2 is initial value of velocity autocorrelation function which is equal to $3k_BT/m$ in which m is molecular mass.

Table 5.2. Initial values of k(t) and VACF (velocity auto correlation functions) for hydrophilic and hydrophobic samples in different. NVT ensemble was used for C320, C500 and C720 but NVE ensemble used for C1500.

	C320	C500	C720	C1500
$k_{t=0}$ (Hphil) / ps^{-1}	3.07	3.67	3.98	3.57
$k_{t=0}$ (Hphob) / ps^{-1}	3.35	3.68	3.69	3.67
$VACF^{Hphil}_{t=0}$ ($Å^2/ps^2$)	269.15	275.00	279.40	267.83
$VACF^{Hphob}_{t=0}$ ($Å^2/ps^2$)	260.25	273.88	249.34	277.42

Function n(t) represents a measure of local strain in the hydrogen bond network (Figures 5.9a-5.9b ; 5.10a-5.10b ; 5.11a-5.11b; 5.12a-5.12b).

$$n(t) = \int_0^t dt' k_{in}(t') \tag{5-3}$$

$$k_{in}(t) = \frac{-\left\langle \dot{h}(0)[1-h(t)]H(t)\right\rangle}{\left\langle h\right\rangle} \tag{5-4}$$

which is the restrictive reactive flux function.

$$H(t) = \begin{cases} 1 \; if \; R_{OO}(t) < R_{OO}^C \\ 0 \; otherwise \end{cases} \tag{5-5}$$

For bulk water, R_{OO}^C is a cut-off value equal to 3.5 Å, in which $R_{OO}(t)$ is the distance between the oxygen atoms of a tagged pair[85]. This value has been estimated from radial distribution function of bulk water. For our simulation this value is adapted from bulk value which is an approximation for our confinements.

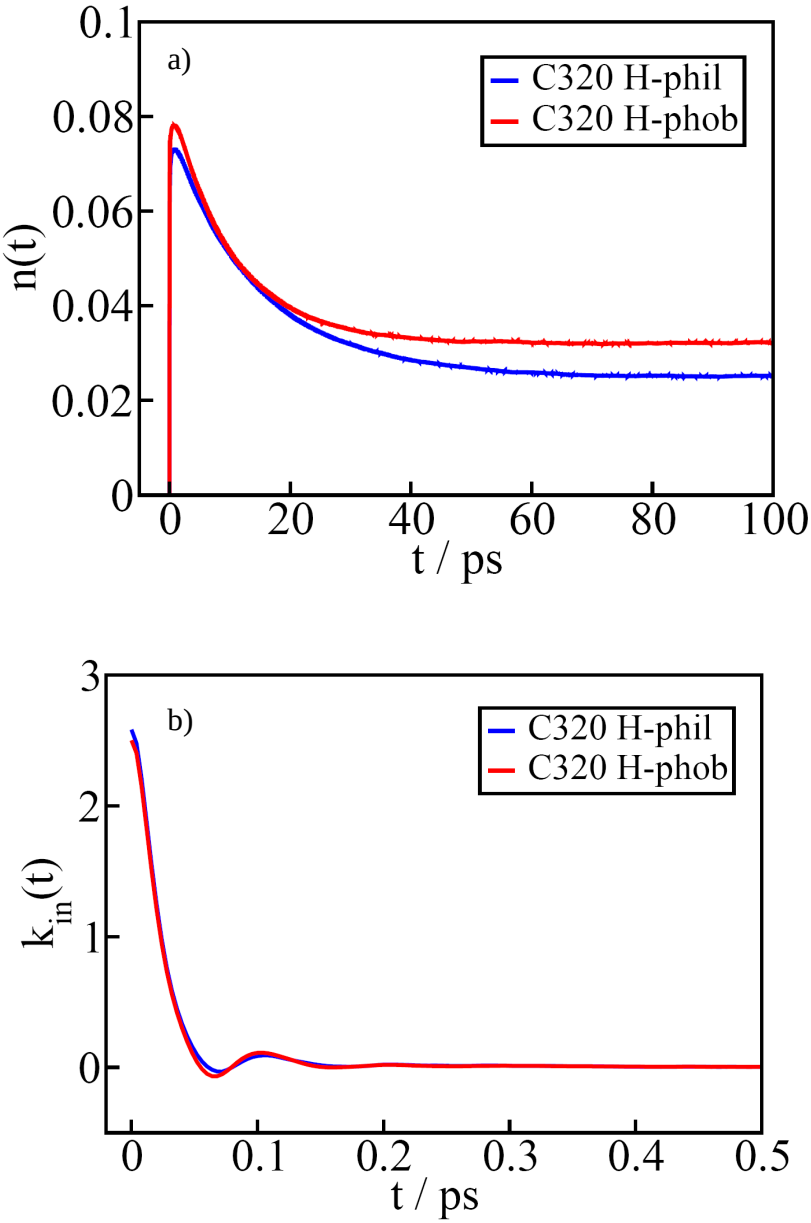

Figure 5.9. C320 sample, hydrophilic (blue) and hydrophobic (red), with 20 water molecules inside. a) function representing local strain in the hydrogen bond network, n(t), b) restrictive reactive flux function, $k_{in}(t)$.

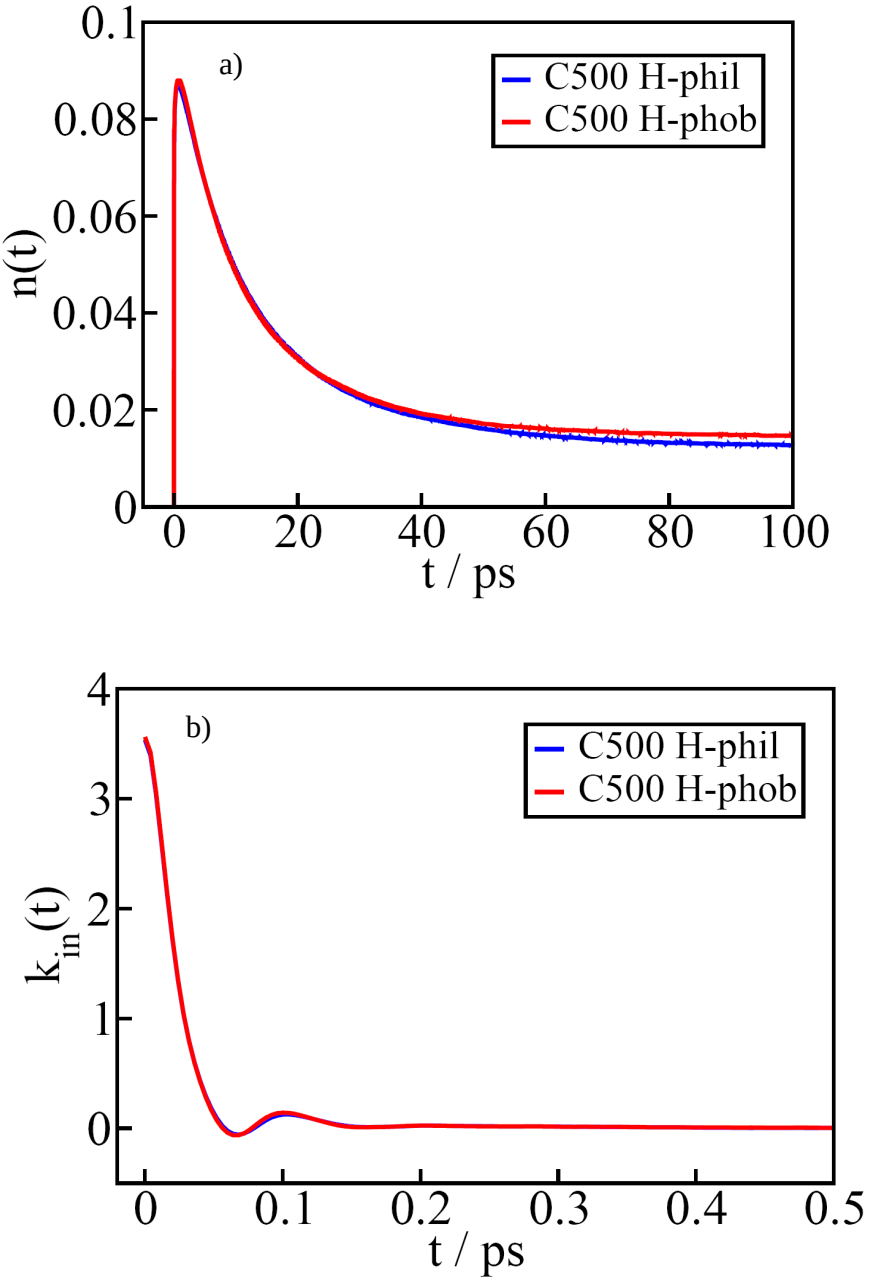

Figure 5.10. C500 sample, hydrophilic (blue) and hydrophobic (red), with 57 water molecules inside. a) function representing local strain in the hydrogen bond network, n(t), b) restrictive reactive flux function, $k_{in}(t)$.

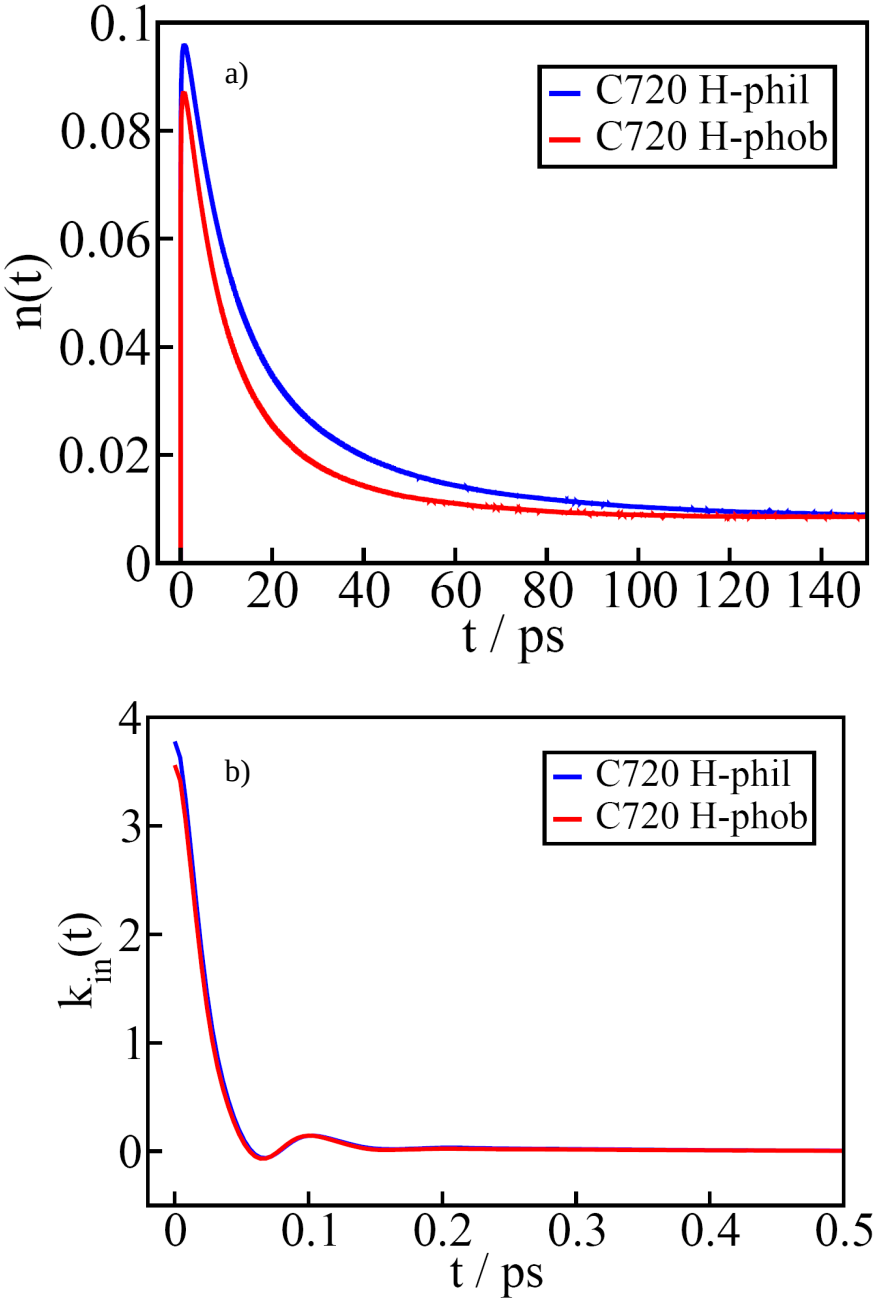

Figure 5.11. C720 sample, hydrophilic (blue) and hydrophobic (red), with 100 water molecules inside. a) function representing local strain in the hydrogen bond network, n(t), b) restrictive reactive flux function, $k_{in}(t)$.

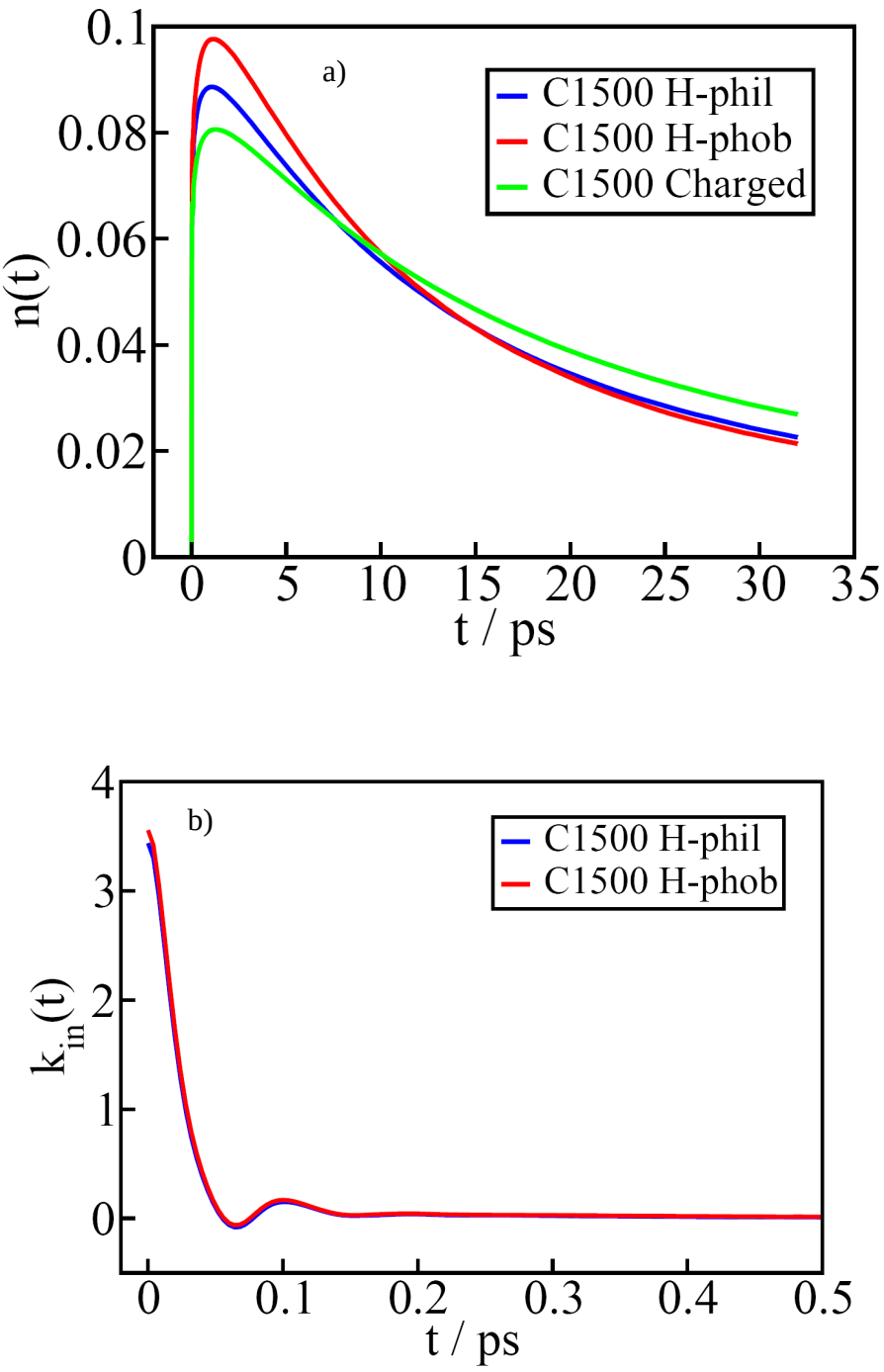

Figure 5.12. C1500 sample, hydrophilic (blue) and hydrophobic (red), and charged sample (green), with 500 water molecules inside. a) function representing local strain in the hydrogen bond network, n(t), b) restrictive reactive flux function, $k_{in}(t)$.

Considering A $\underset{k}{\overset{k'}{\rightleftarrows}}$ B, the reaction kinetics for t > $t_{transient}$ is described by (Figures 5.13a-5.13b ; 5.14a-5.14b ; 5.15a-5.15b; 5.16a-5.16b):

$$k(t) = k\,c(t) - k'\,n(t) \qquad (5\text{-}5)$$

By transient time, we mean librations and inter-oxygen vibrations on a short time scale. From Figures. 5.5d, 5.6d, 5.7d and 5.8d it is clear that transient time is ~ 0.2 ps which is not different from bulk water's transient time.

If one can find a unique values for k and k' that can satisfy equation (5-5), that means the model is working and we have a first order kinetic. To find the best values for k and k' we have two choices. Either we can use a fitting procedure or we can do try and error procedure to find correct values. We used the combination of both methods to find the best k and k' in each system.

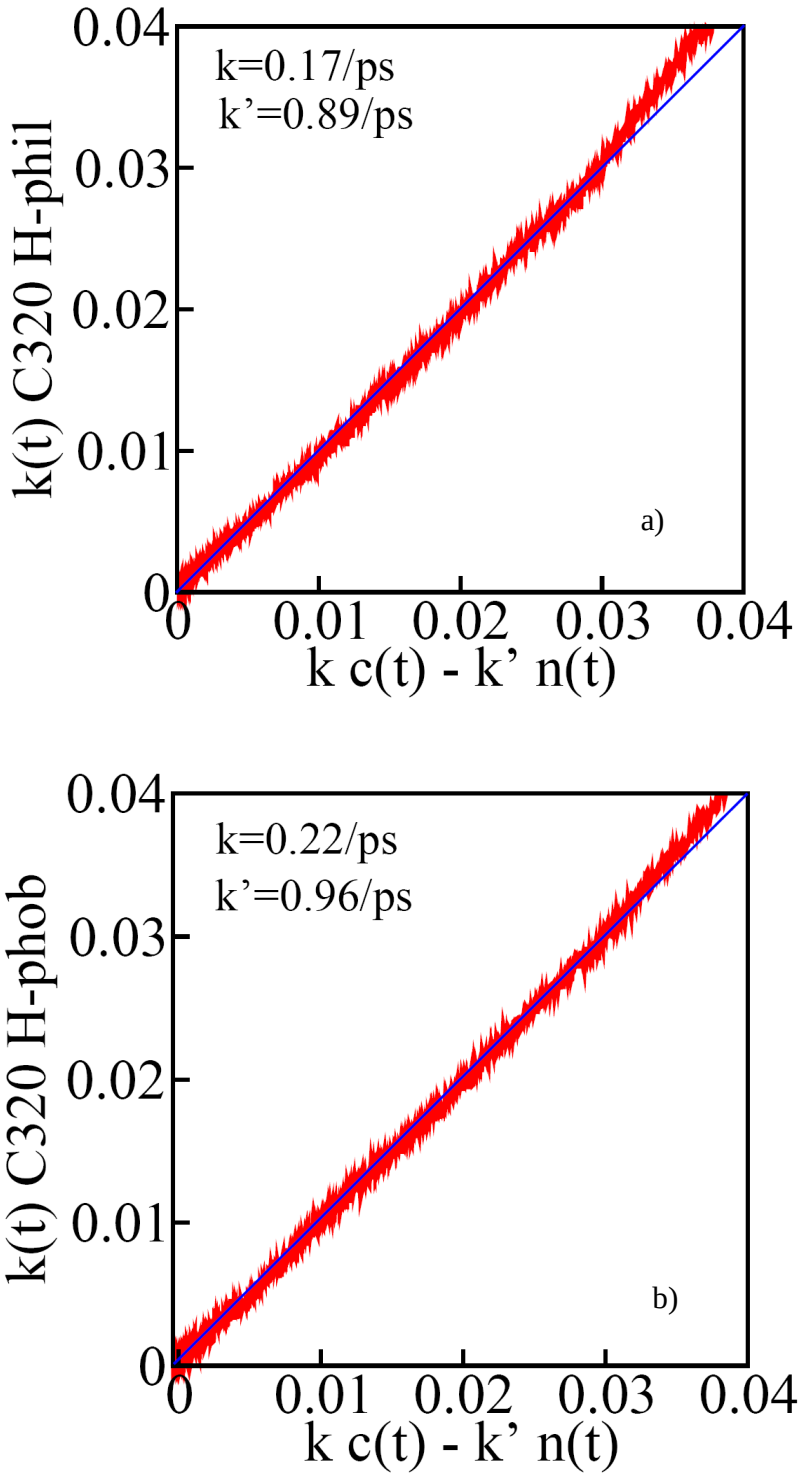

Figure 5.13. Correlation plot for C320 sample, with 20 water molecules inside. a) Hydrophilic, deviation is starting at 6.4 ps. b) Hydrophobic deviation is starting at 5.8 ps.

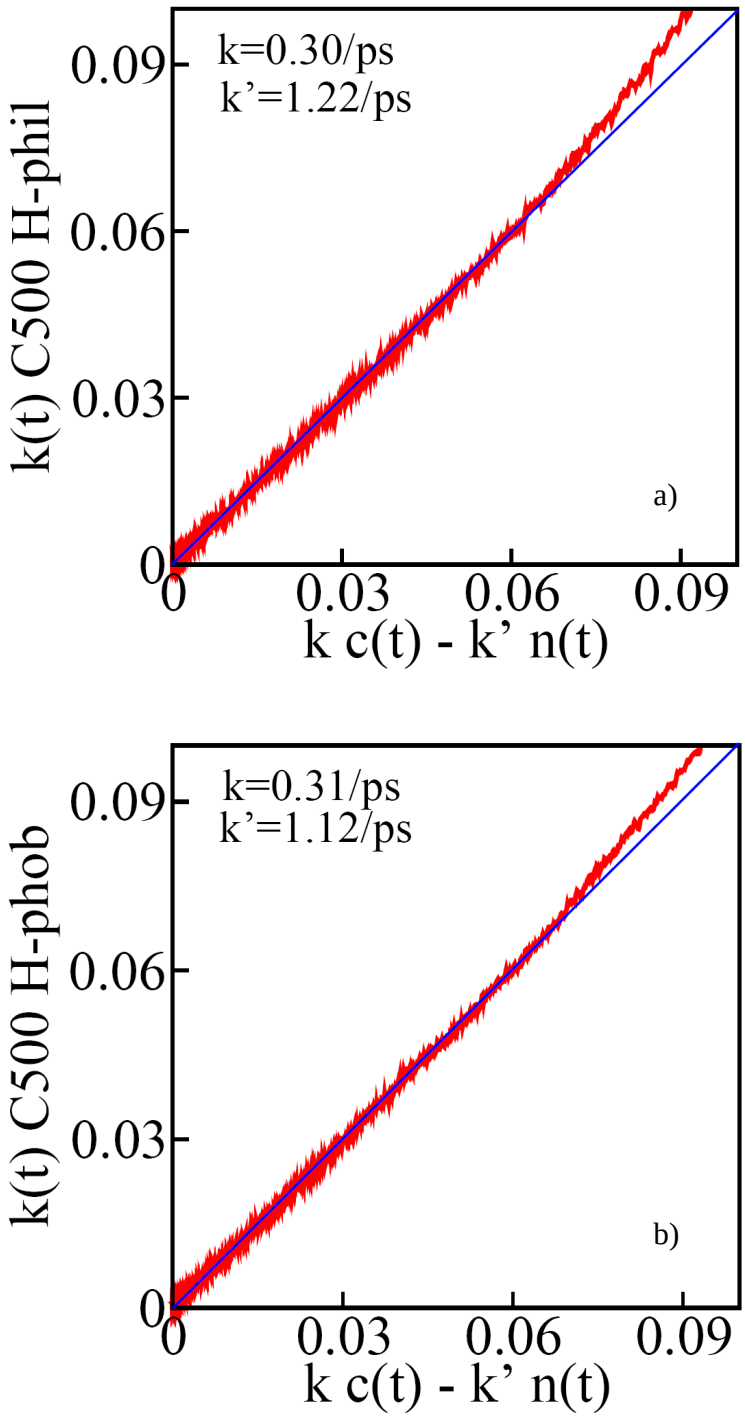

Figure 5.14. Correlation plot for C500 sample, with 57 water molecules inside. a) Hydrophilic, deviation is starting at 2.45 ps. b) Hydrophobic deviation is starting at 3.0 ps.

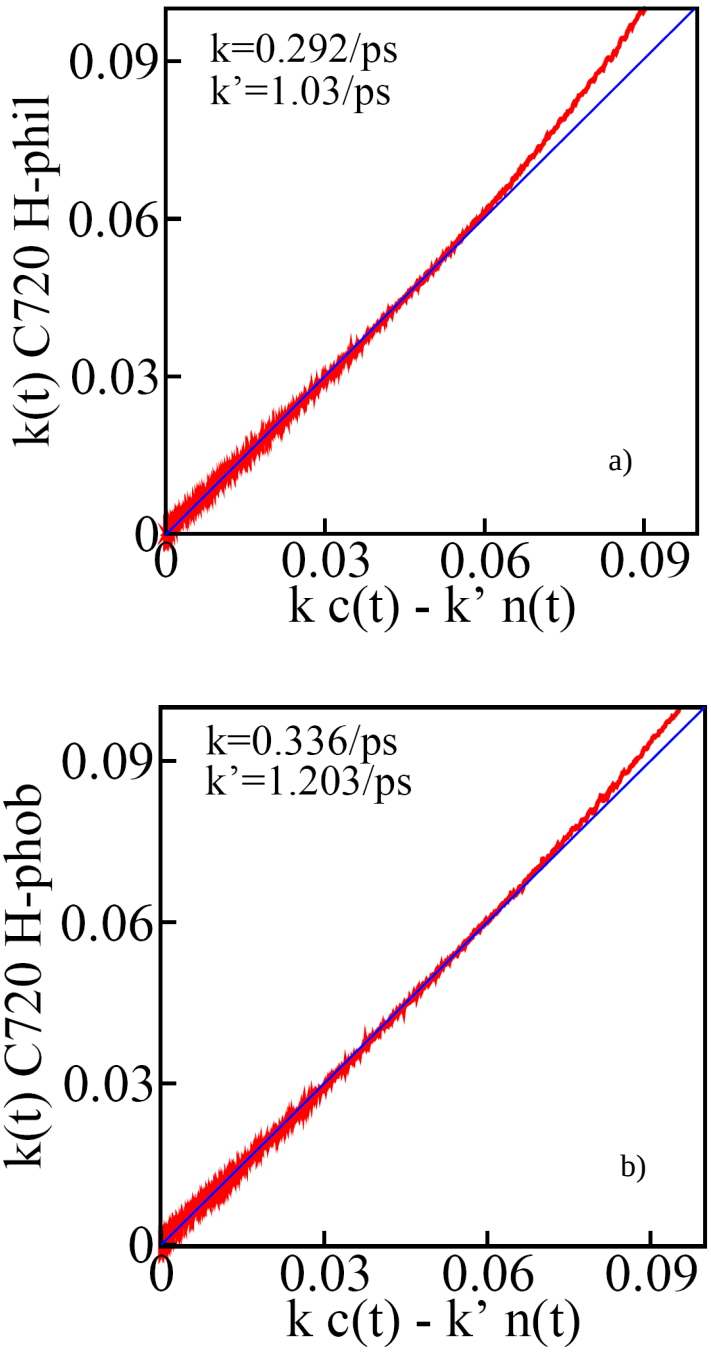

Figure 5.15. Correlation plot for C720 sample, with 100 water molecules inside. a) Hydrophilic, deviation is starting at 2.8 ps. b) Hydrophobic, deviation is starting at 2.7 ps.

Results and discussion. Initial calculations have been done in NVT ensemble (Table 5.3). From these correlation plots, we obtain very similar rate constant characterizing water hydrogen bond dynamics in hydrophilic and hydrophobic systems. Note that τ_{HB}, hydrogen bonds life time, is equal to 1/k and time for reforming a bond is 1/k'[85].

Table 5.3. Summary of the results of MD simulation in NVT ensemble.

NVT		k (1/ps)	k'(1/ps)	τ_{HB} (ps)
C320 20 water	hydrophilic	0.18	0.93	5.7
	hydrophobic	0.23	0.99	4.4
C500 57 water	hydrophilic	0.30	1.22	3.3
	hydrophobic	0.31	1.12	3.2
C720 100 water	hydrophilic	0.29	1.03	3.4
	hydrophobic	0.34	1.20	3.0
C1500 500 water	hydrophilic	0.30	-	3.3
	hydrophobic	0.37	-	2.7

Up to now the difference between hydrophilic and hydrophobic samples is only based on different Lennard-Jones energy parameters, ε. To make this difference even more pronounced we also made a charged confinement by having partial charges distributing over all atoms using the method presented in the work of[86] Berkowitz. These charges formed dipoles with dipolar density ~1dipole/50Å^2, which is close to the dipolar density in some of the zwitterionic model biomembranes (Table 5.5). The whole sample however, is neutral.

In our C_x samples (x=320, 500, 720, 1500), we calculate the amount of partial charge that must add to individual molecules. We have even number of carbon-like atoms in each case therefore we have half of them to get positive charge and the other half to get negative charge. This makes the overall structure to be neutral. Table 5.4 has the value of partial charges in each case that are evenly distributed over all carbon-like atoms.

Table 5.4. Partial charge values on different confinements.

Sample	C320	C500	C720	C1500
Partial charges	± 0.0875	± 0.088	± 0.089	± 0.0888

These charged nano-spheres are interesting to study because the results of their study can be compared with well known Molybdenum based nanocapsules that are based on very robust structure of $[Pentagon]_{12}(Linker)_{30}$ and can be modified in different ways. In these structures each pentagonal unit is containing six Mo-atoms. Using different functional groups (i.e. PHOS and ACET) for internal layer of these nanocapsules, experimentalists made respectively hydrophilic and hydrophobic spherical confinements[87,88]. Water trapping during the synthesis of these compounds made it possible to study water dynamics in well ordered, spherical, confinements. For example, this is structural formula for these nanocpsules:

$[(NH_2)_3C]_{32}(H_2O)_{100}\{(NH_2)_3C\}_{20}\{(Mo)Mo_5O_{21}(H_2O)_6\}_{12}\{Mo_2O_4(SO_4)\}_{10}\{Mo_2O_4(H_2PO_2)\}_{20}]$

Also we calculate diffusion coefficients by integration of velocity autocorrelation functions, VACF, (Figures 5.17a,b-5.18a,b-5.19a,b-5.20a,b). Also we calculate mean square displacement, MSD. As it is clear from the results, especially Figure 5.19b, there is a ballistic motion followed by almost linear motion of water molecules, but because of confinement as it is clear from Figures 5.17b and 5.18b, MSD reaches to an almost constant value.

As another dynamics property we calculate rotational relaxation times using second Legendre polynomial, $P_2(t)$, (Figures 5.21a,b,c,d). We switch ensemble to NVE that is more reliable for studying the dynamics of systems from simulations starting from well equilibrated configurations. However, there is a small difference between the results of calculation in NVT and NVE ensemble. For example for neutral hydrophilic C320 sample with NVT we got 0.7 ps and with NVE we got 0.8 ps for rotational relaxation time. Table 5.5 has the results of dynamics properties calculated in NVE ensemble for hydrogen bond life times, diffusion coefficients and rotational relaxation time. For comparison purpose Table 5.6 shows the simulation results of bulk SPC/E water from literatures.

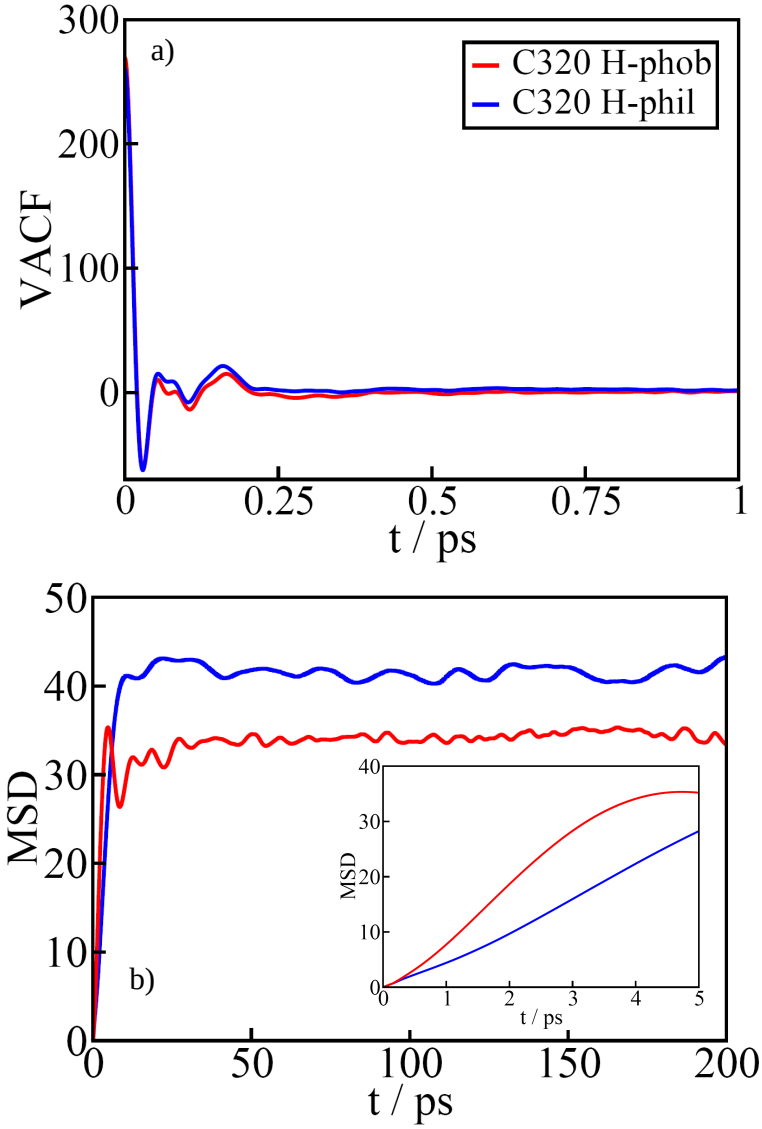

Figure 5.17. C320 sample with 20 water molecules (blue) hydrophilic and (red) hydrophobic. a) Velocity auto-correlation function, b) Mean square displacement. Inset shows MSD up to 5 ps.

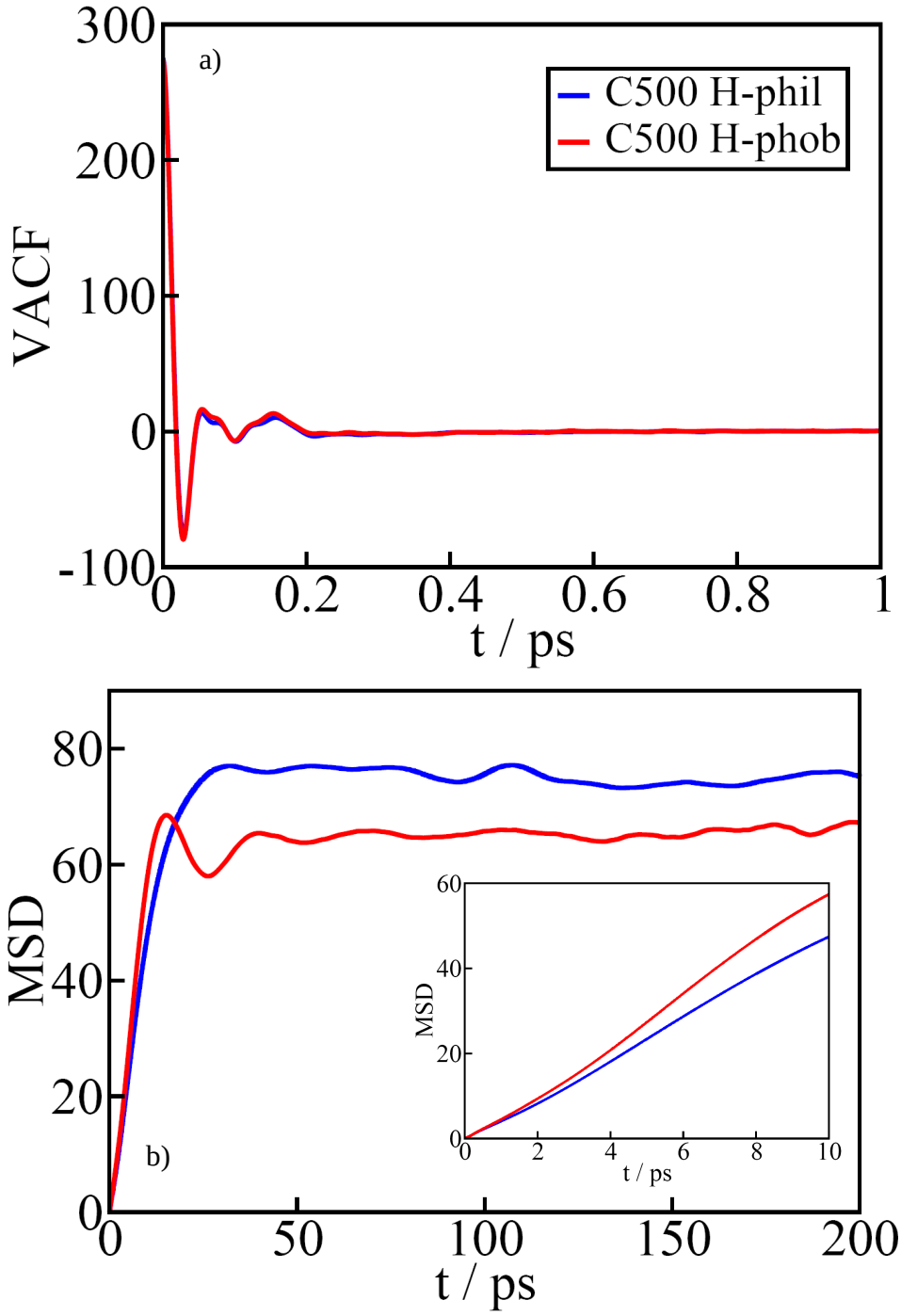

Figure 5.18. C500 sample with 57 water molecules (blue) hydrophilic and (red) hydrophobic. a) Velocity auto-correlation function, b) Mean square displacement. Inset shows MSD up to 10 ps.

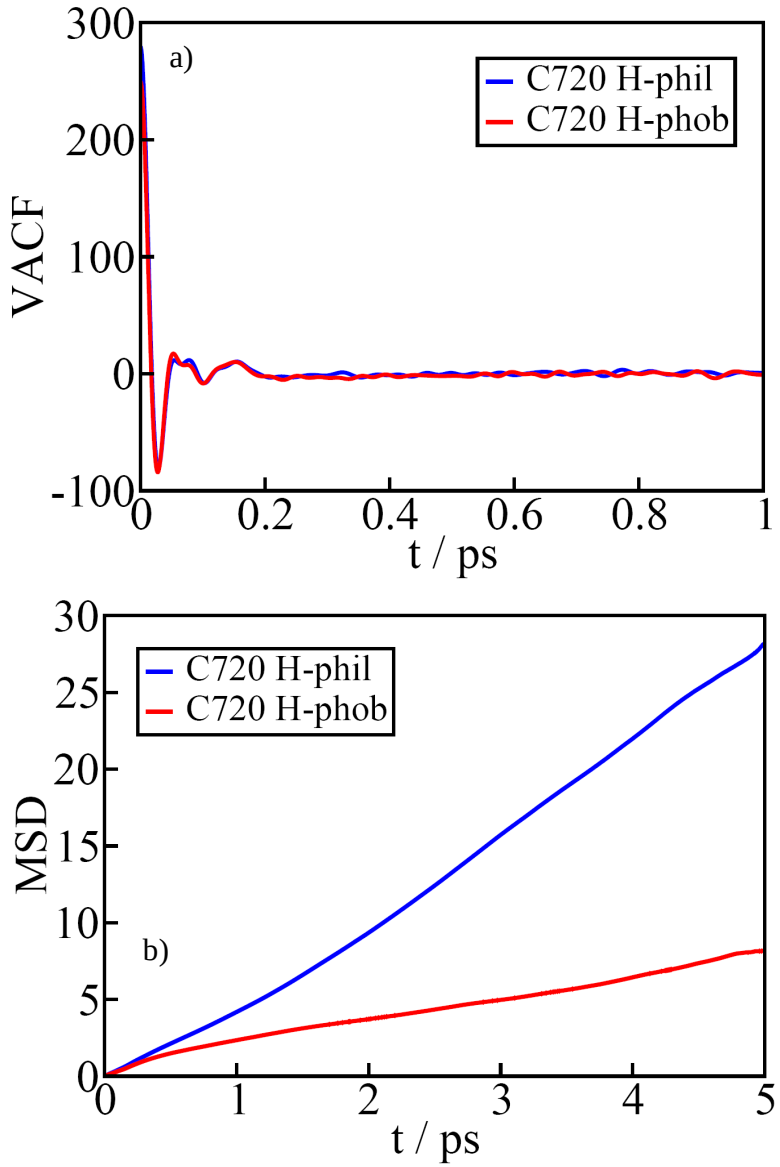

Figure 5.19. C720 sample with 100 water molecules (blue) hydrophilic and (red) hydrophobic. a) Velocity auto-correlation function, b) Mean square displacement.

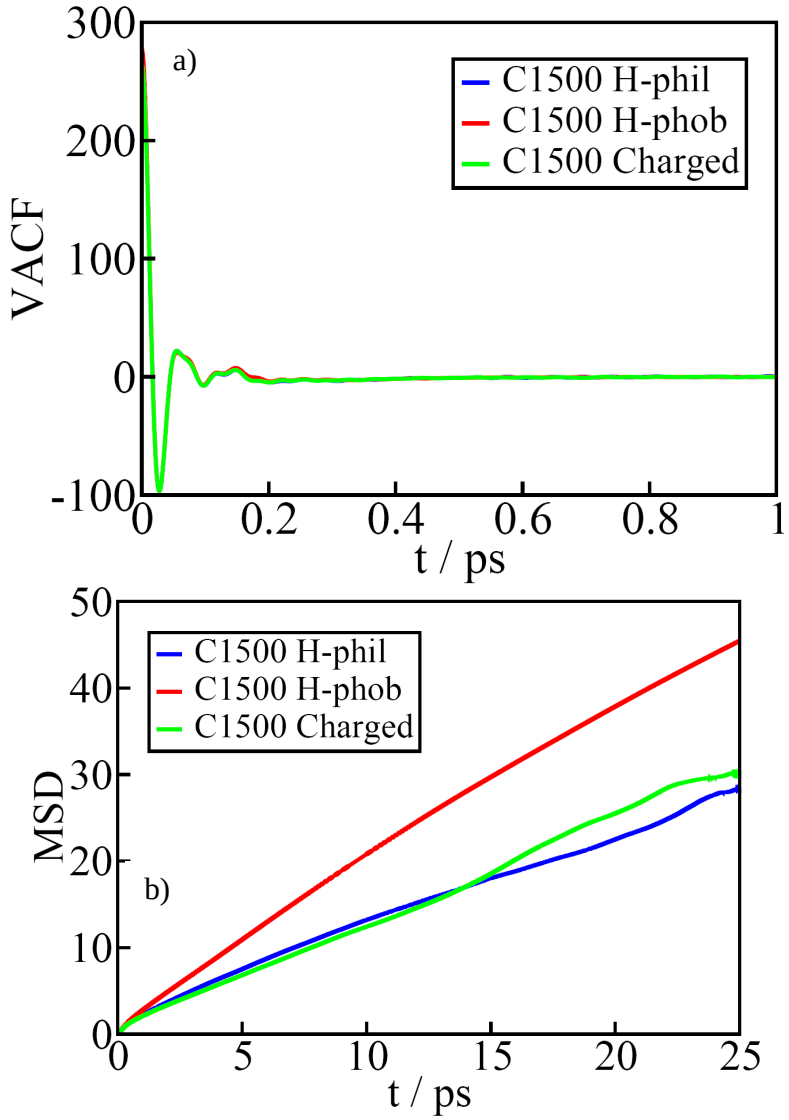

Figure 5.20. C1500 sample with 500 water molecules (blue) hydrophilic and (red) hydrophobic. a) Velocity auto-correlation function, b) Mean square displacement.

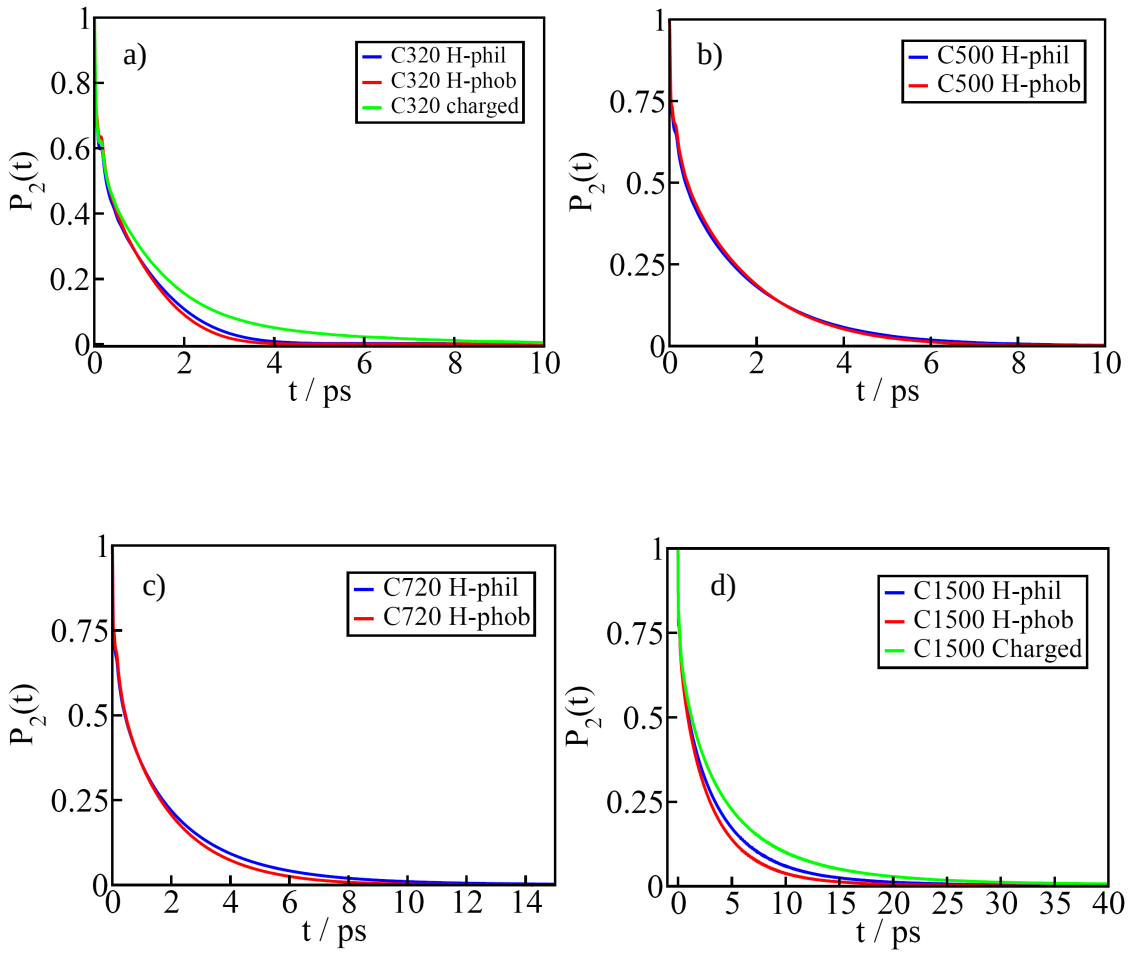

Figure 5.21. Second Legendre polynomial to calculate rotational relaxation times, (blue) hydrophilic and (red) hydrophobic and (green) charged samples. a) C320 sample with 20 water molecules. b) C500 sample with 57 water molecules. c) C720 sample with 100 water molecules. d) C1500 sample with 500 water molecules.

Table 5.5. The results of MD simulation in NVE ensemble for hydrogen bonds dynamics (τ_{HB}), diffusion coefficients (D) and rotational relaxation times ($\tau_{rotation}$) at 300K for hydrophobic and hydrophilic and charged samples.

NVE		τ_{HB} (ps)	$t_{Reforming}$(ps)	$D\times10^{-8}$ m^2/s	$\tau_{rotation}$(ps)
C320 20 water	Philic/charged	6.6	1.03	0.4	1.0
	Philic/neutral	6.4	0.94	0.44	0.8
	Hydrophobic	6.9	1.12	0.5	1.2
C500 57 water	Philic/charged	6.2	1.37	0.2	1.4
	Philic/neutral	6.2	0.82	0.4	1.2
	Hydrophobic	6.5	0.89	0.6	2.0
C720 100 water	Philic/charged	3.9	1.25	0.5	1.8
	Philic/neutral	3.7	1.01	1.0	1.5
	Hydrophobic	4.0	0.83	0.2	2.2
C1500 500 water	Philic/charged	4.7	1.47	0.17	3.7
	Philic/neutral	3.8	1.17	0.18	2.7
	Hydrophobic	3.2	1.15	0.32	2.3

Table 5.6. The results of MD simulation for SPC/E bulk water at T=300K.

SPC/E	τ_{HB} (ps)	$t_{Reforming}$(ps)	$D\times10^{-8}$ m^2/s	$\tau_{Rotation}$(ps)
Bulk Water	1.7[85]	1.1[85]	0.24[89,41]	1.4[90,91]

From the results obtained for dynamics properties for different confinement sizes, it is clear that there is insignificant difference in water dynamics confined within these different samples. Considering system sizes and number of water molecules we can definitely say that this is not due to smallness of these samples. Therefore there is a distinct difference between hydration water outside the spheres (studied by Baglioni[92]) and water confined inside the spheres. We have a reasonable explanation of what is this difference due to. A water molecule outside of the sphere (which is a usual hydration

water), has a force and there is attraction between sphere and this molecule. In other words, net force on this water molecule is acting to attract it to the surface. However, a water molecule inside the sphere has a force pulling it towards all atoms of the sphere in all directions and so the net force is pretty much balanced out, i.e. it is weak. That means molecules inside these spheres are more free than molecules outside, because force from opposite directions will greatly balance (Figure 5.22). This is about radial (i.e. perpendicular) motion, but lateral motion will have wells and bumps, depending on surface roughness/heterogeneity. The interior surface can be very smooth or less smooth (as it can be seen from snapshots). If inside is very smooth it would be easy to move laterally but water may be less attracted to the surface because it is affected by the other side of the surface. That means that we should expect a difference between lateral and radial motions/diffusion for a water cluster inside confined spheres that calls for calculating separately $D_{\parallel}$ and $D_{\perp}$ which is left for future work.

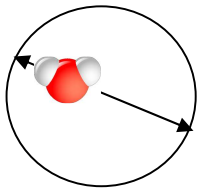

Figure 5.22. Water in the confinement feels attraction and repulsion from all cage's atoms in all different directions.

Our results in Table 5.5 show that we got diffusion coefficients (which in our case are overall diffusion constants) that in some cases are bigger than the bulk value, especially for smaller confinements. Berne and co-workers[93] have calculated lateral and radial diffusion for a system of rectangular confinement with a flat interface that $D_{zz} \neq D_{xx}=D_{yy}$ and they found $D_{xx}=D_{yy}=D_{\parallel} \approx 0.8 Å^2/ps$ and for $D_{zz}=D_{\perp} \approx 0.5 Å^2/ps$ which means diffusion coefficient close to the interface is bigger than the one far from the interface (i.e. bulk water). For bulk water they compute the diffusion coefficients in slabs of water of width 3.5 Å perpendicular to the z-axis and they found $D_{xx} = 0.30 \pm 0.02$ $Å^2/ps$ and $D_{yy} = 0.30 \pm 0.02$ $Å^2/ps$ and for homogeneous system using Einstein relation they found $D = 0.307$ $Å^2/ps$. We have a possible explanation for our results based on Berne's results. In these nanospheres water droplet is in nanoscale size and since nano-size materials have high surface to volume ratio, therefore the most portion of water

molecules are located on the outer layer of the droplet (i.e. surface of the droplet) and therefore the most molecules are interfacial water molecules (i.e. they are near the interface either solid interface in the case of filled confinement or vapour-solid interface in the case of partially filled samples that discussed a little later). According to Berne's results the diffusion coefficient of these interfacial water molecules is bigger than the bulk value and even though the diffusion coefficient for the molecules of inner layers is smaller than the bulk value, the overall value will be bigger than the bulk value. Near interface, the number of hydrogen-bonds decreases, compared to the bulk value, therefore fewer hydrogen-bonds reduce the effective friction felt by the water molecules, resulting in a larger diffusion coefficient. Of course in the case of spherical confinement this effect will enhance, since interfacial water molecules are the majority of total molecules. Therefore higher diffusion coefficient would be expected compare to rectangular confinement. In our case the geometry of these confinements makes it easier for molecules to move and continue to move. Rotational relaxation times in Table 5.5 also differ compared to the bulk water value that has been reported by experimentalists as[94] $\tau_{rotatioanl}$=2.8ps.

In third column of Table 5.5 we have reported rotational relaxation times. As a first thought it might be confusing why reorientational times are faster than hydrogen bond life times. This argument is relevant for bulk water since water molecules need to break few hydrogen bonds in order to be able to rotate. In bulk water all water molecules are attached to others through hydrogen bonds. However in the case of confined water especially nanoscale confinement, question can be answered considering large number of interfacial water molecules that are not as bind as in bulk water because interfacial water molecules have dangling OH bonds (especially in partially filled, like our C720 sample, or hydrophobic confinements that interface is pronounced) but water molecules in the bulk do not have that. Therefore interfacial water molecules are more free to rotate and although rotation is a local process, actually faster diffusion that has been discussed before, might help them to rotate even faster. This property has been proved recently by experimentalists at AMOLF using femtosecond vibrational spectroscopy[95].

Another question might be raised about these confined nanodroplets is whether these water molecules stay in a cluster and therefore showing a collective motion or they don't. As one knows cluster undergoes thermal motion and it is easier to see this in a partially filled pore than in a fully filled pore, but in both cases molecules move with exactly the same kinetic energy. In the filled one they have spatial constrains that prevent us to see this as clearly as in the partially filled case. Therefore in order to find the right answer to this question we made a partially filled sample on purpose which is C720 with 100 water molecules, and then we calculate the distance between all pairs. We plot the average distance between a molecule and all other molecules over time. This was done for two molecules, molecule 1 and molecule 2 and then we plot the average distance versus number of frames that is an indication of time. It is clear from Figure 5.23 that the distance remains almost the same. Therefore we conclude that in the case of partial filled confinement (Figure 5.24), waters remaining the form of tight cluster to minimize interfacial free energy.

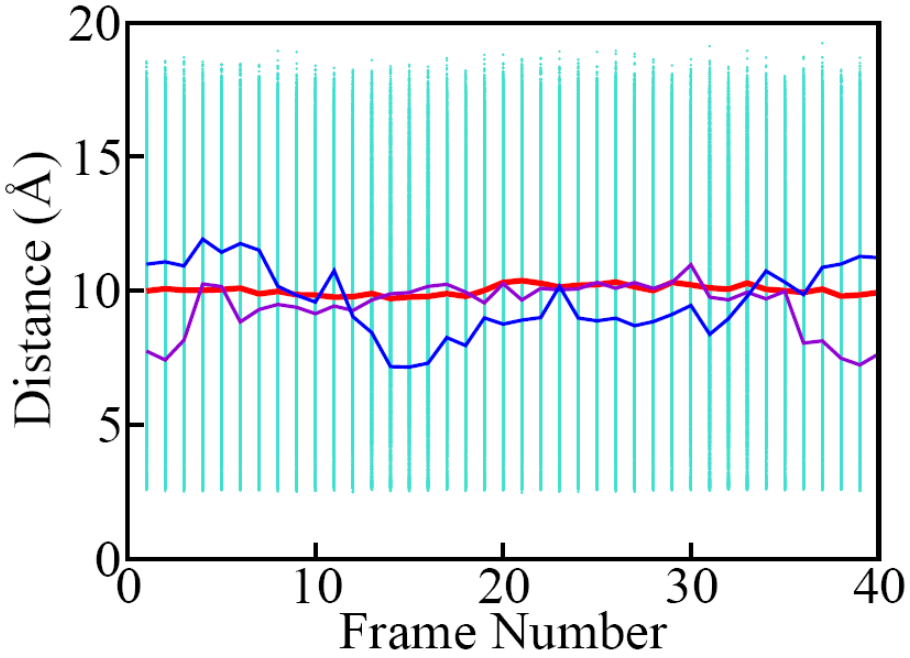

Figure 5.23. Average distance between a water molecule and all other water molecules over time for partially filled sample C720 with 100 water molecules inside. X-axis is number of frames which are 40 and the total time is 100 fs. Tick red color shows the average of averaged distance for molecule1 and molecule2.

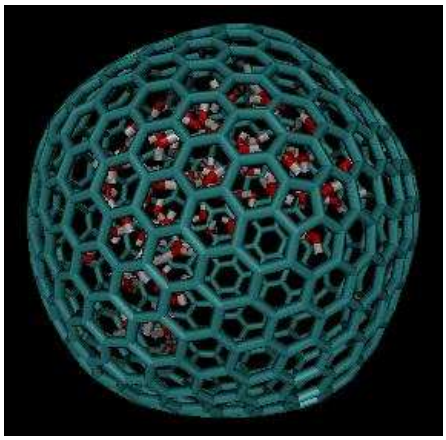

Figure 5.24. Snapshot of partial filled sample, charged C720 with 100 water molecules inside.

Figure 5.24 is a snapshot of simulation box for charged C720 with 100 water molecules. As it was seen during the whole simulation water molecules stay together for the entire time, that is suggesting a cluster motion but because of its thermal motion this cluster is rolling around the wall.

Comparing real nanocapsules[87] with our system, we should notice of few Mo atoms that are distributed around the sphere. Therefore if we consider lateral motion of water close to wall, there must be some points close to Mo atoms that are slowing down water motion. As a result we expect an additional time scale related to this type of motion. We can mimic this behaviour by replacing partial charge distribution of all atoms with only two charges as a dipole (with the same density as before) or having a quadrupole instead.

Conclusion. From our results we can conclude having hydrophilic or hydrophobic sample do not make any significant difference in dynamic properties. The reason is all forces applied to molecules inside these spherical confinements from different directions are balanced out that is an interesting and new finding. The only simulation study on similar systems[39] considered only the hydrophilic sample therefore they were not able to distinguish this. We considered different sizes of the spherical confinement and we realized that in the case of smaller confinement, since the ratio of surface molecules to bulk molecules is high, the overall diffusion is greater than the bulk value. On the basis of the current data we have so far we may predict water confined in C_x based nanospheres

(x=320, 500, 720, 1500) can show up to three different time scales: first one is a small time scale related to hydrogen bonds dynamics, second is a time scale related to slowing down motion by charged atoms and third one is a time scale of collective motion when the whole droplet can stay as a cluster. To validate these prediction additional computations will need to be performed.

Future tasks that need to be completed. Calculation of lateral diffusion and comparing with radial and overall diffusion to get more details about water dynamics inside spherical nano confinements is planned. Also using GCMC code to get the right number of water molecules inside each of hollow buckyballs, and recalculate all properties based on that is another interest. Replacing partial charge distribution of all atoms with a dipole or a quadrupole with the same density as original charged sample is among the future works too.

Appendix I:

The whole sets of surfaces for topological heterogeneity (with radius of patch in each case) with snapshots of water droplet on corresponding surfaces.

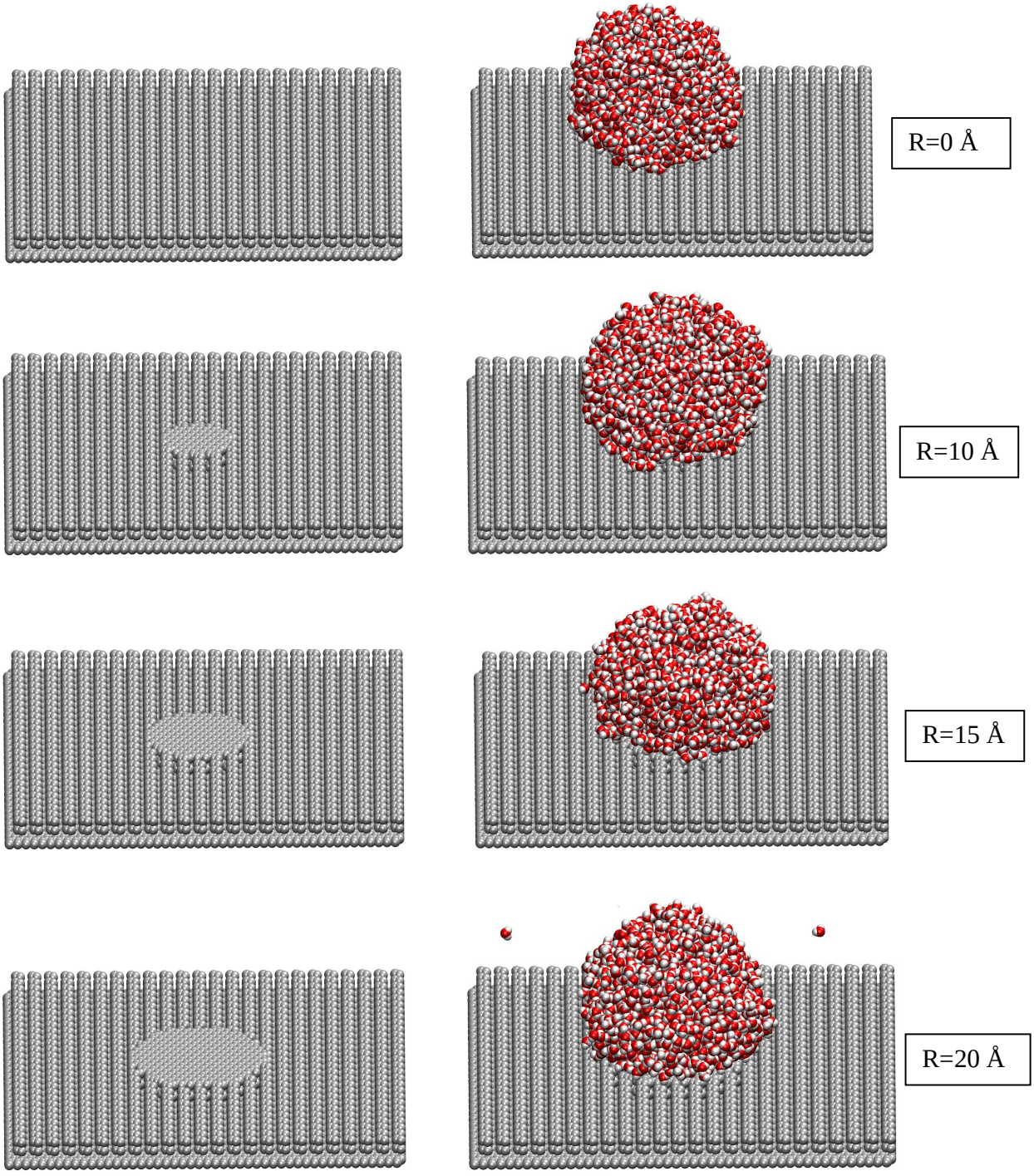

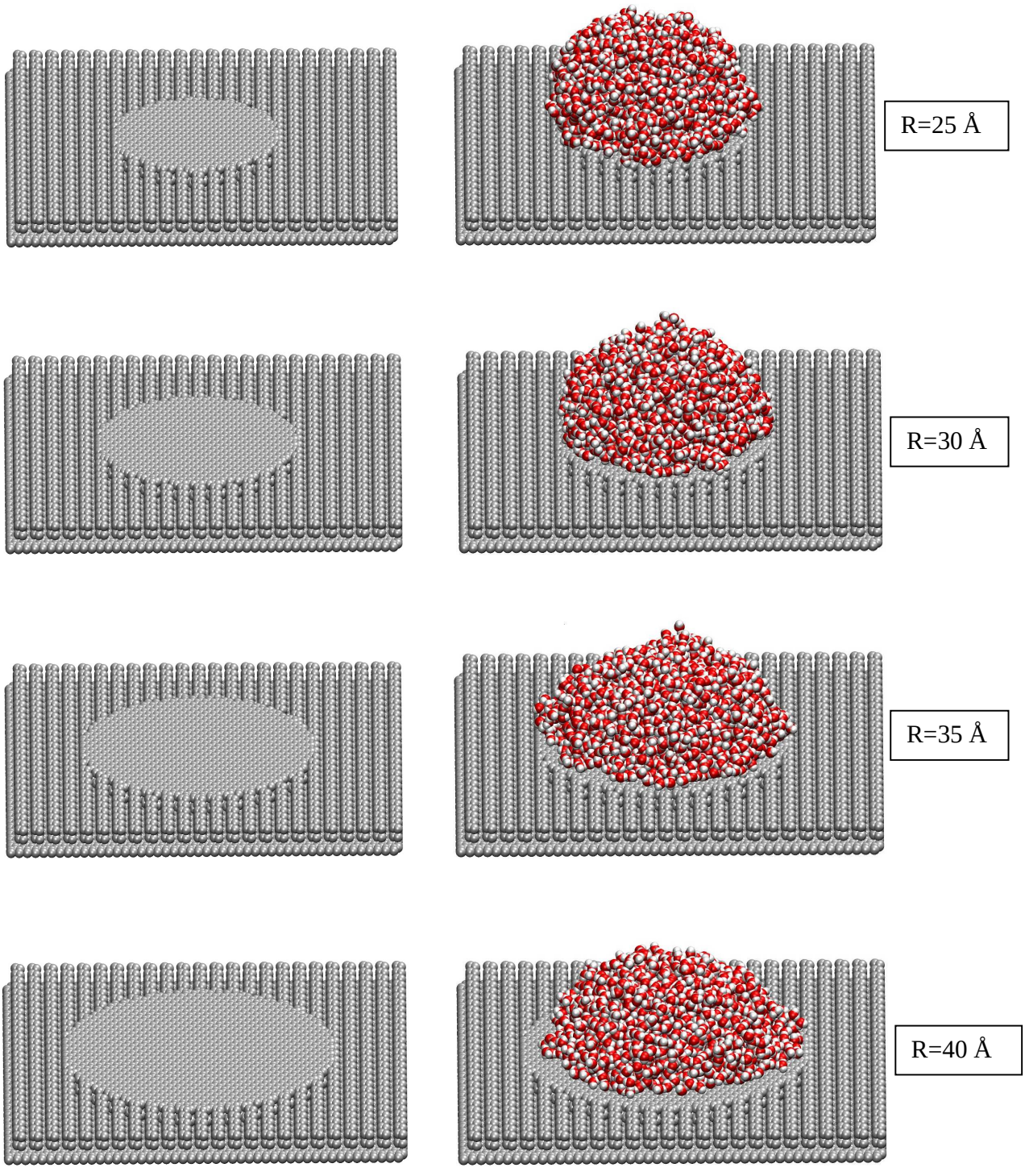
R=25 Å
R=30 Å
R=35 Å
R=40 Å

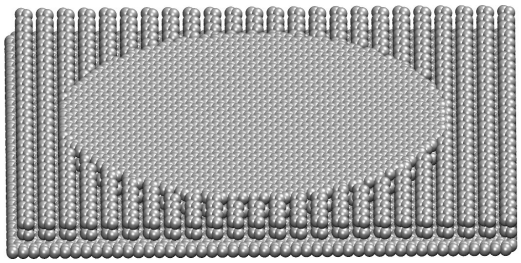

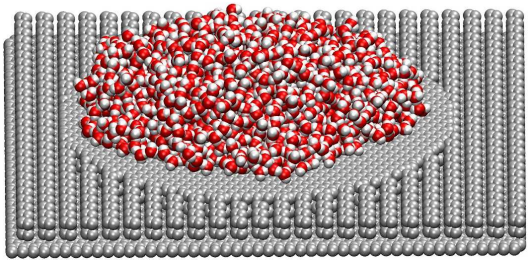

R=45 Å

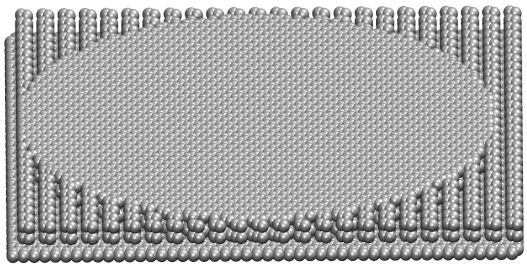

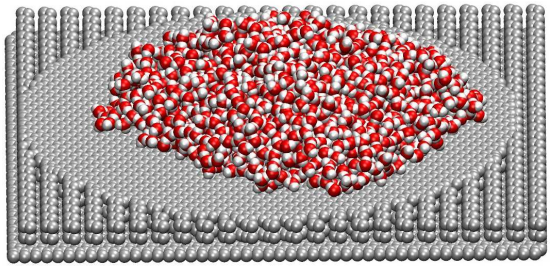

R=50 Å

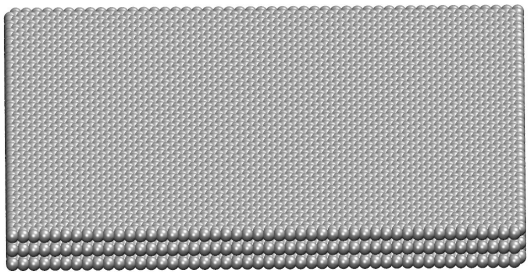

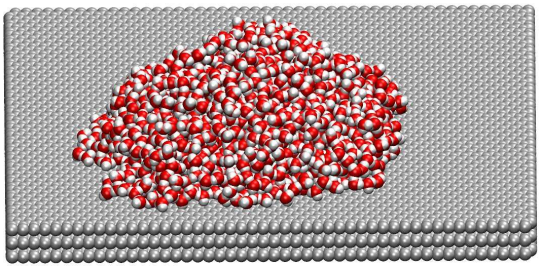

R=∞

Appendix II:

Table form T Werder, J H Walther, R L Jaffe, T Halicioglu and P Koumoutsakos; "On the water-carbon interaction for use in MD simulations of graphite and carbon nanotubes", *J. Phys. Chem. B*, 107, **2003**, 1345-1352.

TABLE 2: Overview of the MD Simulations of Water Droplets on Graphite[a]

case	σ_{CO}	ϵ_{CO}	σ_{CH}	ϵ_{CH}	N_{H_2O}	ΔE	r_B	θ (deg)
1	3.190	0.3135			2000	−5.07	25.3	111.3
2[b]	3.190	0.3135			2000	−5.07	25.7	110.0
3[c]	3.190	0.3135			2000		25.3	111.2
4[d]	3.190	0.3135			2000	−5.07	24.3	114.5
5	3.190	0.3135			1000	−5.07	17.7	115.5
6	3.190	0.3135			4000	−5.07	32.5	109.2
7	3.190	0.3135			8379	−5.07	41.8	108.8
8	3.190	0.3135			17576	−5.07	54.0	107.7
9	3.190	0.4389			1000	−7.09	24.2	85.9
10	3.190	0.4389			2000	−7.09	32.8	85.5
11	3.190	0.4389			4000	−7.09	42.2	82.6
12	3.190	0.4389			8379	−7.09	54.4	81.1
13	3.190	0.1881			1000	−3.04	10.9	143.3
14	3.190	0.1881			2000	−3.04	16.4	138.8
15	3.190	0.1881			4000	−3.04	19.5	141.3
16	3.190	0.1881			8379	−3.04	26.9	138.1
17	3.190	0.2508			2000	−4.05	20.1	127.8
18	3.190	0.3762			2000	−6.08	28.2	101.2
19	3.190	0.5016			2000	−8.11	37.4	69.9
20	3.190	0.5643			2000	−9.12	44.6	50.7
21	3.190	0.6270			2000	−10.13	58.0	29.4
22	3.190	0.3910	2.82	0.253	2000	−12.18		0.0
23	3.280	0.3890	2.81	0.129	2000	−9.70	42.4	55.9
24	3.275	0.4785			2000	−8.12	39.4	65.4
25	3.296	0.5781	2.58	0.323	2000	−16.54		0.0
26[e]	3.275	0.4785			2000	−8.12	46.7	48.0
27	3.296	0.4389			2000	−7.53	35.6	76.8
28	3.190	0.3920			2000	−6.33	30.1	95.3

[a] The water−carbon interaction is modeled through Lennard-Jones potentials with parameters ϵ_{CO} (kJ mol^{-1}), σ_{CO} (Å), ϵ_{CH} (kJ mol^{-1}), and σ_{CH} (Å). The resulting binding energy of a water molecule on a double layer of graphite is denoted by ΔE (kJ mol^{-1}). N_{H_2O} is the number of water molecules in the droplets, and r_B and θ are the droplet base radius and the contact angle as obtained from the simulation. [b] Case 1 with a cutoff radius of 25 Å for the electrostatics. [c] Case 1 with flexible graphite. [d] Case 1 with different initial conditions. [e] Case 24 with the TIP3P water model.

Appendix III:

```
      v=60000.
      write(*,*)'input z'
C     read(*,*)z
      do z=24,0,-.2
      pi=3.14159
      rs=0.
      do i=1,10001
      rsold=rs
      zcomold=zcom
      cosb=(i-1)*.0002-1.
      b=2.-3.*cosb+cosb**3
      r=(3.*v/pi/b)**(1./3.)
      sinb=sqrt(1.-cosb**2)
      rs=r*sinb
      h=r*(1-cosb)
C     new zCOM equation
      zc=h-r
      z1=h**2*r**2/2.-h**4/4.+2.*h**3/3.*zc-h**2*zc**2/2.
      z2=h*r**2-h**3/3.+h**2*zc-h*zc**2
      zcom=z1/z2
      drdz=(rs-rsold)/(zcom-zcomold)
      if(zcom.lt.z)goto 3
      if(i.eq.10000)write(*,*)'no solution'
      enddo
      write(*,*)cosb,180./pi*acos(cosb),rs,drdz,h,zcom
      write(12,*)cosb,180./pi*acos(cosb),rs,drdz,h,zcom
      if(i.eq.1)write(*,*)'no solution'
      write(13,*)z,rs,drdz
      enddo
      stop
      end
```

Appendix IV[72]:

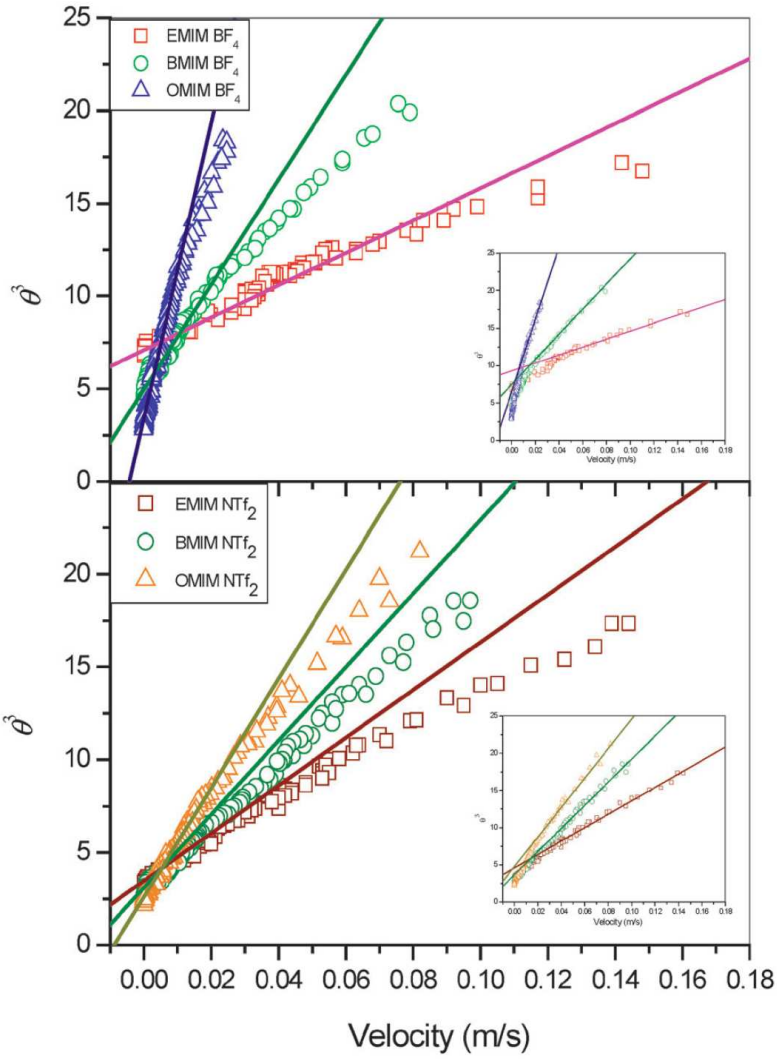

Fig. 4 Experimental data from Fig. 3 presented in the characteristic hydrodynamic scale θ^3 *versus* V. The solid lines are the best fits of the hydrodynamic model to the data in the low velocity range. The best fits in the high velocity range are shown in the insets. The hydrodynamic parameters are given in Table 2.

Table 2 Hydrodynamic parameters for ionic liquids spreading on Teflon AF1600 surfaces

		EMIM BF_4	BMIM BF_4	OMIM BF_4	EMIM NTf_2	BMIM NTf_2	HMIM NTf_2
High velocity range	$\ln L/L_S$	8.6	7.1	6.5	11.2	10.4	8.6
	θ_0^{HD}	120	112	107	95	89	97
Low velocity range	$\ln L/L_S$	15.4	12.1	9.0	15.9	13.3	12.8
	θ_0^{HD}	108	98	86	87	84	79
θ_A		104	95	80	83	78	75

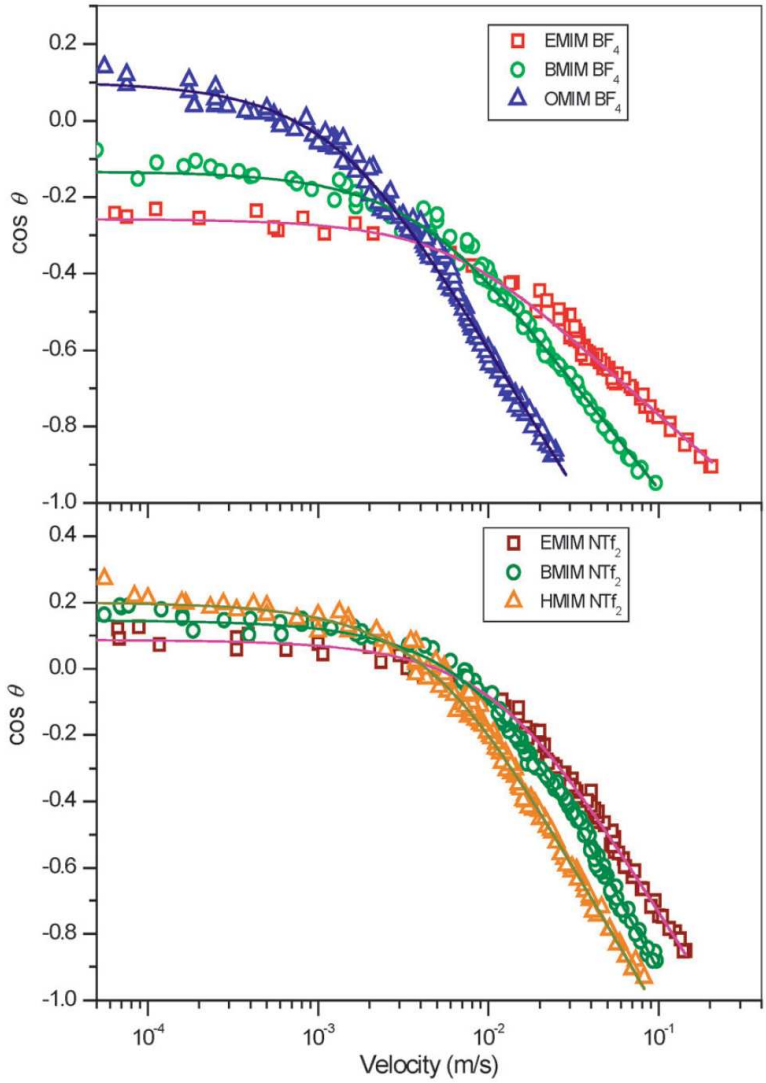

Fig. 5 Experimental data from Fig. 3 presented as $\cos\theta$ *versus* V (logarithmic scale). The solid lines show the best fits of the MK model to data over the whole velocity regime. MK parameters are given in Table 3.

Table 3 MK parameters for ionic liquids spreading on Teflon AF1600 surfaces

	EMIM BF_4	BMIM BF_4	OMIM BF_4	EMIM NTf_2	BMIM NTf_2	HMIM NTf_2
${\theta_0}^{MK}/^\circ$	105	99	83	85	81	78
k_0/MHz	7.2	3.5	1.0	12.8	10.0	4.8
λ/nm	0.9	0.9	0.9	0.8	0.8	0.8

Appendix V:

Subroutines developed in Dr. Luzar's group to use in DLPOLY:
Original codes adapted from Christopher Daub for bulk water and modified by Jamileh Seyed-Yazdi to use for water in the confinement, last modifications January 2010.

Hydrogen-bond correlation functions:

```
SUBROUTINE CORRH2O(DELT0,DELT,XXX,YYY,ZZZ,NSTEP,NSTEQL,
     :      ICTSUM,INTSUM,IRTSUM,IBIGRTSUM,IH0,IH0POINT,IH0LIST,
     :  IBIGH0,IHT,IBIGHT,NTIMEC,TSTEP,CELL,NT0,IT0,
     :  ROOWMAX,ROOMAX,ROHMAX,COSMIN,DOH,HAVSUM,HSUMSUM,
     :  HSUMTOTAV,NNBSUM,NNBAV,BIGHAVSUM,BIGHSUMSUM,BIGHSUMTOTAV,
     :  HBLIP,BIGHBLIP)

C     Subroutine to calculate time correlation functions for H2O
C     simulations.  Calculates c(t) and k(t).
C     Kr(t), <Hdot(0)H(t)>/<H>
      INCLUDE 'dl_params.inc'
C     ------------- INTEGER DECLARATIONS ----------
      INTEGER NSTEP,NSTEQL,NRUN, DELT
      INTEGER I1, I2, II, J1, J0, JP, JF, T, DT
      INTEGER JBEG, JEND
      INTEGER J0BEG, J0END, J0PBEG, J0PEND, J0FBEG, J0FEND
      INTEGER NNBSUM, DELT0, NT0,IT0, T0IDX
      INTEGER HSUM, HSUMSUM
      INTEGER BIGHSUM, BIGHSUMSUM
      INTEGER HBLIP, BIGHBLIP
      DIMENSION NTIMEC(MAXNC)
C     -------------Neighbour list stuff--------------
      DIMENSION IH0LIST(MAXNB,MAXNT0)
      DIMENSION IH0POINT(MXMOLS,MAXNT0)
      INTEGER*1 IH0(MAXNB,MAXNT0), IHT(MAXNB)
      INTEGER*1 IBIGH0(MAXNB,MAXNT0), IBIGHT(MAXNB)
      INTEGER*1 IHOLD(MAXNB), IBIGHOLD(MAXNB)
      DIMENSION ICTSUM(MAXNC), INTSUM(MAXNC)
      DIMENSION IRTSUM(MAXNC), IBIGRTSUM(MAXNC)
C     ------------- REAL DECLARATIONS ---------------
      DOUBLE PRECISION NBAV, NNBAV
      DOUBLE PRECISION HAV, HTOTAV, HAVSUM, HSUMTOTAV
      DOUBLE PRECISION BIGHAV, BIGHTOTAV, BIGHAVSUM, BIGHSUMTOTAV
      DOUBLE PRECISION TSTEP, TSAMP, L, RTEMP
      DOUBLE PRECISION XOO,YOO,ZOO
      DOUBLE PRECISION XOH1, YOH1, ZOH1
      DOUBLE PRECISION XOH2, YOH2, ZOH2
      DOUBLE PRECISION XOH3,YOH3,ZOH3
      DOUBLE PRECISION XOH4,YOH4,ZOH4
      DOUBLE PRECISION ROOSQ, ROH1SQ, ROH2SQ, ROH3SQ, ROH4SQ
      DOUBLE PRECISION COS
C     ---These are the HB criteria, read in from the 'CONTROL' file:
      DOUBLE PRECISION ROOWMAX, ROOMAX, ROHMAX, COSMIN
```

```
      DOUBLE PRECISION ROOWMAXSQ, ROOMAXSQ, ROHMAXSQ
C     --------------H2O internal geometry:-----------
      DOUBLE PRECISION DOH, DOHSQ

      DIMENSION CELL(9)
      DIMENSION XXX(MXATMS), YYY(MXATMS), ZZZ(MXATMS)
C     ------------------------------------------------
      ROOWMAXSQ = ROOWMAX*ROOWMAX
      ROOMAXSQ = ROOMAX*ROOMAX
      ROHMAXSQ = ROHMAX*ROHMAX
      DOHSQ = DOH*DOH
      L = CELL(1)
C     NRUN = 1 on first call on 1st step after eq,
C     +1 for each call.
      NRUN = (NSTEP - NSTEQL - 1)/DELT + 1
C     Initialize on the first call:
      IF (NRUN .EQ. 1) THEN
        DO I = 1, MAXNC
          ICTSUM(I) = 0
          INTSUM(I) = 0
          IRTSUM(I) = 0
          IBIGRTSUM(I) = 0
          NTIMEC(I) = 0
        ENDDO
        DO I = 1, MAXNB
          IHOLD(I) = 0
          IBIGHOLD(I) = 0
          DO J = 1, MAXNT0
            IH0(I,J) = 0
            IBIGH0(I,J) = 0
            IH0LIST(I,J) = 0
          ENDDO
        ENDDO
        NT0 = 0
        IT0 = 1
        HAV = 0.0D0
        HAVSUM = 0.0D0
        BIGHAV = 0.0D0
        BIGHAVSUM = 0.0D0
        HSUMSUM = 0
        BIGHSUMSUM = 0
        NNBSUM = 0
C     IHOLD is the past value of IHT, needed for the blip counter.
      ELSE
        DO I = 1, MAXNB
          IHOLD(I) = IHT(I)
          IBIGHOLD(I) = IBIGHT(I)
        ENDDO
      ENDIF
C     Reset HSUM, IHT, IBIGHT to zero every time:
      HSUM = 0
      BIGHSUM = 0
      DO I = 1, MAXNB
        IHT(I) = 0
```

```
        IBIGHT(I) = 0
      ENDDO

C     Check if a new T0 is being added whether NRUN>MAXNC or not.

      IF (NRUN .LE. MAXNC) THEN
        IF ((NRUN. EQ. 1) .OR.
     :           (MOD(NRUN-1,DELT0/DELT).EQ.0))THEN
          NT0 = NT0 + 1
         ENDIF
      ELSE
        IF (MOD(NRUN-1, DELT0/DELT) .EQ. 0) THEN
          IT0 = MOD((NRUN-1)/(DELT0/DELT),NT0) + 1
          DO II = 1, MAXNB
            IH0(II,IT0) = 0
            IBIGH0(II,IT0) = 0
          ENDDO
        ENDIF
      ENDIF

C     Neighbour list.
C     Neighbour list update interval = DELT0
      IF ((NRUN .EQ. 1) .OR.
     :           (MOD(NRUN-1,DELT0/DELT) .EQ. 0)) THEN
C     zero the I1 counter:
        I1 = 0
C     Look for neighbours:
        DO I = 1, MXMOLS - 1
          IF (NRUN .LE. MAXNC) THEN
            IH0POINT(I,NT0) = I1 + 1
          ELSE
            IH0POINT(I,IT0) = I1 + 1
          ENDIF
          DO II = I+1, MXMOLS
            XOO = DABS(XXX(320+3*I-2) - XXX(320+3*II-2))
            IF (XOO .GT. L/2) XOO = L-XOO
            YOO = DABS(YYY(320+3*I-2) - YYY(320+3*II-2))
            IF (YOO .GT. L/2) YOO = L-YOO
            ZOO = DABS(ZZZ(320+3*I-2) - ZZZ(320+3*II-2))
            IF (ZOO .GT. L/2) ZOO = L-ZOO
            ROOSQ = XOO*XOO + YOO*YOO + ZOO*ZOO
            IF (ROOSQ .LT. ROOWMAXSQ) THEN
              I1 = I1 + 1
              IF ((NRUN .EQ. 1) .OR.
     :                (MOD(NRUN-1,DELT0/DELT).EQ.0))THEN
                  IF (NRUN .LE. MAXNC) THEN
                    IH0LIST(I1,NT0) = II
                  ELSE
                    IH0LIST(I1,IT0) = II
                  ENDIF
                ENDIF
            ENDIF
          ENDDO
        ENDDO
```

```
        IF (NRUN .LE. MAXNC) THEN
          IH0POINT(MXMOLS,NT0) = I1+1
        ELSE
          IH0POINT(MXMOLS,IT0) = I1+1
        ENDIF
      ENDIF
C     End of Neighbour list!
C     checking the pairs with ROO < ROOWMAX to see if any of the
C     4 ROH's are < ROHMAX, and then check the appropriate angles:
      DO I = 1, MXMOLS - 1
C     Neighbours of molecule I:
        IF (NRUN .LE. MAXNC) THEN
          JBEG = IH0POINT(I,NT0)
          JEND = IH0POINT(I+1,NT0) - 1
        ELSE
          JBEG = IH0POINT(I,IT0)
            JEND = IH0POINT(I+1,IT0) - 1
        ENDIF

        IF (JBEG .LE. JEND) THEN
          DO J1 = JBEG, JEND
            IF (NRUN .LE. MAXNC) THEN
              II = IH0LIST(J1,NT0)
            ELSE
            II = IH0LIST(J1,IT0)
            ENDIF
            XOO = DABS(XXX(320+3*I-2) - XXX(320+3*II-2))
            YOO = DABS(YYY(320+3*I-2) - YYY(320+3*II-2))
            ZOO = DABS(ZZZ(320+3*I-2) - ZZZ(320+3*II-2))
            IF (XOO .GT. L/2) XOO=XOO-L
            IF (YOO .GT. L/2) YOO=YOO-L
            IF (ZOO .GT. L/2) ZOO=ZOO-L
            ROOSQ = XOO*XOO + YOO*YOO + ZOO*ZOO
            IF (ROOSQ .LT. ROOMAXSQ) THEN
            IBIGHT(J1) = 1
            BIGHSUM = BIGHSUM + 1
              IF ((NRUN .EQ. 1) .OR.
     :               (MOD(NRUN-1,DELT0/DELT).EQ.0))THEN
                IF (NRUN .LE. MAXNC) THEN
                IBIGH0(J1,NT0) = 1
                ELSE
                IBIGH0(J1,IT0) = 1
                ENDIF
            ENDIF
              XOH1 = DABS(XXX(320+3*I-2) - XXX(320+3*II-1))
              YOH1 = DABS(YYY(320+3*I-2) - YYY(320+3*II-1))
              ZOH1 = DABS(ZZZ(320+3*I-2) - ZZZ(320+3*II-1))
              IF (XOH1 .GT. L/2) XOH1 = L-XOH1
              IF (YOH1 .GT. L/2) YOH1 = L-YOH1
              IF (ZOH1 .GT. L/2) ZOH1 = L-ZOH1
              XOH2 = DABS(XXX(320+3*I-2) - XXX(320+3*II))
              YOH2 = DABS(YYY(320+3*I-2) - YYY(320+3*II))
              ZOH2 = DABS(ZZZ(320+3*I-2) - ZZZ(320+3*II))
              IF (XOH2 .GT. L/2) XOH2 = L-XOH2
```

```
              IF (YOH2 .GT. L/2) YOH2 = L-YOH2
              IF (ZOH2 .GT. L/2) ZOH2 = L-ZOH2
              XOH3 = DABS(XXX(320+3*I-1) - XXX(320+3*II-2))
              YOH3 = DABS(YYY(320+3*I-1) - YYY(320+3*II-2))
              ZOH3 = DABS(ZZZ(320+3*I-1) - ZZZ(320+3*II-2))
              IF (XOH3 .GT. L/2) XOH3 = L-XOH3
              IF (YOH3 .GT. L/2) YOH3 = L-YOH3
              IF (ZOH3 .GT. L/2) ZOH3 = L-ZOH3
              XOH4 = DABS(XXX(320+3*I) - XXX(320+3*II-2))
              YOH4 = DABS(YYY(320+3*I) - YYY(320+3*II-2))
              ZOH4 = DABS(ZZZ(320+3*I) - ZZZ(320+3*II-2))
              IF (XOH4 .GT. L/2) XOH4 = L-XOH4
              IF (YOH4 .GT. L/2) YOH4 = L-YOH4
              IF (ZOH4 .GT. L/2) ZOH4 = L-ZOH4
              ROH1SQ = XOH1*XOH1 + YOH1*YOH1 + ZOH1*ZOH1
              ROH2SQ = XOH2*XOH2 + YOH2*YOH2 + ZOH2*ZOH2
              ROH3SQ = XOH3*XOH3 + YOH3*YOH3 + ZOH3*ZOH3
              ROH4SQ = XOH4*XOH4 + YOH4*YOH4 + ZOH4*ZOH4
C---------------------------------------------
              IF (ROH1SQ .LT. ROHMAXSQ) THEN
                COS = (ROOSQ + DOHSQ - ROH1SQ)/(2*DSQRT(ROOSQ)*DOH)
                IF (COS .GT. COSMIN) THEN
                  HSUM = HSUM + 1
                IHT(J1) = 1
                  IF ((NRUN.EQ.1).OR.
     :                 (MOD(NRUN-1,DELT0/DELT).EQ.0))THEN
                  IF (NRUN .LE. MAXNC) THEN
                      IH0(J1,NT0) = 1
                    ELSE
                      IH0(J1,IT0) = 1
                    ENDIF
                  ENDIF
                ENDIF
              ELSE IF (ROH2SQ .LT. ROHMAXSQ) THEN
                COS = (ROOSQ + DOHSQ - ROH2SQ)/(2*DSQRT(ROOSQ)*DOH)
                IF (COS .GT. COSMIN) THEN
                  HSUM = HSUM + 1
                IHT(J1) = 1
                  IF ((NRUN .EQ. 1) .OR.
     :                 (MOD(NRUN-1,DELT0/DELT).EQ.0))THEN
                  IF (NRUN .LE. MAXNC) THEN
                      IH0(J1,NT0) = 1
                    ELSE
                      IH0(J1,IT0) = 1
                    ENDIF
                  ENDIF
                ENDIF
              ELSE IF (ROH3SQ .LT. ROHMAXSQ) THEN
                COS = (ROOSQ + DOHSQ - ROH3SQ)/(2*DSQRT(ROOSQ)*DOH)
                IF (COS .GT. COSMIN) THEN
                  IHT(J1) = 1
                  HSUM = HSUM + 1
                  IF ((NRUN .EQ. 1).OR.
     :                 (MOD(NRUN-1,DELT0/DELT).EQ.0))THEN
```

```
                  IF (NRUN .LE. MAXNC) THEN
                      IH0(J1,NT0) = 1
                    ELSE
                      IH0(J1,IT0) = 1
                    ENDIF
                  ENDIF
                ENDIF
              ELSE IF (ROH4SQ .LT. ROHMAXSQ) THEN
                COS = (ROOSQ + DOHSQ - ROH4SQ)/(2*DSQRT(ROOSQ)*DOH)
                IF (COS .GT. COSMIN) THEN
                  IHT(J1) = 1
                  HSUM = HSUM + 1
                  IF ((NRUN .EQ. 1).OR.
     :                 (MOD(NRUN-1,DELT0/DELT).EQ.0))THEN
                  IF (NRUN .LE. MAXNC) THEN
                      IH0(J1,NT0) = 1
                    ELSE
                      IH0(J1,IT0) = 1
                    ENDIF
                  ENDIF
                ENDIF
              ENDIF
            ENDIF
          ENDDO
        ENDIF
      ENDDO
C---------------------------------------
C     Calculation of <h> based on the last sample configuration:
      HAV = 2.0D0*DBLE(HSUM) / DBLE (MXMOLS*(MXMOLS-1))
C     NBAV = avg. number of h bonds per molecule, without
C     double counting (about 3/2=1.5)
      NBAV = DBLE(HSUM)/DBLE(MXMOLS)
C     Accumulate HAVSUM, and HSUMSUM, and NNBSUM, the total
C     number of neighbours:
C     BIGHAV = <H>, avg. # of neighbours per H2O:
      BIGHAV = 2.0D0*DBLE(BIGHSUM) / DBLE(MXMOLS*(MXMOLS-1))
      HAVSUM = HAVSUM + HAV
      HSUMSUM = HSUMSUM + HSUM
      BIGHAVSUM = BIGHAVSUM + BIGHAV
      BIGHSUMSUM = BIGHSUMSUM + BIGHSUM
      IF (NRUN .LE. MAXNC) THEN
        NNBSUM = NNBSUM + IH0POINT(MXMOLS,NT0) -1
      ELSE
        NNBSUM = NNBSUM + IH0POINT(MXMOLS,IT0) -1
      ENDIF
C     h and h(0) and H and H(0) done
        IF (NRUN .GT. 1) THEN
          DO I = 1, MXMOLS - 1
          IF (NRUN .LE. MAXNC) THEN
              JBEG = IH0POINT(I,NT0)
              JEND = IH0POINT(I+1,NT0) - 1
          ELSE
            JBEG = IH0POINT(I,IT0)
            JEND = IH0POINT(I+1,IT0) - 1
```

```
      ENDIF
        IF (JBEG. LE. JEND) THEN
          IF (MOD(NRUN-1,DELT0/DELT).EQ.0) THEN
       IF (NRUN .LE. MAXNC) THEN
             JPBEG = IH0POINT(I,NT0-1)
             JPEND = IH0POINT(I+1,NT0-1) - 1
       ELSE
         IF (IT0 .EQ. 1) THEN
           JPBEG = IH0POINT(I,NT0)
           JPEND = IH0POINT(I+1,NT0) - 1
         ELSE
           JPBEG = IH0POINT(I,IT0-1)
           JPEND = IH0POINT(I+1,IT0-1) - 1
         ENDIF
       ENDIF
           DO J = JBEG,JEND
             IF (JPBEG .LE. JPEND) THEN
             DO JP = JPBEG,JPEND
           IF (NRUN .LE. MAXNC) THEN
                 IF (IH0LIST(J,NT0).EQ.IH0LIST(JP,NT0-1))THEN
                   IF (IHT(J) .NE. IHOLD(JP))
:            HBLIP = HBLIP + 1
                   IF (IBIGHT(J) .NE. IBIGHOLD(JP))
:           BIGHBLIP = BIGHBLIP + 1
                 ENDIF
           ELSE
             IF (IT0 .EQ. 1) THEN
               IF (IH0LIST(J,1).EQ.IH0LIST(JP,NT0))THEN
                     IF (IHT(J) .NE. IHOLD(JP))
:           HBLIP = HBLIP + 1
                     IF (IBIGHT(J) .NE. IBIGHOLD(JP))
:           BIGHBLIP = BIGHBLIP + 1
                   ENDIF
             ELSE
              IF(IH0LIST(J,IT0).EQ.IH0LIST(JP,IT0-1))THEN
                     IF (IHT(J) .NE. IHOLD(JP))
:           HBLIP = HBLIP + 1
                     IF (IBIGHT(J) .NE. IBIGHOLD(JP))
:           BIGHBLIP = BIGHBLIP + 1
                   ENDIF
             ENDIF
           ENDIF
              ENDDO
              ENDIF
            ENDDO
          ELSE
            DO J = JBEG, JEND
              IF (IHT(J) .NE. IHOLD(J)) HBLIP = HBLIP + 1
              IF (IBIGHT(J) .NE. IBIGHOLD(J))
:                   BIGHBLIP = BIGHBLIP + 1
            ENDDO
          ENDIF
        ENDIF
      ENDDO
```

```
        ENDIF

C     n(t), and kin(t), with BIGHT, also r(t) and R(t)




C     DT=1 if t=t0.
      DO T = 1, NT0
        IF (NRUN .LE. MAXNC) THEN
          DT = NRUN - (DELT0/DELT)*(T-1)
          T0IDX = T
        ELSE
          DT = MOD(NRUN,MAXNC) + (DELT0/DELT)*(NT0-T-IT0+1)
          IF (DT.LT.1) DT = DT + MAXNC
          T0IDX = MOD(T+IT0,NT0)
          IF (T0IDX .EQ. 0) T0IDX = NT0
        ENDIF
      C----------------------
             DO I = 1, MXMOLS - 1
          IF (NRUN .LE. MAXNC) THEN
            JBEG = IH0POINT(I,NT0)
            JEND = IH0POINT(I+1,NT0) - 1
          ELSE
            JBEG = IH0POINT(I,IT0)
            JEND = IH0POINT(I+1,IT0) - 1
          ENDIF
          J0BEG = IH0POINT(I,T0IDX)
          J0END = IH0POINT(I+1,T0IDX) – 1
C----------------------------------------
          IF (JBEG .LE. JEND) THEN
          DO J1 = JBEG, JEND
            NTIMEC(DT) = NTIMEC(DT) + 1
                  IF (J0BEG .LE. J0END) THEN
            DO J0 = J0BEG, J0END
            IF (NRUN .LE. MAXNC) THEN
                IF (IH0LIST(J1,NT0) .EQ. IH0LIST(J0,T0IDX)) THEN
                IRTSUM(DT)=IRTSUM(DT)
     :                 + IBIGHT(J1)*IBIGH0(J0,T0IDX)
                IBIGRTSUM(DT) = IBIGRTSUM(DT)
     :                 + IBIGHT(J1)*IH0(J0,T0IDX)
                ICTSUM(DT) = ICTSUM(DT)
     :                 + IHT(J1)*IH0(J0,T0IDX)
                INTSUM(DT) = INTSUM(DT)
     :                 + (1-IHT(J1))*IH0(J0,T0IDX)*IBIGHT(J1)
              ENDIF
            ELSE
              IF (IH0LIST(J1,IT0) .EQ. IH0LIST(J0,T0IDX)) THEN
                IRTSUM(DT)=IRTSUM(DT)
     :                 + IBIGHT(J1)*IBIGH0(J0,T0IDX)
                    IBIGRTSUM(DT) = IBIGRTSUM(DT)
     :                   + IBIGHT(J1)*IH0(J0,T0IDX)
                    ICTSUM(DT) = ICTSUM(DT)
```

```
     :                 + IHT(J1)*IH0(J0,T0IDX)
                    INTSUM(DT) = INTSUM(DT)
     :                  + (1-IHT(J1))*IH0(J0,T0IDX)*IBIGHT(J1)
              ENDIF
            ENDIF
            ENDDO
            ENDIF
          ENDDO
          ENDIF
        ENDDO
C       print *, t, dt, t0idx, ntimec(dt)
      ENDDO
      HTOTAV = HAVSUM / DBLE(NRUN)
      HSUMTOTAV = DBLE(HSUMSUM) / DBLE(NRUN)
      BIGHTOTAV = BIGHAVSUM / DBLE(NRUN)
      BIGHSUMTOTAV = DBLE(BIGHSUMSUM) / DBLE(NRUN)
      NNBAV = DBLE(NNBSUM) / DBLE(NRUN)
      RETURN
      END
```

Mean square displacement and velocity auto-correlation functions:

```
SUBROUTINE DIFF(NATMS,DELT0,XXX,YYY,ZZZ,XT0,YT0,ZT0,
:          VXX,VYY,VZZ,VX0,VY0,VZ0,NSTEP,NSTEQL,
:          PMSD,VACF,PMSDAV,VACFAV,NTIME,CELL,NT0)
      INCLUDE 'dl_params.inc'
      INTEGER NATMS, NSTEP, NSTEQL, NSRUN,I,J,K,T
      INTEGER DELT0, NT0, DT
      DIMENSION NTIME(MAXSTP)
      DOUBLE PRECISION L, DX, DY, DZ
      DIMENSION CELL(9)
      DIMENSION XT0(MXATMS,MAXNT0),YT0(MXATMS,MAXNT0)
      DIMENSION ZT0(MXATMS,MAXNT0)
      DIMENSION VX0(MXATMS,MAXNT0),VY0(MXATMS,MAXNT0)
      DIMENSION VZ0(MXATMS,MAXNT0)
      DIMENSION XXX(MXATMS),YYY(MXATMS),ZZZ(MXATMS)
      DIMENSION VXX(MXATMS),VYY(MXATMS),VZZ(MXATMS)
      DIMENSION PMSD(MAXSTP), VACF(MAXSTP)
      DIMENSION PMSDAV(MAXSTP), VACFAV(MAXSTP)
      L = CELL(1)
      NRUN = NSTEP - NSTEQL
C     On the first call, initialize MSD and VACF to 0.
      IF (NRUN .EQ. 1) THEN
        NT0 = 0
        DO I = 1, MAXSTP
          PMSD(I) = 0.0D0
          PMSDAV(I) = 0.0D0
          VACF(I) = 0.0D0
          VACFAV(I) = 0.0D0
          NTIME(I) = 0
        ENDDO
      ENDIF
      IF ( (NRUN .EQ. 1) .OR.
     :           (MOD(NRUN-1,DELT0) .EQ. 0)) THEN
        NT0 = NT0 + 1
C       PRINT *, 'FIRST T0 ADDED, NT0=', NT0
      ENDIF
      DO I = 321, NATMS
        IF ( (NRUN .EQ. 1) .OR.
     :           (MOD(NRUN-1,DELT0) .EQ. 0)) THEN
          XT0(I,NT0) = XXX(I)
          YT0(I,NT0) = YYY(I)
          ZT0(I,NT0) = ZZZ(I)
          VX0(I,NT0) = VXX(I)
          VY0(I,NT0) = VYY(I)
          VZ0(I,NT0) = VZZ(I)
        ENDIF
C-----------------------------
        DO T = 1, NT0
          DT = NRUN - DELT0*(T-1)
          DX = DABS(XXX(I) - XT0(I,T))
          IF (DX .GT. L/2) DX = DX - L
          DY = DABS(YYY(I) - YT0(I,T))
          IF (DY .GT. L/2) DY = DY - L
```

```
      DZ = DABS(ZZZ(I) - ZT0(I,T))
      IF (DZ .GT. L/2) DZ = DZ - L
      PMSD(DT) = PMSD(DT) + DX*DX + DY*DY + DZ*DZ
      VACF(DT) = VACF(DT)+ VXX(I)*VX0(I,T) +
     :           VYY(I)*VY0(I,T) + VZZ(I)*VZ0(I,T)
      IF (I .EQ. 321) THEN
        NTIME(DT) = NTIME(DT)+1
      ENDIF
    ENDDO
  ENDDO
  DO J = 1, NRUN
    PMSDAV(J) = PMSD(J)/(DBLE(NATMS)*DBLE(NTIME(J)))
    VACFAV(J) = VACF(J)/(DBLE(NATMS)*DBLE(NTIME(J)))
  ENDDO

  RETURN
  END
```

Rotational relaxation time $P_2(t)$.

```
      SUBROUTINE CORRH2O(DELT0,DELT,XXX,YYY,ZZZ,NSTEP,NSTEQL,
     :     XHH0,YHH0,ZHH0,TSTEP,CELL,NT0,IT0,P2SUM,NTIMEC,
     :     XHHT,YHHT,ZHHT)
      INCLUDE 'dl_params.inc'
C     ------------- INTEGER DECLARATIONS ----------
      INTEGER NSTEP,NSTEQL,NRUN, DELT
      INTEGER I1, I2, II, J1, J0, JP, JF, T, DT
      INTEGER DELT0, NT0,IT0, T0IDX
      DIMENSION NTIMEC(MAXNC)
C     ------------- REAL DECLARATIONS ---------------
      DOUBLE PRECISION TSTEP, TSAMP, L, RTEMP
      DOUBLE PRECISION XHH,YHH,ZHH
      DOUBLE PRECISION DOT
      DIMENSION CELL(9)
      DIMENSION XXX(MXATMS), YYY(MXATMS), ZZZ(MXATMS)
      DIMENSION P2SUM(MAXNC)
      DIMENSION XHH0(MXMOLS,MAXNT0)
      DIMENSION YHH0(MXMOLS,MAXNT0)
      DIMENSION ZHH0(MXMOLS,MAXNT0)
      DIMENSION XHHT(MXMOLS)
      DIMENSION YHHT(MXMOLS)
      DIMENSION ZHHT(MXMOLS)
C     -------------------------------------------------
      L = CELL(1)
C     NRUN = 1 on first call on 1st step after eq,
C     +1 for each call.
      NRUN = (NSTEP - NSTEQL - 1)/DELT + 1
C     Initialize on the first call:
      IF (NRUN .EQ. 1) THEN
        DO I = 1, MAXNC
          NTIMEC(I) = 0
          P2SUM(I) = 0.0D0
        ENDDO
        DO I = 1, MXMOLS
          DO J = 1, MAXNT0
            XHH0(I,J) = 0.0D0
            YHH0(I,J) = 0.0D0
            ZHH0(I,J) = 0.0D0
          ENDDO
        ENDDO
        NT0 = 0
        IT0 = 1
      ENDIF
C     Check if a new T0 is being added: whether NRUN>MAXNC or not.
C     reset ILIST0 when an old T0 being replaced.
      IF (NRUN .LE. MAXNC) THEN
        IF ((NRUN. EQ. 1) .OR.
     :           (MOD(NRUN-1,DELT0/DELT).EQ.0))THEN
          NT0 = NT0 + 1
          DO I = 1, MXMOLS
            XHH0(I,NT0) = 0.0D0
            YHH0(I,NT0) = 0.0D0
```

```
            ZHH0(I,NT0) = 0.0D0
          ENDDO
          ENDIF
        ELSE
          IF (MOD(NRUN-1, DELT0/DELT) .EQ. 0) THEN
            IT0 = MOD((NRUN-1)/(DELT0/DELT),NT0) + 1
            DO I = 1, MXMOLS
              XHH0(I,IT0) = 0.0D0
              YHH0(I,IT0) = 0.0D0
              ZHH0(I,IT0) = 0.0D0
            ENDDO
          ENDIF
        ENDIF

C     neighbour list.
C     Neighbour list update interval = DELT0
      IF ((NRUN .EQ. 1) .OR.
     :           (MOD(NRUN-1,DELT0/DELT) .EQ. 0)) THEN
C     H-H distance is 1.633 A, so to get the unit vector, div. all
C     components by 1.633.
C     need the vector components
          DO I = 1, MXMOLS
            XHH = XXX(320+3*I) - XXX(320+3*I-1)
            IF (XHH .GT. L/2) XHH = L-XHH
            IF (XHH .LT. -L/2) XHH = L+XHH
            YHH = YYY(320+3*I) - YYY(320+3*I-1)
            IF (YHH .GT. L/2) YHH = L-YHH
            IF (YHH .LT. -L/2) YHH = L+YHH
            ZHH = ZZZ(320+3*I) - ZZZ(320+3*I-1)
            IF (ZHH .GT. L/2) ZHH = L-ZHH
            IF (ZHH .LT. -L/2) ZHH = L+ZHH
            XHH = XHH/1.633
            YHH = YHH/1.633
            ZHH = ZHH/1.633
C           print *, xhh,yhh,zhh
            XHHT(I) = XHH
            YHHT(I) = YHH
            ZHHT(I) = ZHH
            IF (NRUN .LE. MAXNC) THEN
              XHH0(I,NT0) = XHH
              YHH0(I,NT0) = YHH
              ZHH0(I,NT0) = ZHH
            ELSE
              XHH0(I,IT0) = XHH
              YHH0(I,IT0) = YHH
              ZHH0(I,IT0) = ZHH
            ENDIF
          ENDDO
        ENDIF

        DO T = 1, NT0
          IF (NRUN .LE. MAXNC) THEN
            DT = NRUN - (DELT0/DELT)*(T-1)
            T0IDX = T
```

```
        ELSE
          DT = MOD(NRUN,MAXNC) + (DELT0/DELT)*(NT0-T-IT0+1)
          IF (DT.LT.1) DT = DT + MAXNC
          T0IDX = MOD(T+IT0,NT0)
          IF (T0IDX .EQ. 0) T0IDX = NT0
        ENDIF
        DO I = 1, MXMOLS
C     Do e(t).e(0)
          DOT = XHHT(I)*XHH0(I,T0IDX)
     :           + YHHT(I)*YHH0(I,T0IDX)
     :           + ZHHT(I)*ZHH0(I,T0IDX)
C     second Legendre polynomial of DOT
          P2SUM(DT) = P2SUM(DT)
     :           + ((3.0D0*DOT*DOT)-1.0D0)/2.0D0
        ENDDO
        NTIMEC(DT) = NTIMEC(DT) + 1
      ENDDO
      RETURN
      END
```

References:

[1] T Young; "An Essay on the Cohesion of Fluids", *Philos. Trans. R. Soc. London*, 95, **1805**, 65-87.

[2] A B D Cassie and S Baxter; "Wettability of Porous Surfaces", *Trans. Faraday Soc*., 40, **1944**, 546-551.

[3] Gao, T J McCarthy; "How Wenzel and Cassie Were Wrong", *Langmuir*, 23, **2007**, 3762-3765.

[4] J Wang, D Bratko, A Luzar; "Probing surface tension additivity on chemically heterogeneous surfaces by a molecular approach", *Proceeding of the National Academy of Science of the United States of America*, 108, **2011**, 6374-6379.

[5] G McHale; "Cassie and Wenzel: Were they really so wrong?", *Langmuir*, 23, 2007, 8200-8205.

[6] G. McHale, N. J. Shirtcliffe, M. I. Newton; "Super-hydrophobic and super-wetting surfaces: Analytical potential?", *Analyst*, 129, **2004**, 284-287.

[7] Brandon, N Haimovich, E Yeger, and A Marmur; "Partial wetting of chemically patterned surfaces: The effect of drop size", *J. Colod Interface Sci.*, 263, **2003**, 237-243.

[8] A Marmur and E Bittoun,; "When Wenzel and Cassie are right: Reconciling local and global considerations", *Langmuir*, 25, **2009**, 25, 1277-1281.

[9] Y Kwon, S Choi, N Anantharaju, J Lee, M V Panchagnula and N A Patankar; "Is the Cassie-Baxter formula relevant?", *Langmuir*, 26, **2010**, 17528-17531.

[10] J F Joanny and P G de Gennes; "A model for contact angle hysteresis", *J. Chem.Phys.*, 81, **1984**, 552-562.

[11] L Gao, T J McCarthy; "Comment on how Wenzel and Cassie were wrong", *Langmuir*, 23, **2007**, 13243-13243.

[12] J Ritchie, J Seyed-Yazdi, D Bratko, A Luzar; **2011**, to be published.

[13] S L Gras, T Mahmud, G Rosengarten, A Mitchell, K Kalantar-zadeh "Intelligent control of surface hydrophobicity", *ChemPhysChem*, 8, **2007**, 2036-2050.

[14] T Roques-Carmes, A Gigante, J M Commenge, S Corbel; "Use of surfactants to reduce the driving voltage of switchable optical elements based on electrowetting", 25, **2009**, 12771-12779.

[15] J Lahann, J S Mitragotri, T Tran, H Kaido, J Sundaram, I S Choi, S Hoffer, G A Somorjai and R Langer, "A Reversibly Switching Surface", *Science*, 299, **2003**, 371-374.

[16] R Fetzer, M Ramiasa and J Ralston; "Dynamics of liquid-liquid displacement", Langmuir, 25, 2009, 8069-8074.

[17] S Ray, R Sedev, C Priest, J Ralston; "Influence of the work of adhesion on the dynamic wetting of chemically heterogeneious surfaces", *Langmuir*, 24, **2008**, 13007-13012.

[18] C Priest, R Sedev, J Ralston; "Asymmetric wetting hysteresis on chemical defects", *Phys. Rev. Lett.*, 99, **2007**, 026103.

[19] L Bocquet, E Charlaix; "Nanofluidics, from bulk to interfaces", *Chem. Soc. Rev.*, 39, **2010**, 1073-1095.

[20] J Marti, G Nagy, E Guardia, M C Gordillo; "Molecular dynamics simulation of liquid water confined inside graphite channels: dielectric and dynamical properties", *J. Phys. Chem. B*, 110, **2006**, 23987-23994.

[21] L Huang, L Zhang, Q Shao, J Wang, L Lu, X Lu, S Jiang, W Shen; "Molecular dynamics simulation study of the structural characteristics of water molecules confined in functionalized carbon nanotubes", *J. Phys. Chem. B*, 110, **2006**, 25761-25768.

[22] O Byl, J Liu, Y Wang, W Yim, J K Johnson, J T Yates Jr.; "Unusual hydrogen bonding in water-filled carbon nanotubes", *J. Am. Chem. Soc.*, 128, **2006**,12090-12097.

[23] J Shiomi, T Kimura, S Maruyama; "Molecular dynamics of ice-nanotube formation inside carbon nanotubes", *J. Phys. Chem. C*, 111, **2007**, 12188-12193.

[24] M Rovere, P Gallo; "Effects of confinement on static and dynamical properties of water", Eur. Phys. J. E, 12, 2003, 77-81.

[25] M Rovere, M A Ricci, D Vellati, F Bruni; "A molecular dynamics simulation of water confined in a cylindrical SiO_2 pore", J. Chem. Phys., 108, 1998, 9859-9867.

[26] A Malani, K G Ayappa, S Murad; "Influence of hydrophilic surface specificity on the structural properties of confined water", J. Phys. Chem. B, 113, 2009, 13825-13839.

[27] P L Luisi, B E Straub; "Reverse micelles: biological and technological relevance of amphiphilic structures in apolar media", Plenum, New York, 1984.

[28] T De, A Maitra; "Solution behavior of aerosol OT in non-polar solvents", *Adv. Colloid Interface Sci.*, 59, **1995**, 95-193

[29] N E Levinger; "Water in confinement", *Science*, 298, **2002**, 1722-1723.

[30] J Faeder, B M Ladanyi; "Molecular dynamics simulations of the interior of aqueous reverse micelles", *J. Phys. Chem. B*, 104, **2000**, 1033-1046.

[31] D E Rosenfeld, C A Schmuttenmaer; "Dynamics of water confined within reverse micelles", *J. Phys. Chem. B*, 110, **2006**, 14304-14312.

[32] P A Pieniazek, Y S Lin, J Chowdhary, B M Ladanyi, J L Skinner; "Vibrational spectroscopy and dynamics of water confined inside reverse micelles", *J. Phys. Chem.*, 113, **2009**, 15017-15028.

[33] M R Harpham, B M Ladanyi, N E Levinger, K W Herwig; "Water motion in reverse micelles studied by quasielastic neutron scattering and molecular dynamics simulations", *J. Phys. Chem.*, 121, **2004**, 7855-7866.

[34] D S Venables, K Huang, C A Schmuttenmaer; "Effect of reverse micelle size on the librational band of confined water and methanol", *J. Phys. Chem. B*, 105, 2001, 9132-9138.

[35] G Onori, A Santucci; "IR Investigations of Water Structure in Aerosol OT Reverse Micellar Aggregates", *J. Phys. Chem.*, 97 1993, 5430-5434.

[36] I R Piletic, D E Moilanen, D B Spry, N E Levinger, M D Fayer; "Testing the Core/Shell Model of Nanoconfined Water in Reverse Micelles Using Linear and Nonlinear IR Spectroscopy", *J. Phys. Chem. A*, 110, 2006, 4985-4999.

[37] A M Dokter, S Woutersen, H Bakker; "Inhomogeneous dynamics in confined water nanodroplets", *J. Proc. Natl. Acad. Sci. U.S.A.*, 103, **2006**, 15355-15358.

[38] T Mitra, P Miro, A R Tomsa, A Merca, H Bogge, J B Avalos, J M Poblet, C Bo, A Muller; "Gated and Differently Functionalized (New) Porous Capsules Direct Encapsulates' Structures: Higher and Lower Density Water", *A. Chem. Eur. J.*, 15, **2009**, 1844-1852.

[39] M Garcia-Ratés, P Miró, J M Poblet, C Bo, J Bonet Avalos*;* "Dynamics of encapsulated water inside Mo(132*)* cavities", *J. Phys. Chem. B*, 115, **2011**, 5980-5992.

[40] H J C Berendsen, J R Grigera, T P Straatsma; "The missing term in effective pair potentials", *J. Phys. Chem.*, 91, **1987**, 6269-6271.

[41] B Guillot; "A reappraisal of what we have learnt during three decades of computer simulations on water", *J. Mol. Liq.*, 101, **2002**, 219-260.

[42] C Vega, J L F Abascal, M M conde, J L Aragones; "What ice can teach us about water interactions: A critical comparison of the performance of different water models", *Faraday Discuss.*, **141**, 2009, 251-276.

[43] D Frenkel, B Smit; "Understanding Molecular Simulation from Algorithms to Applications", 2nd ed., Academic Press: San Diego, **2002**, Vol. 1.

[44] M P Allen, D. J. Tildesley; "Computer Simulation of Liquids", Oxford University Press: New York, **1991**

[45] S Plimpton, "Fast Parallel Algorithms for Short-Range Molecular Dynamics", *J. Comput. Phys.*, 117, **1995**, 1-19.

[46] W Smith, T R Forester; "DL_POLY_2.0: a general-purpose parallel molecular dynamics simulation package", *J. Mol. Graphics*, 14, **1996**, 136-141.

[47] S W Deleeuw, J W Perram, E R Smith; "Simulation of Electrostatic Systems in Periodic Boundary-Conditions. 1. Lattice Sums and Dielectric-Constants", *Proceedings of the Royal Society of London Series a-Mathematical Physical and Engineering Sciences*, 373, **1980**, 27-56.

[48] U Essmann, L Perera, M L Berkowitz; "A Smooth Particle Mesh Ewald Method", *J. Chem.Phys.*, 103, **1995**, 8577-8593.

[49] A Y Toukmaji, J A Board; "Ewald summation techniques in perspective: a survey", *Comp. Phys. Comm.*, 95, **1996**, 73-92.

[50] T Werder, J H Walther, R L Jaffe, T Halicioglu and P Koumoutsakos;" On the water-carbon interaction for use in molecular dynamics simulations of graphite and carbon nanotubes", *J. Phys. Chem. B*, 107, **2003**, 1345-1352.

[51] M J de Ruijter, T D Blake, J De Coninck; "Dynamic wetting studied by molecular modeling simulations of droplet spreading", *Langmuir*, 15, **1999**, 7836-7847.

[52] A Luzar and D Chandler; "Effect of environment on hydrogen bond dynamics in liquid water", Phys. Rev. Lett., 76, **1996**, 928-931.

[53] M Mezei, D L Beveridge; "Theoretical studies of hydrogen-bonding in liquid water and dilute aqueous-solution", J. Chem. Phys., 74, 1981, 622-632.

[54] A Rahman, F. H. Stillinger; "Molecular dynamics study of liquid water", J. Chem. Phys., 55, **1971**, 3336-3359.

[55] L Jorgensen, J Chandrasekhar, J Madura, R W Impey, M L Klein; "Comparison of simple potential functions for simulating liquid water", J.Chem. Phys., 79, **1983**, 926-935.

[56] D Chandler; "Introduction to modern statistical mechanics", *Oxford, New York*, **1987**.

[57] C W Extrand; "Contact Angles and Hysteresis on Surfaces with Chemically Heterogeneous Islands", *Langmuir*, 19, **2003**, 3793-3796.

[58] J Ritchie; "Contact Angle Of A Nano-Drop On A Heterogeneous Surface", *Master Thesis*, VCU, **2010**.

[59] S Nose, "A molecular dynamics method for simulations in the canonical ensemble", *Molecular Physics*, 52, 1984, 255-268.

[60] J P Ryckaert, G Ciccotti, H J C Berendsen; "Numerical integration of the Cartesian equations of motion of a system with constraints: molecular dynamics of n-alkanes", *J. Comput. Phys*., 23, **1977**, 327-341.

[61] R N Wenzel; "Resistance of Solid Surfaces to Wetting by Water", *Ind. Eng. Chem*., 28, **1936**, 988-994.

[62] C D Daub, J Wang, S Kudesia, D Bratko, A Luzar; "The influence of molecular-scale roughness on the surface spreading of an aqueous nanodrop ", *Faraday Disscus.*, 146, **2010**, 67-77.

[63] J Mittal, G Hummer; "Interfacial thermodynamics of confined water near molecularly rough surfaces", *Faraday Discuss.*, 146, **2010**, 341-352.

[64] H Gelderblom, A G Marin, H Nair, A Houselt, L Lefferts, J H Snoeijer and D Lohse; "How water droplets evaporate on a superhydrophobic substrate", *Phys. Rev. E*, 83, **2011**, 026306.

[65] Y ChangWei, H Feng and H PengFei; "The apparent contact angle of water droplet on the micro-structured hydrophobic surface ", *Science China-Chemistry*, 53, 2010, 912-916.

[66] J Ralston, M Popescu, R Sedev; "Dynamics of Wetting from an Experimental Point of View", *Annual Review of Materials Research*, 38, **2008**, 23-43.

[67] T D Blake and J De Coninck; "The influence of pore wettability on the dynamics of imbibition and drainage", *Colloids and Surfaces A: Physicochemical and Engineering Aspects*, 250, **2004**, 395-402.

[68] M Paneru, C Priest, R Sedev, J Ralston; "Static and dynamic electrowetting of an ionic liquid in a solid/liquid/liquid system", *J. Am. Chem. Soc.*, 132, **2010**, 8301-8308.

[69] R Fetzer, J Ralston; "Influence of Nanoroughness on Contact Line Motion", J. Phys. Chem. C, 114, 2010, 12675-12680.

[70] G McHale, M I Newton; "Frenkel's method and the dynamic wetting of heterogeneous planar surfaces", *Colloids and Surfaces A*, 206, **2002**, 193-201.

[71] T D Blake, J M Haynes; "Kinetics of liquid/liquid displacement", *J. Colloid Interface Sci.*, 30, **1969**, 421-423.

[72] H Li, R Sedev and J Ralston; "Dynamic wetting of a fluoropolymer surface by ionic liquids", *Phys. Chem. Chem. Phys.*, 13, **2011**, 3952-3959.

[73] R G Cox; "The dynamics of the spreading of liquids on a solid surface. Part 2. Surfactants", *Journal of Fluid Mechanics*, 168, **1986**, 195-220.

[74] O V Voinov; "Hydrodynamics of wetting", *Fluid Dyn.*, 11, **1976**, 714-721.

[75] T D Blake, J De Coninck; "The influence of solid-liquid interactions on dynamic wetting", *Adv. colloid interface sci.*, 96, **2002**, 21-36.

[76] P G Petrov and J G Petrov; "A combined molecular-hydrodynamic approach to wetting kinetics", *Langmuir*, 8, **1992**, 1762-1767.

[77] C Vega, E de Miguel; "Surface tension of the most popular models of water by using the test-area simulation method", *J. Chem. Phys.*, 126, **2007**, 154707(1-10).

[78] P E Smith, W F van Gunsteren; "The viscosity of SPC and SPC/E water at 277 and 300K", *Chem. Phys. Lett.*, 215, **1993**, 315-318.

[79] J Seyed-Yazdi, D Bratko, A Luzar; "Switchable nano-wetting dynamics", to be published.

[80] M Henry; "Quantitative Modelization of Hydrogen-Bonding in Polyoxometalate Chemistry", *Journal of Cluster Science*, 13, **2002**, 437-458.

[81] M Henry; "Unraveling water structure inside and between nanocapsules", *Journal of Cluster Science*, 14, **2003**, 267-287.

[82] A Muller, H Bogge, E Diemann; "Structure of a cavity-encapsulated nanodrop of water ", *Inorg. Chem. Commun.*, 6, **2003**, 52-53.

[83] S Nose; "A molecular dynamics method for simulation in the canonical ensemble", *Mol. Phys.*, 52, **1984**, 255-268.

[84] A Luzar, D Chandler; "Hydrogen-bond kinetics in liquid water", Nature, 379, 1996, 55-57.

[85] A Luzar, "Resolving the hydrogen bond dynamics conundrum", *J. Chem. Phys.*, 113, **2000**, 10663-10675.

[86] L Lu and M L Berkowitz; "Hydration force between model hydrophilic surfaces: Computer simulations", *Chem. Phys.*, 124, 2006, 101101 (4p).

[87] A Muller, M Henry; "Nanocapsule water-based chemistry", *C. R. Chimie*, 6, **2003**, 1201-1208.

[88] A Muller, B Hartmut, M Henry; "Coordination chemistry under confined conditions: a simplified illustrative view", *C. R. Chimie*, 8, **2005**, 47-56.

[89] S W Rick, S J Stuart, B J Berne; "Dynamical fluctuating charge force fields: Application to liquid water", *J. Chem. Phys.*, 101, **1994**, 6141-6156.

[90] C Daub, A Luzar; to be published.

[91] R W Impey, P A Madden, I R McDonald; "Spectroscopic and transport properties of water model calculations and the interpretation of experimental results", *Mol. Phys.*, 46, **1982**, 513-539.

[92] A Faraone, E Fratini, A M Todea, B Krebs, A Muller, P Baglioni; "Dynamics of water in voids between well-defined and densely packed spherical nanocages acting as polyprotic inorganic acids", *J. Phys.Chem. C*, 113, **2009**, 8635-8644.

[93] P Liu, E Harder, B J Berne; "On the calculation of diffusion coefficients in confined fluids and interfaces with an application to the liquid-vapor interface of water", *J. Phys. Chem. B*, 108, **2004**, 6595-6602.

[94] D A Turton, J Hunger, G Hefter, R Buchner, K Wynne; "Glasslike behavior in aqueous electrolyte solutions", *J. Chem. Phys. (Comm.)*, 128, **2008**, 161102-161105.

[95] C S Hsieh, R Kramer Campen, A C Vila Verde, P Bolhuis, H K Nienhuys, M Bonn; "Ultrafast reorientation of dangling OH groups at the air-water interface using femtosecond vibrational spectroscopy", *Physical Review Letters*, 107, **2011**, 116102.

Vita

Jamileh Seyed Yazdi was born on Dec. 13th in Rafsanjan, Iran.

Education:

Bachelor of Science, Ferdowsi University, Physics, Iran –September 1997.

Master of Science, Shiraz University, Physics, Iran –September 2000.

Master of Science, UvA Amsterdam, ENS Lyon and Sapienza Rome –July 2007.

Ph.D, Iran University of Science and Technology, Physics –January 2009.

Master of Science, Chemistry, Virginia Commonwealth University, Richmond, VA –December 2011.

Fellowships, Scholarships and Awards (VCU):

Altria Fellowship, VCU, Summer 2010.

Lidia M. Vallarino Scholarship, Summer 2010.

Outstanding Teaching Assistant Award, March 2011.

Global Ambassador Scholarship, August 2011.

Scientific Contributions:

Jamileh Seyed Yazdi, Jihang Wang, Dusan Bratko, Alenka Luzar; "*Switchable Nanowetting Dynamics*", Poster Presentation at Faraday Discussion, Richmond VA, 2010.

John Ritchie, Jamileh Seyed Yazdi, Dusan Bratko, Alenka Luzar; "*Shape of a Droplet atop a Surface Heterogeneity at the Nanoscale*", to be submitted December 2011.

"*Switchable Nanowetting Dynamics*", to be completed.

"*Water Dynamics inside Nanospheres*", to be completed.